UNIVERSITY OF SOUTHAMPTON

Borel Singularities in the High Energy Limit of QCD

by

Kevin David Anderson

A thesis submitted for the degree of

Doctor of Philosophy

Department of Physics

June 1998

Dedicated to my family

UNIVERSITY OF SOUTHAMPTON

ABSTRACT

FACULTY OF SCIENCE

PHYSICS

Doctor of Philosophy

Borel Singularities in the High Energy Limit of QCD

Kevin David Anderson

This thesis discusses evidence for corrections of possible non-perturbative origin to the leading logarithmic ($1/x$) approximation of QCD. It is found that gluon radiation generated by a high energy quark-antiquark system provides a framework to incorporate a running gauge coupling appropriate for sampling a wide range of momenta. By using the Borel transform, the argument of the coupling in terms of impact parameters is deduced in this framework and an integral equation is formulated in Borel space to describe the evolution of the gluon density with rapidity. It is shown that the action of the kernel of this equation reproduces the BFKL result in the fixed coupling limit. The action of the kernel on a conformally invariant function is studied to determine deviations from the fixed coupling limit and a series of singularities in the Borel plane are detected. The relevance of these singularities to physical processes is discussed. A scheme to determine the Borel plane singularities of the gluon cascade arising in deep inelastic scattering is introduced and the position of these singularities is found after transforming the kernel to a form amenable to numerical analysis. The existence of a leading pole in the Borel plane corresponding to $1/Q^2$ power corrections is established. The importance of these power corrections relative to the perturbative result is estimated.

Contents

List of Figures

List of Tables

Preface

The material presented in Chapters 5-8 constitutes research carried out in collaboration with D. A. Ross and M. G. Sotiropoulos and has appeared in part in

K. D. Anderson, D. A. Ross and M. G. Sotiropoulos, *How to run the coupling in the dipole approach to the BFKL equation*, Phys. Lett. **B380**, 127–133 (1996), hep-ph/9602275.

K. D. Anderson, D. A. Ross and M. G. Sotiropoulos, *Running coupling and Borel singularities at small* x, Nuc. Phys. **B515**, 249–268 (1998), hep-ph/9705466.

No claim is made to the originality of the results presented in other chapters and references to the original literature are supplied where appropriate.

Acknowledgements

Firstly, I must acknowledge the support and advice that my supervisor Douglas Ross has given me over the last three years. His wealth of experience in the BFKL ladder formalism has been especially valuable to me. My understanding of small-x physics has also been greatly enhanced by discussions with my other research team member, Michael Sotiropoulos. I must also thank all the other members of SHEP who have shared their understanding and listened to my ideas over the last three years.

The Southampton High Energy Physics group has always provided a friendly and supportive atmosphere in which to work and needless to say this has produced many memories which will remain with me long after I leave.

Outside the office. I should thank a collection of long suffering housemates who have had to put up with my erratic hours over the years. I also owe a great deal to my parents for their support throughout my time of study here so thanks Mum and Dad.

Finally, I acknowledge the support provided to me by PPARC by their award of a research studentship.

Chapter 1

Introduction

Quantum chromodynamics (QCD) is now an accepted part of the standard model of particle physics, successfully describing many experimentally observed aspects of the strong interaction. In spite of this statement, there are many challenging problems which still require to be addressed. One such challenge concerns processes where two large but disparate momentum scales are present. Starting from a perturbative framework, this study concentrates on identifying the nature of the corrections to these processes which are due to effects arising from low momentum scales.

Hadron-hadron scattering processes which are governed solely by low momentum scales have been studied for many decades and it is observed that the total hadronic cross section rises slowly with centre of mass energy. This kinematic regime cannot be investigated using perturbative QCD. Regge theory, which will be reviewed in chapter 2, is currently the only tool available to model processes at low momentum scales. Over the last twenty years, an understanding has emerged on the treatment of high energy scattering processes in which there is a sufficiently hard momentum scale present so that QCD perturbation theory can be applied but in which there exists a much larger scale also.

Deep inelastic lepton-hadron scattering at small Bjorken-x is such a process where a highly virtual photon probe provides a hard scale and the square of the centre of mass energy of the photon-proton system provides another much larger scale. It is found that in order to make any predictions, the full perturbation series in α_s has to be approximated by considering a resummed set of leading terms only. These terms contain large logarithms in $(1/x)$ which dominate the perturbation series at all orders. At fixed coupling, the evolution equation in $\ln(1/x)$ which results is known as the BFKL equation [1, 2]. Its solution predicts that F_2, the proton structure function, should rise far more rapidly with the centre of mass energy than is observed in the case of total hadronic cross sections. In chapter 2, the BFKL formulation will be reviewed and evidence to suggest that a running coupling should be employed within this approximation will be presented.

The fact that such different types of behaviour are observed when contrasting processes governed by soft and hard momentum scales may not be surprising but it is interesting to ask whether there is any way in which they can be related. Note that it is not expected that one should be able to describe soft scattering from first principles in perturbative QCD: however it might be hoped that the understanding which has been gained from the perturbative approach could be extended to indicate how the BFKL behaviour could be 'softened'. Further motivation for the need to extend the BFKL formalism comes from recent results published by the HERA *ep* scattering facility which shall be discussed in more detail later. Although the structure functions are observed to rise rapidly with centre of mass energy, the rise is lower than the leading logarithmic BFKL prediction. Another problem with the original BFKL prediction is that it violates the Froissart bound which states that cross sections cannot rise faster than $\ln^2 s$ at high energies without violating unitarity constraints. Incorporating unitarity corrections into the BFKL equation has also attracted much effort recently [3] but will not be considered in this study.

It shall be demonstrated that the colour dipole formalism [4, 5] which also generates the leading logarithmic approximation in $1/x$ provides a clear way of introducing a running coupling. The colour dipole method with fixed coupling is reviewed in chapter 3. Fully incorporating a running coupling into the scattering amplitudes would of course be an enormous task and a full set of next to leading order terms would also have to be evaluated. In this study, the effect of diffusion into the infra-red region will be studied using the renormalon calculus where amplitudes are transformed into the Borel plane. A brief review of the renormalon formalism is presented in chapter 4.

In chapter 5, a Borel transformed expression for the running coupling in momentum space is used to determine Borel space amplitudes in the dipole approach. By formally inverting the Borel transform, the argument of the running coupling in the dipole approach is determined in terms of transverse coordinate variables. An integral equation in Borel space describing how the number of gluons (or dipoles) changes with centre of mass energy is also developed here. Naturally, it is important that the application of the kernel of this equation yields the same results as the BFKL kernel in the fixed coupling limit. This issue is addressed in chapter 6 where the properties of the kernel in Borel space are also studied.

It will be shown that it is possible to model structure functions in terms of dipole scattering cross sections and the approach used in this study is discussed in chapter 7. By convoluting the kernel with an expression for the process $\gamma^* \to q\bar{q}$, where the virtual photon γ^* has virtuality $-Q^2$, the singularity structure of the dipole cascade can be found. Due to the complexity of the integrations which need to be performed, this is carried out numerically.

Having identified the leading singularity in the Borel plane, a possible scheme for estimating the magnitude of the power corrections which emerge when inverting the Borel transform is introduced in chapter 8. The importance of the power correction terms over a range of Q^2 is examined.

Chapter 2

A Review of the Strong Interaction in the Regge Limit

In this chapter, the study of the strong interaction in the high energy limit is reviewed. The first part of this chapter provides a very brief overview of the fundamental results of QCD. A more rigourous and wide ranging treatment of QCD than that which is presented here can be found in a standard text [6]. The Regge limit of the strong interaction is introduced and the nature of hadron-hadron scattering amplitudes in this limit is reviewed in terms of Regge theory. Following the definition of the scaling variable x in section 2.3 the small-x limit of QCD perturbation theory is reviewed and the BFKL equation is introduced. Reasons for implementing a running gauge coupling in the BFKL equation are presented and the difficulty of choosing the appropriate argument with which to run the coupling in order to study low momentum regions in this approach is highlighted. Finally in this review, a link is established between BFKL predictions and the recent experimental low Bjorken-x deep inelastic scattering data from the HERA collider.

2.1 Quantum Chromodynamics and Running α_s

Quantum chromodynamics (QCD) is the non-Abelian gauge theory which describes the strong interaction within the Standard Model of particle interactions. In QCD, the observed particle spectrum of hadrons and mesons are composed of elementary particles called quarks and antiquarks whose interactions are mediated by gluons. All these elementary particles carry colour charge and transform according to representations of the gauge group $SU(3)$. The richness of the particle interactions which occurs within QCD can be traced to the classical Lagrangian density,

$$\mathcal{L}_{QCD} = -\frac{1}{4}F_A^{\mu\nu}F^A_{\mu\nu} + \sum_{flavour} \bar{q}_a(i\not{\partial} - m_f - g_s t^A \not{A}_A)_{ab} q_b \tag{2.1}$$

where

$$F^A_{\mu\nu} = \partial_\mu A^A_\nu - \partial_\nu A^A_\mu - g_s f^{ABC} A^B_\mu A^C_\nu \tag{2.2}$$

Note that as only the classical Lagrangian density has been considered here, gauge fixing and ghost terms have not been included, see [6] for details. In (2.1,2.2) the indices a, b run over the three degrees of freedom of the quarks and the indices A, B, C run over the eight degrees of freedom that the gluons possess. The matrices t^A are the generators of the fundamental representation of $SU(3)$ and f_{ABC} are the structure constants of $SU(3)$. The last term on the right hand side of (2.2) allows self interactions between gluons with the possibility of three or four gluon interaction terms. Using the full Lagrangian of QCD, a set of Feynman rules can be derived to describe the tree level vertices and propagators of the theory [6].

If one wishes to extend the tree level amplitudes which can be calculated directly from these QCD Feynman rules, quantum loop corrections must be inserted into the basic graphs. This process introduces infinities which emerge by performing integrals over internal momenta and these divergences must be removed consistently. Renormalisation of the parameters in the Lagrangian has been developed to treat these divergences. The process of renormalisation is not central to this study and an introduction can be found in Sterman [7]. A feature of renormalisation which is important however, is that renormalisation schemes introduce an arbitrary momentum scale μ into the theory. Using the renormalisation group equations, it can be shown that the effect of changing the momentum scale on a physical observable can be encoded in an effective or running coupling $\tilde{g}_s(g_s, t)$ defined in terms of the renormalised QCD coupling g_s and the scaling variable $t = \frac{1}{2}\ln(Q^2/\mu^2)$ where Q^2 is the momentum scale governing the process under consideration. The running coupling is then found to obey

$$\frac{\partial \tilde{g}_s(g_s, t)}{\partial t} = \beta(\tilde{g}_s(g_s, t)) \quad , \quad \tilde{g}_s(g_s, 0) = g_s \tag{2.3}$$

where the β function relates changes in g_s to changes in μ. The nature of the β function will determine the behaviour of the theory in the asymptotic limit. A study of the β function in QCD [8, 9] showed that QCD is an asymptotically free theory so that the coupling vanishes at large momentum scales. The β function can be approximated by

$$\beta = -\beta_0 \tilde{g}_s^3 + \mathcal{O}(\tilde{g}_s^5) \quad , \quad \beta_0 = \frac{1}{4\pi}\left(\frac{11}{3}N_c - \frac{2}{3}N_f\right) \tag{2.4}$$

where the coefficient β_0 can be determined by evaluating one loop corrections to tree level vertices. Solving (2.3) with this approximation, it is found that the scale dependence of the coupling is

$$\alpha_s(Q^2) = \frac{\alpha_s(\mu^2)}{1 + \beta_0 \alpha_s(\mu^2)\ln(Q^2/\mu^2)} \tag{2.5}$$

where α_s is defined in terms of g_s by

$$\alpha_s = \frac{g_s^2}{4\pi} \tag{2.6}$$

A perturbative expansion in α_s is reliable as long as Q^2 is large, so that $\alpha_s \ll 1$. In this case, Q^2 is termed to be a *hard* momentum scale. In order to quantify what 'large' means, it is useful to introduce a scale Λ_{QCD}, which is the scale at which the coupling in (2.5) formally diverges

$$\alpha_s(Q^2) = \frac{1}{\beta_0 \ln(Q^2/\Lambda_{QCD}^2)} \tag{2.7}$$

Processes with $Q^2 \approx \Lambda_{QCD}^2$ cannot be treated reliably within perturbation theory. Advances have been made in understanding the strong interaction at these low momentum scales using lattice simulations, although this approach is not available to study the scattering processes which will be considered in future chapters.

2.2 Regge Theory

In the early 1960's the great advances in the understanding of the strong interaction which were motivated by the first results from deep inelastic scattering experiments had not yet been made. The experimental data which was available consisted of hadron-hadron scattering events governed by soft momentum scales of the order of the hadron masses. It was impossible for theorists to formulate a quantum field theory of the strong interaction to interpret this kinematic regime. Instead, using a set of general principles derived from constraints placed on the scattering matrix [10], a theoretical framework was developed following initial work on quantum scattering by Regge [11]. The key results of Regge theory are

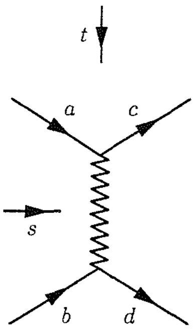

Figure 2.1: Reggeon exchange in 2 → 2 particle scattering

presented here and a more rigourous treatment is provided by Collins [12].

Consider the 2 → 2 particle scattering process $ab \rightarrow cd$, illustrated in fig. 2.1 where s and t are the usual Mandelstam variables. If all the particles have the same mass m, the scattering angle angle for the s-channel process is

$$\cos\theta = 1 + \frac{2t}{s - 4m^2} \tag{2.8}$$

The amplitude of the related t-channel process ($a\bar{c} \rightarrow b\bar{d}$) can be decomposed in terms of a partial wave expansion. This corresponds to the exchange of a series of particles in the t-channel which possess different angular momenta l. Employing the crossing symmetry of Mandelstam variables [10], one finds the s-channel decomposition to be

$$\mathcal{A}(s,t) = \sum_{l=0}^{\infty}(2l+1)a_l(t)\mathrm{P}_l\left(1 + \frac{2s}{t - 4m^2}\right) \tag{2.9}$$

where the transformation $s \leftrightarrow t$ has been made in (2.8). In (2.9), P_l is a Legendre polynomial of degree l and $a_l(t)$ is the partial wave amplitude. An analytic continuation of (2.9) can be performed converting the series into a contour integration over a complex valued l using a Sommerfeld-Watson transform [13, 14]. After some detailed complex analysis, one finds that $\mathcal{A}(s,t)$ contains a series of poles in the complex l-plane whose positions l_i are determined by Regge trajectories $l_i = \alpha_i(t)$.

The objective in this thesis is the study of the Regge limit of the strong interaction which is defined by the inequality $|t| \ll s$. If one makes the assumption that only one dominant or leading Regge trajectory $\alpha(t)$ contributes, the scattering amplitude has the form

$$\mathcal{A}(s,t) \xrightarrow[s\to\infty]{} f(t)s^{\alpha(t)} \tag{2.10}$$

in the Regge limit. The s dependence of (2.10) suggests that one can regard the zig-zag line in fig. 2.1 as the exchange of an object with angular momentum $\alpha(t)$ called a reggeon. Equivalently, it can be regarded as the combined contribution from the t-channel exchange of a family of particles carrying the correct quantum numbers and which satisfy $\alpha(m^2) = j$ where m and j are the masses and spins of these particles respectively. For a particular family of meson states, Chew and Frautschi [15, 16] determined that the reggeon trajectory is linear with an intercept $\alpha_{\mathbb{R}} \sim 0.5$. When these predictions were used to fit data for the differential cross section of a process where the relevant quantum numbers were exchanged, it was found that they provided a good fit to the data.

The total cross section can be related to the amplitude using the optical theorem which in general relates the total cross section for the scattering of a two particle state $|i>$ to the imaginary part of the elastic scattering amplitude $\mathcal{A}_{ii}$. In the Regge limit, the optical theorem takes the form

$$s\sigma_{tot} = \Im\mathrm{m}\mathcal{A}_{ii}(s,0) = \sum_n |\mathcal{A}_{i\to n}|^2 \tag{2.11}$$

It is observed that all data for *total* hadronic cross sections shows a gradual rise at large s. If one retains the intercept of the leading Regge trajectory $\alpha(0)$ only, it can be shown that

$$\sigma_{tot} \propto s^{\alpha(0)-1} \tag{2.12}$$

If $\alpha_{\mathbb{R}}(0)$ were the intercept of the dominant Regge trajectory then (2.12) indicates that the total cross section should vanish in the asymptotic limit, contrary to the observed data. According to the Pomeranchuk theorem [17], a further universal Regge trajectory carrying the quantum numbers of the vacuum and with intercept $\alpha_{\mathbb{P}}(0) > 1$ should be introduced to account for this rise. This Regge trajectory was initially called the pomeron. As the scattering processes in which it participates are governed by soft scales alone, it is now often referred to as the *soft pomeron*. Donnachie and Landshoff [18] have fitted total cross sections for pp and $p\overline{p}$ scattering , using the fit

$$\sigma_{tot} = Xs^{0.08} + Ys^{-0.45} \tag{2.13}$$

where X and Y are fit parameters. One can make the identification $\alpha_{\mathbb{P}}(0) \simeq 1.08$. As can be seen from fig. 2.2, reproduced from [18], the fit agrees over a wide range of centre of mass energies.

It is perhaps not surprising to learn that the soft pomeron is very poorly understood within QCD. Given the low momentum scales governing the processes in which it appears, a perturbative description is not possible. A model motivated by QCD to describe the soft pomeron has been developed by Landshoff and Nachtmann [19] and some of the results from this approach have been successfully tested on the lattice [20]. At the current time however, Regge theory still provides the best method of modelling total hadronic cross sections.

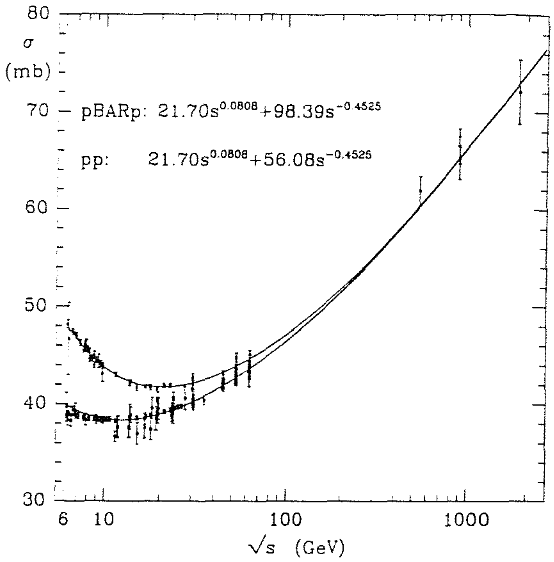

Figure 2.2: Total cross section data for pp and $p\bar{p}$, fitted by (2.13)

2.3 The High Energy Limit of QCD Perturbation Theory

The approximation to the complete QCD perturbation series which is discussed in this section is relevant to hadronic processes where only a very small fraction of the initial large energy of the colliding particles takes part in the hard collision. Such a process will contain two large scales, generically labelled here by q^2 and s, where $q^2 \ll s$. It is useful to define the ratio

$$x = \frac{q^2}{s} \tag{2.14}$$

so that the high energy limit of QCD describes the small-x kinematic regime. Note that $q^2 \gg \Lambda^2_{QCD}$ so that perturbation theory can be applied to analyse this process. The small-x region of perturbation theory is also sometimes called the semihard or Regge region.

The perturbative series for an observable $O(x, q^2)$ takes the form

$$O(x, q^2) = \sum_{n=0} \alpha_s^n \sum_{m=0}^{n} \ln^m \left(\frac{1}{x}\right) c_{nm} \tag{2.15}$$

At each order in perturbation theory, the small coupling α_s is accompanied by a large logarithm in $(1/x)$ and so all orders of the perturbation series contain a contribution of the form $(\alpha_s \ln(1/x))^n \sim 1$. The result of this is that the perturbation series cannot be truncated reliably at finite order. The leading logarithmic approximation in $1/x$ (LLA $(1/x)$) approximates the full perturbation series by retaining the dominant term at each order only,

$$O(x, q^2)_{LLA\ (1/x)} = \sum_{n=0} \alpha_s^n \ln^n \left(\frac{1}{x}\right) c_{nn} \tag{2.16}$$

Terms of the form $\alpha_s^n \ln(1/x)^m$ with $n > m$ which are formally non-leading are neglected in this approximation. It should also be noted that depending on the process being considered, the momentum dependent coefficients c_{nm} may contain large logarithms in q^2 at all orders in perturbation theory. In this discussion, it is assumed that these logarithms are dominated by the leading terms in $\ln(1/x)$ at each order and are therefore neglected. Away from the small-x region, the QCD perturbation series may be dominated by such large logarithmic momentum terms and this kinematic regime is treated by the DGLAP equation [21, 22, 23, 24].

In order to make predictions using the LLA $(1/x)$ approach it is necessary to resum the leading terms to all orders in perturbation theory. In the case of colour singlet exchange, the LLA $(1/x)$ resummation results in the BFKL equation. At lowest order, colour singlet exchange is obtained by the exchange of two gluons in the t-channel. The BFKL equation resums all the radiative corrections to the Born level contribution within LLA $(1/x)$. In analogy to colour singlet exchange in Regge theory, the amplitude for colour singlet scattering derived from the

LLA $(1/x)$ is called the BFKL or hard pomeron.

2.4 The BFKL Equation

In this section, results which arise from the conventional t-channel approach to generating the leading logarithmic $(1/x)$ corrections will be quoted without proof. It is important to understand that the results presented here can be derived from perturbative QCD and therefore are based on modern quantum field theoretical methods. The LLA $(1/x)$ resummation was first developed by Balitsky, Fadin, Kuraev and Lipatov [2, 25] (hence BFKL). A recent detailed review which constructs the BFKL pomeron from first principles is presented in [26]. The original BFKL evolution equation was constructed at fixed α_s and α_s remains frozen in this section also.

Using the optical theorem (2.11), the imaginary part of the BFKL pomeron amplitude at zero momentum transfer can be related to the elastic scattering amplitude for 2 quarks → 2 quarks + n gluons with no net colour exchange in the t-channel. The evolution of the amplitude in rapidity $(= \ln(1/x))$ is independent of the particles which are scattered and quark scattering has been chosen here without loss of generality. It should be noted however, that the scale which the coupling α_s is chosen to take is determined by a hard momentum scale coming from the scattered particle.

Retaining leading logarithmic $(1/x)$ terms only (where $x = \boldsymbol{k}^2/s$, with k^2 being a typical gluon transverse momentum, see (2.19)), it can be shown that the imaginary part of the pomeron amplitude is a ladder like configuration of gluons, illustrated in fig. 2.3. Assuming the limit of massless quarks, in the quark-quark

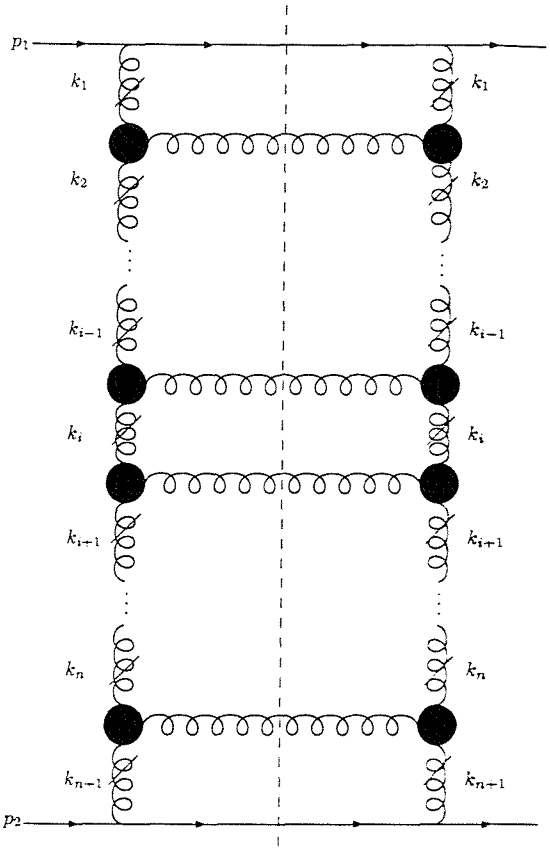

Figure 2.3: n gluon contribution to the imaginary part of the BFKL pomeron amplitude. The dashed line represents the unitarity cut implicit in (2.11)

centre of mass frame where the incoming quarks are aligned with the z axis,

$$\begin{aligned} p_1^\mu &= \frac{\sqrt{s}}{2}(1,\mathbf{0},1) \\ p_2^\mu &= \frac{\sqrt{s}}{2}(1,\mathbf{0},-1) \end{aligned} \tag{2.17}$$

where the two dimensional second coordinate represents the plane transverse to incoming quarks. It is also convenient to write the momentum of the vertical gluons in the ladder in terms of Sudakov parameters,

$$k_i^\mu = \alpha_i p_1^\mu + \beta_i p_2^\mu + k_{i\perp}^\mu \tag{2.18}$$

$k^{\mu}_{i\perp}$ is the momentum transverse to the incoming quarks and is denoted by $\boldsymbol{k}_i$. In the LLA $(1/x)$, the Sudakov parameters and transverse momenta obey the inequalities

$$\begin{aligned}
1 &\gg \alpha_1 \gg \alpha_2 \gg \cdots \gg \alpha_{n+1} \\
1 &\gg |\beta_{n+1}| \gg |\beta_n| \gg \cdots \gg |\beta_2| \gg |\beta_1| \\
\boldsymbol{k}_1^2 &\simeq \boldsymbol{k}_2^2 \simeq \cdots \simeq \boldsymbol{k}_{n+1}^2 \simeq \boldsymbol{k}^2 \qquad (2.19)
\end{aligned}$$

where $\boldsymbol{k}^2$ in the last set of approximate equalities denotes a typical transverse momentum scale in the ladder. The longitudinal momentum components are strongly ordered going down or up the ladder. There is no strong ordering of the transverse momenta in the ladder which is a very important property of the gluon ladder in LLA $(1/x)$ and this will be discussed in more detail in section 2.4.2.

The ladder of fig. 2.3 does not have a straightforward interpretation in terms of Feynman diagrams but instead should be viewed as a schematic representation of the large number of diagrams which contribute to the leading logarithmic amplitude. More specifically, the black blob between the vertical lines with momenta k_i and k_{i+1} in fig. 2.3 is not an ordinary triple gluon vertex but an effective vertex which encodes all the ways of adding a gluon with momentum $k_i - k_{i+1}$ to the ladder within the LLA $(1/x)$. The virtual contributions to the amplitude due to loop effects can be treated by reggeising all the vertical gluon lines (reggeised gluons are graphically represented by a gluon with a bar). In analogy to the reggeised particles discussed in section 2.2, the propagator of the i^{th} reggeised gluon is enhanced by a factor of

$$\left(\frac{s_i}{\boldsymbol{k}^2}\right)^{\alpha_G(\boldsymbol{k}_i^2)-1} \qquad (2.20)$$

over a normal gluon where s_i is the centre of mass energy in the i^{th} section of the ladder and $\alpha_G(t)$ can be thought of as the gluon Regge trajectory, where $\alpha_G(0) = 1$, indicating that the massless gluon of spin one lies on the trajectory. More details of effective vertices and the reggeised gluon can be found in [26, 27] and references therein.

The full amplitude for 2 quark → 2 quark scattering at zero momentum transfer $\mathcal{A}(s, 0)$ can be found by summing the contributions from the $2 \to 2+n$ amplitudes for $0 \leq n < \infty$. Before discussing the integral equation which embodies the resummation, the universal BFKL pomeron amplitude $F(x, \boldsymbol{k}_1, \boldsymbol{k}_2)$ is defined from $\mathcal{A}(s, 0)$ by

$$\frac{\mathcal{A}(s,0)}{s} = \frac{\mathcal{C}}{(2\pi)^4} \int \frac{\mathrm{d}^2\boldsymbol{k}_1}{k_1^2} \frac{\mathrm{d}^2\boldsymbol{k}_2}{k_2^2} \Phi_1(\boldsymbol{k}_1)\Phi_2(\boldsymbol{k}_2) F(x, \boldsymbol{k}_1, \boldsymbol{k}_2) \tag{2.21}$$

where $\mathcal{C} = C_F/2N_C$ is the colour factor and Φ_1, Φ_2 are known as impact factors which describe the way in which the BFKL pomeron couples to the the scattered particles. The parameterisation of the amplitude in (2.21) as a convolution of the pomeron amplitude and impact factors is used when the elastic scattering of hadrons is considered later. It should be noted that the parameterisation of the full elastic scattering amplitude is not uniquely defined by (2.21) as the BFKL amplitude F can be written as a convolution of two BFKL amplitudes, some of which may be absorbed into the definition of the impact factors

$$F(x, \boldsymbol{k}_1, \boldsymbol{k}_2) = \int \mathrm{d}^2\hat{\boldsymbol{k}} F(\hat{x}, \boldsymbol{k}_1, \hat{\boldsymbol{k}}) F(x/\hat{x}, \hat{\boldsymbol{k}}, \boldsymbol{k}_2) \tag{2.22}$$

where $\hat{x} = \boldsymbol{k}^2/\hat{s}$ and for any $\hat{s} < s$. In the dipole approach which is reviewed in chapter 3, the partitioning of the scattering amplitude will be treated differently.

The BFKL equation is the integral equation which describes how the BFKL pomeron $F(x, \boldsymbol{k}_1, \boldsymbol{k}_2)$ evolves in $\ln(1/x)$. For zero momentum transfer, the BFKL equation can be written as

$$F(x,\boldsymbol{k}_1,\boldsymbol{k}_2)=\frac{\delta^2(\boldsymbol{k}_1-\boldsymbol{k}_2)}{\boldsymbol{k}_1^2\boldsymbol{k}_2^2}+\int_x^1\frac{\mathrm{d}x'}{x'}\int \mathrm{d}^2\boldsymbol{k}'\mathcal{K}_{BFKL}(\boldsymbol{k}_1,\boldsymbol{k}')F(x',\boldsymbol{k}',\boldsymbol{k}_2) \tag{2.23}$$

with

$$\int \mathrm{d}^2\boldsymbol{k}'\mathcal{K}_{BFKL}(\boldsymbol{k}_1,\boldsymbol{k}')F(x',\boldsymbol{k}',\boldsymbol{k}_2)$$

$$=\frac{N_c\alpha_s}{\pi^2}\int\frac{\mathrm{d}^2\boldsymbol{k}'}{(\boldsymbol{k}_1-\boldsymbol{k}')^2}\left\{F(x',\boldsymbol{k}',\boldsymbol{k}_2)-\frac{\boldsymbol{k}_1^2}{\boldsymbol{k}'^2+(\boldsymbol{k}_1-\boldsymbol{k}')^2}F(x',\boldsymbol{k}_1,\boldsymbol{k}_2)\right\} \tag{2.24}$$

The first term in the BFKL kernel $\mathcal{K}_{BFKL}$ encodes the emission of a new gluon rung which couples to the vertical section of the ladder via an effective vertex and corresponds to a real gluon correction. The second term is related to the reggeisation of the t-channel gluons in the vertical sides of the ladder and corresponds to the treatment of virtual gluon corrections. The BFKL kernel is infra-red finite. This can be seen by noting that the kernel vanishes when $\boldsymbol{k}'=\boldsymbol{k}_1$ so that there is a cancellation of real and virtual gluon singularities. Viewing the BFKL equation as a Bethe-Salpeter equation, it is possible to generate the ladder structure of fig. 2.3 by an iterative technique. A diagrammatic representation of (2.23) is illustrated in fig. 2.4. The BFKL equation may also be expressed in integro-differential form

$$\frac{\partial F(x,\boldsymbol{k}_1,\boldsymbol{k}_2)}{\partial\ln(1/x)}=\int \mathrm{d}^2\boldsymbol{k}'\mathcal{K}_{BFKL}(\boldsymbol{k}_1,\boldsymbol{k}')F(x,\boldsymbol{k}',\boldsymbol{k}_2) \tag{2.25}$$

Often the BFKL equation is written in terms of the rapidity variable $Y=\ln(1/x)$ for clarity and thus describes the evolution of the pomeron amplitude $F(y=\ln(1/x),\boldsymbol{k}_1,\boldsymbol{k}_2)$ with increasing rapidity.

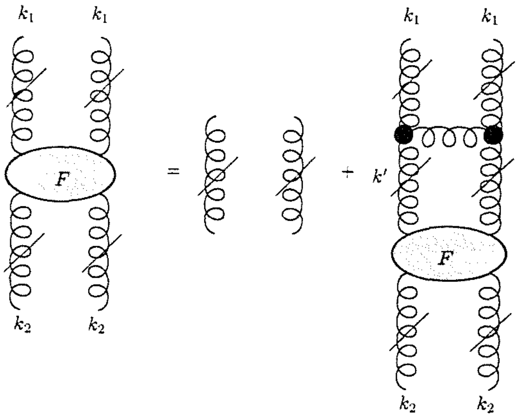

Figure 2.4: Schematic representation of the BFKL integral equation for the pomeron amplitude F.

2.4.1 Approximate Solution of the BFKL Equation

The solution of the BFKL equation at zero momentum transfer was developed in [1, 2, 28]. The integral equation is solved by using eigenvalue techniques. Eigenfunctions of the kernel $\phi_\nu(\boldsymbol{k})$ behave like a power of $k^{2\nu}$ and are used to define the BFKL spectral function $\chi(\nu)$

$$\mathcal{K}_{BFKL} \otimes \phi_\nu(\boldsymbol{k}) = \frac{\alpha_s N_C}{\pi} \chi^{(0)}(\nu) \phi_\nu(\boldsymbol{k}) \tag{2.26}$$

and $\chi^{(0)}(\nu)$ is the BFKL spectral function which has the leading order expansion

$$\chi^{(0)}(\nu) = 2\psi(1) - \psi(1-\nu) - \psi(\nu) \tag{2.27}$$

where ψ is the logarithmic derivative of the Euler gamma function. As χ will be used again in the running coupling case, the index 0 has been applied to the BFKL spectral function to denote that this term corresponds to the fixed coupling limit. Retaining only terms which are consistent with the leading logarithmic

$(1/x)$ limit, the solution for the amplitude F is found to be

$$F(x, \boldsymbol{k}_1, \boldsymbol{k}_2) = \frac{1}{2\pi} \frac{1}{\sqrt{\boldsymbol{k}_1^2 \boldsymbol{k}_2^2}} \frac{x^{-\omega_L}}{\sqrt{C\pi \ln(1/x)}} \exp\left(-\frac{\ln^2(\boldsymbol{k}_1^2/\boldsymbol{k}_2^2)}{4C\ln(1/x)}\right) \tag{2.28}$$

where

$$\omega_L = \frac{4\alpha_s N_C}{\pi} \ln 2 \tag{2.29}$$

$$C = \frac{14\alpha_s N_C}{\pi} \zeta(3) \tag{2.30}$$

where ζ is the Riemann zeta function. The leading order solution exhibits an x dependence which invites comparisons with Regge theory. Recalling that $x = \boldsymbol{k}^2/s$ and using (2.21) the leading behaviour for the amplitude of a scattering process $\mathcal{A}(s, 0)$ in which a BFKL pomeron is exchanged is

$$\mathcal{A}(s, 0) \simeq \frac{s^{1+\omega_L}}{\sqrt{\ln s}} \tag{2.31}$$

A much stronger s dependence emerges from the perturbative treatment of the Regge limit than is observed at low momentum scales, where it was observed that $\alpha_{\mathbb{P}} \simeq 1.08$. For example, if the coupling is evaluated at $10GeV^2$, $1 + \omega_L \simeq 0.5$. The presence of the $\sqrt{\ln s}$ indicates that the leading BFKL singularity is a branch cut in angular momentum space, not an isolated pole like the soft pomeron. The reason for this can be traced to the fact that a fixed coupling has been used. Lipatov [28] has pointed out that the inclusion of a running coupling will transform the branch cut into an isolated pole.

2.4.2 Running the Coupling in the BFKL Equation

It has been stated that the BFKL equation does not possess any infra-red singularities and also that the scale used to determine α_s is set by the impact factors which are convoluted with the BFKL pomeron. The inclusion of a running coupling is formally outside the scope of the leading logarithmic $(1/x)$ approximation also. Why then should one include a running coupling in the BFKL equation ? It can be shown that the solution of the BFKL equation (2.28) allows for diffusion in transverse momenta away from the ends of the ladder, see [26]. The logarithm of the transverse momentum at some intermediate vertical section of the ladder, $\ln \boldsymbol{k}'^2$ is normally distributed with mean

$$\ln\left(\sqrt{\boldsymbol{k}_1^2\boldsymbol{k}_2^2}\right) + \ln\left(\frac{\boldsymbol{k}_1^2}{\boldsymbol{k}_2^2}\right)\left(2 - \frac{Y'}{Y}\right) \tag{2.32}$$

and variance

$$\frac{28\alpha_s N_C \zeta(3)}{\pi} Y' \left(1 - \frac{Y'}{Y}\right) \tag{2.33}$$

where $Y' \leq Y$ represents the rapidity at this point on the ladder. Therefore at any point of the ladder, there is a probability that arbitrarily large or small transverse momenta appear in the loop integrals. This means that non-perturbative physics which arises from the region of small momenta cannot be cleanly factorised from the perturbative region. The situation for BFKL evolution is therefore in marked contrast to DGLAP evolution where the ladder structure obtained from retaining leading logarithmic terms in momenta shows strong ordering in transverse momentum. In the DGLAP regime, the non-perturbative physics can be completely separated from the perturbative using factorisation theorems [29]. A study of the non-perturbative corrections to the BFKL amplitude is the subject will be presented in chapters 5-8.

As the diffusion in transverse momentum along the ladder means that a wider range of transverse momenta contributes to the BFKL amplitude, the amplitude is indeed sensitive to the argument of the running coupling at each rung of the ladder. One may now ask with which momentum scale should the coupling run in the BFKL equation (2.25); $\alpha_s(\boldsymbol{k}_1)$ or $\alpha_s(\boldsymbol{k}')$? It makes little difference whether the argument of the coupling at a particular rung is set equal to the transverse momentum above or below that rung provided that both $\alpha_s(\boldsymbol{k})$ and $\alpha_s(\boldsymbol{k}')$ are small. In terms of the integral equation this means that one has the freedom to set the argument of the coupling equal to the external (unintegrated) value, $\boldsymbol{k}_1$, rather than the integrated one $\boldsymbol{k}'$. The reason for this is that although far enough along the ladder transverse momenta whose magnitude differs substantially from the value set by the impact factors may be found. the transverse momenta of two adjacent sections of the ladder are indeed of the same order. As far as perturbation theory is concerned, therefore, a discussion about which transverse momentum should be used in the running of the coupling will only affect the solutions to the BFKL equation at the sub-leading logarithm level.

However, if one wishes to consider in more detail the infrared contributions to the BFKL amplitude and run the coupling down to scales comparable to Λ_{QCD}, where small changes in the argument lead to substantial changes in the value of the coupling, one no longer has the above freedom and a study of the precise prescription for running the coupling becomes pertinent. Such a precise prescription is necessary for an analysis of the renormalon structure of the BFKL amplitude aimed at identifying non-perturbative power corrections to the amplitude. Levin [30] has conjectured that the correct prescription for the coupling is

$$\frac{\alpha_s(\boldsymbol{k}'^2)\,\alpha_s((\boldsymbol{k}_1-\boldsymbol{k}')^2)}{\alpha_s(\boldsymbol{k}_1)} \tag{2.34}$$

His analysis, however, was based on the idea of considering the running of the coupling at one rung of the ladder only, whilst keeping the coupling fixed throughout the rest of the ladder. A systematic treatment requires a prescription which can be extended to the entire ladder. The colour dipole method will provide a framework in which to introduce the running coupling systematically.

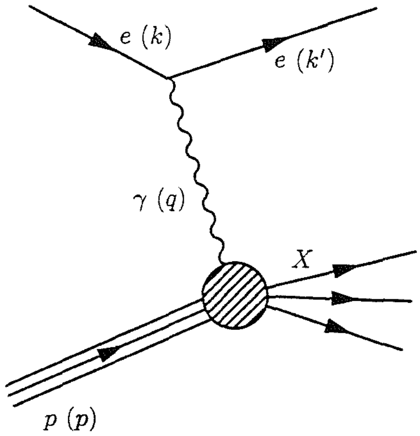

Figure 2.5: Deep inelastic *ep* scattering mediated by a virtual photon.

2.5 Deep Inelastic Scattering at Small-x

A brief review of deep inelastic electron proton scattering (DIS) in the small-x regime is given here. A more rigourous and wide ranging discussion of DIS can be found in [31] which also treats the DGLAP approach to DIS not considered here. A generic electron-proton scattering process is shown in fig. 2.5. The four momenta of the particles taking place in the scattering are shown in parentheses. In order to describe the scattering cross section, the following kinematic invariants are defined

$$\begin{aligned} Q^2 &= -q^2 > 0 \\ W^2 &= (p+q)^2 \\ y &= \frac{p\cdot q}{p\cdot k} \\ x &= \frac{Q^2}{2p\cdot q} \end{aligned} \tag{2.35}$$

For convenience, the positive invariant Q^2 has been defined to describe the space-like momentum of the virtual photon. The centre of mass energy of the photon-proton system is given by W and y expresses the fraction of the incoming electron energy which the photon carries in the proton rest frame. For deep inelastic scattering in the high energy limit the following inequalities apply

$$W^2 \gg Q^2 \gg m_p^2 \tag{2.36}$$

Neglecting the masses of the external particles in this limit, the Bjorken-x variable can be approximated by

$$x \simeq \frac{Q^2}{W^2} \Rightarrow x \ll 1 \tag{2.37}$$

The presence of the large momentum scale Q^2 allows a perturbative approach to be used. The hadronic contribution to the differential *ep* cross section can be written in terms of two structure functions F_2 and F_L. Using symmetry and Lorentz invariance arguments, it can be shown that

$$\frac{\mathrm{d}^2\sigma}{\mathrm{d}x\mathrm{Q}^2} = \frac{2\pi\alpha_{em}^2}{xQ^4}\left(\left[1+(1-y)^2\right]F_2(x,Q^2) - y^2F_L(x,Q^2)\right) \tag{2.38}$$

Generally, a third structure function F_3 is also present which describes weak vector boson exchange. In the small x limit however, this third structure function will not enter as $Q^2 \ll m_Z^2$. The structure functions F_2 and F_L can be written in a form more amenable to calculation by expressing them in terms of σ_T and σ_L, the cross sections for scattering with transverse and longitudinal virtual photons respectively.

$$\begin{aligned} F_2(x,Q^2) &= \frac{Q^2}{4\pi^2\alpha_{em}}\left\{\sigma_L(x,Q^2) + \sigma_T(x,Q^2)\right\} \\ F_L(x,Q^2) &= \frac{Q^2}{4\pi^2\alpha_{em}}\sigma_L(x,Q^2) \end{aligned} \tag{2.39}$$

The cross sections σ_T and σ_L can be calculated using the optical theorem by considering the imaginary part of the amplitude for elastic photon-proton scattering. Using (2.21), the cross section σ_T can be written as

$$\sigma_T(x, Q^2) = \frac{\mathcal{C}}{(2\pi)^4} \int \frac{\mathrm{d}^2\boldsymbol{k}_1^2}{\boldsymbol{k}_1^2} \frac{\mathrm{d}\boldsymbol{k}_2^2}{\boldsymbol{k}_2^2} \Phi_T(\boldsymbol{k}_1)\Phi_p(\boldsymbol{k}_2)F(x, \boldsymbol{k}_1, \boldsymbol{k}_2) \tag{2.40}$$

where Φ_T is the impact factor for the transversely polarised photon and Φ_p is the impact factor for the proton (similarly for σ_L). In (2.40), the BFKL amplitude $F(x, \boldsymbol{k}_1, \boldsymbol{k}_2)$ contains the full x dependence of σ_T. According to (2.28) the cross sections σ_T and σ_L and hence from (2.39) the structure function F_2 has a theoretical x dependence

$$F_2(x, Q^2) \propto \frac{x^{-\omega_L}}{\sqrt{\ln(1/x)}} \tag{2.41}$$

Results reported by the ZEUS group at HERA for their 1994 data [32] at low x and for a range of Q^2 are shown in fig. 2.6 which have been reproduced from [32]. The data exhibited in fig. 2.6 shows that there is a rapid rise in F_2 with decreasing x. At $Q^2 = 10GeV^2$, it is found that the rise is proportional to $x^{-0.33}$. This rise cannot be explained in terms of soft pomeron exchange. On the other hand, the prediction from strict LLA $(1/x)$ BFKL theory predicts a rise which is also too fast, proportional to $x^{-0.5}$.

In this chapter, the major tools used to study QCD in the high energy limit have been introduced and results from recent deep inelastic scattering experiments have been briefly discussed. An argument has been provided indicating why a running QCD coupling should be used in the LLA $(1/x)$ approach. In this study, the running coupling will be implemented in the QCD dipole approach which is discussed in the next chapter.

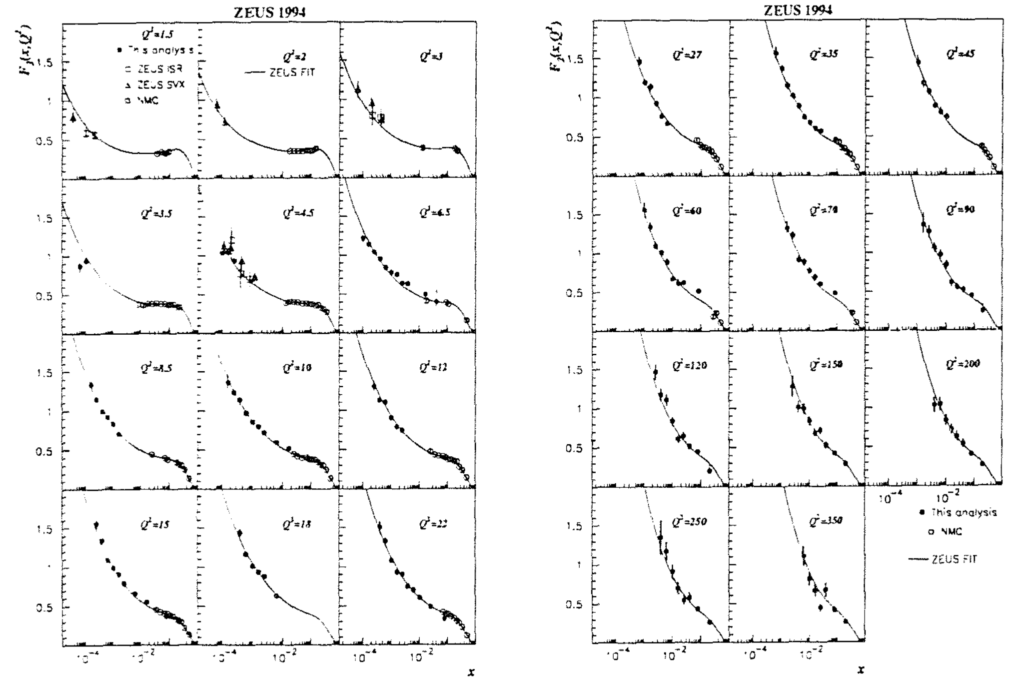

Figure 2.6: Structure function F_2 as a function of x for fixed values of Q^2 measured in GeV^2

Chapter 3

The QCD Dipole Picture of Small-x Processes

In this chapter the colour dipole description of small-x processes will be reviewed. Introduced independently by Mueller [4] and Nikolaev and Zakharov [5], the dipole approach formulates small-x scattering processes in terms of sequential emission of colour dipoles in the s-channel from a quark-antiquark bound state called an *onium*. Using an impact parameter representation, it shall be demonstrated that the pattern of gluon radiation from the onium in the small-x limit admits a simple probabilistic interpretation. An integral equation which describes the change in the number of dipoles with increasing rapidity will be discussed and it will be shown that the solution to this equation is the same as the BFKL equation discussed in Chapter 2. Although the formulations of Mueller and Nikolaev and Zakharov are equivalent, the approach taken for most of this chapter is closest to Mueller and the reader is referred to [3, 4, 33, 34] for more details.

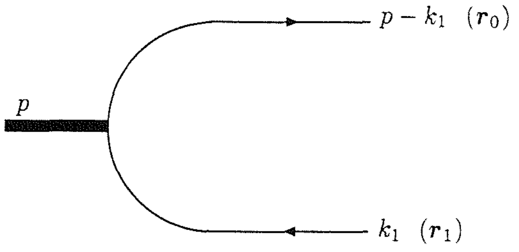

Figure 3.1: $q\bar{q}$ state with no gluon emission

3.1 Development of the Dipole Kernel

The first step in the development of the dipole integral equation is to understand the structure of an onium state in the high energy limit. For the purposes of this discussion, it is assumed that the mass of the onium is large relative to Λ_{QCD} in order that perturbation theory is applicable. Consider an onium with four-momentum p, composed of an antiquark and a quark with four-momenta k_1 and $p - k_1$ respectively. The lowest order configuration is where no gluons have been emitted and is illustrated in fig. 3.1. The light-cone wavefunction for this state $\Psi^{(0)}(\boldsymbol{k}_1, z_1)$ is written in terms of the antiquark's transverse momentum $\boldsymbol{k}_1$ and z_1 which is the longitudinal momentum fraction of the antiquark relative to the onium. For reasons of clarity, the spinor indices have been dropped throughout this chapter. It is also necessary to introduce the transverse coordinate representation of the wavefunction which is determined by means of a Fourier transform

$$\Psi^{(0)}(\boldsymbol{r}_{10}, z_1) = \int \frac{\mathrm{d}^2\boldsymbol{k}_1}{(2\pi)^2} e^{i\boldsymbol{k}_1\cdot\boldsymbol{r}_{10}} \Psi^{(0)}(\boldsymbol{k}_1, z_1) \tag{3.1}$$

The quark and antiquark possess transverse coordinates $\boldsymbol{r}_0$ and $\boldsymbol{r}_1$ respectively. In this derivation, it can be assumed that the quark has transverse coordinate $\boldsymbol{r}_0 = \boldsymbol{0}$. In this study, the conventions $\boldsymbol{r}_{ij} \equiv \boldsymbol{r}_i - \boldsymbol{r}_j$ and $r_{ij}^2 \equiv \boldsymbol{r}_{ij}^2$ are followed.

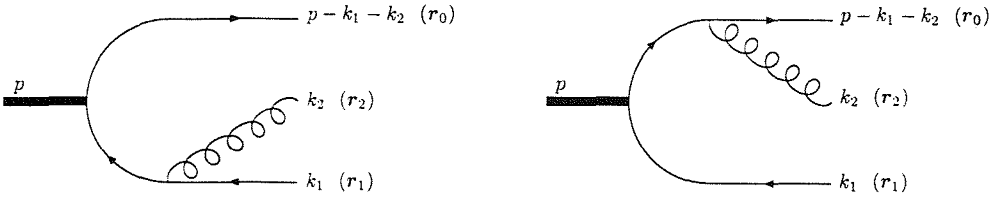

(a) Emission of soft gluon from antiquark line

(b) Emission of soft gluon from quark line

Figure 3.2: Emission of a soft gluon with transverse momentum $\boldsymbol{k}_2$ (impact parameter $\boldsymbol{r}_2$) from a dipole with momentum p, in which the antiquark has transverse momentum $\boldsymbol{k}_1$ (impact parameter $\boldsymbol{r}_1$).

The square wavefunction $\Phi^{(0)}(\boldsymbol{r}_{10}, z_1)$ is defined in the usual manner by

$$\Phi^{(0)}(\boldsymbol{r}_{10}, z_1) = \sum |\Psi^{(0)}(\boldsymbol{r}_{10}, z_1)|^2 \tag{3.2}$$

where the sum is over spinor indices. $\Phi^{(0)}(\boldsymbol{r}_{10}, z_1)$ represents the probability of an onium state of transverse size $\boldsymbol{r}_{10}$ with no gluon emission, where the antiquark possesses longitudinal momentum fraction z_1 and $\Phi(\boldsymbol{r}_{10}, z_1)$ is normalised such that

$$\int \mathrm{d}^2\boldsymbol{r}_{10} \int_0^1 \mathrm{d}z_1 \Phi^{(0)}(\boldsymbol{r}_{10}, z_1) = 1 \tag{3.3}$$

The first order correction to this onium state due to the emission of a real gluon can arise in two ways as illustrated in fig. 3.2, where a gluon with transverse momentum $\boldsymbol{k}_2$ and impact parameter $\boldsymbol{r}_2$ is emitted from either the antiquark or quark. The contribution of virtual gluons will be treated in section 3.3. In order to generate the leading logarithmic terms in the perturbative expansion it is sufficient to consider the contribution from soft gluons only. The gluon emitted in fig. 3.2 is soft if the longitudinal momentum fraction z_2 of the gluon relative to the onium satisfies the inequalities

$$\frac{z_2}{z_1} \ll 1 \qquad \frac{z_2}{1-z_1} \ll 1. \tag{3.4}$$

Note that in this chapter, the 'small-x' limit has become the 'small-z' limit due to the widely held convention of describing longitudinal momentum fractions in this approach by z. By considering soft gluon emissions only, in light cone gauge, Mueller [4] determines that the amplitude for one gluon emission is

$$\Psi^{(1)a}(\boldsymbol{k}_1, \boldsymbol{k}_2, z_1, z_2) = 2g_s t^a \left[\Psi^{(0)}(\boldsymbol{k}_1 + \boldsymbol{k}_2, z_1) - \Psi^{(0)}(\boldsymbol{k}_1, z_1)\right] \frac{\boldsymbol{k}_2 \cdot \epsilon}{\boldsymbol{k}_2^2} \tag{3.5}$$

where ϵ is the polarisation vector of the gluon. In order to simplify this expression, the impact parameter representation is introduced by performing Fourier transforms on all momentum variables,

$$\Psi^{(1)a}(\boldsymbol{r}_{10}, \boldsymbol{r}_{20}, z_1, z_2) = \int \frac{\mathrm{d}^2\boldsymbol{k}_1}{2\pi} \frac{\mathrm{d}^2\boldsymbol{k}_2}{2\pi} e^{i\boldsymbol{k}_1 \cdot \boldsymbol{r}_{10}} e^{i\boldsymbol{k}_2 \cdot \boldsymbol{r}_{20}} \Psi^{(1)a}(\boldsymbol{k}_1, \boldsymbol{k}_2, z_1, z_2) \tag{3.6}$$

so that inserting (3.5),

$$\Psi^{(1)a}(\boldsymbol{r}_{10}, \boldsymbol{r}_{20}, z_1, z_2) = \frac{i}{2\pi} g_s t^a \Psi^{(0)}(\boldsymbol{r}_{10}, z_1) \left(\frac{\boldsymbol{r}_{21}}{r_{21}^2} - \frac{\boldsymbol{r}_{20}}{r_{20}^2}\right) \cdot \epsilon \tag{3.7}$$

The square of the wavefunction is found by integrating over the phase space of the emitted gluon and summing over all colours, polarisations and spinor labels

$$\Phi^{(1)}(\boldsymbol{r}_{10}, z_1) = \int \frac{\mathrm{d}^2\boldsymbol{r}_{20}}{2\pi} \int^{z_1} \frac{\mathrm{d}z_2}{z_2} \sum |\Psi^{(1)a}(\boldsymbol{r}_{10}, \boldsymbol{r}_{20}, z_1, z_2)|^2. \tag{3.8}$$

If the transverse part of the gluon polarisation vector ϵ in (3.7) is assumed to be

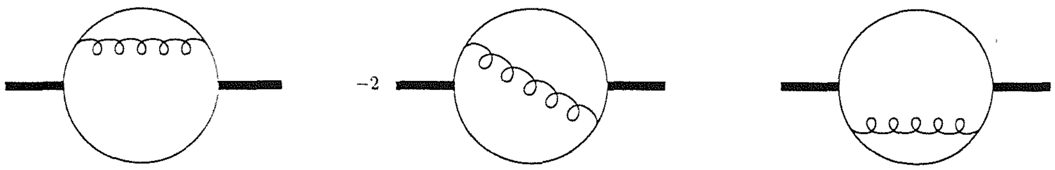

Figure 3.3: Diagrams contributing to $\Phi^{(1)}(\boldsymbol{r}_{10}, z_1)$

real, then $\Phi^{(1)}(\boldsymbol{r}_{10}, z_1)$ can be written as

$$\Phi^{(1)}(\boldsymbol{r}_{10}, z_1) = \int \mathrm{d}^2\boldsymbol{r}_{20} \int^{z_1} \frac{\mathrm{d}z_2}{z_2} \frac{\alpha_s C_F}{\pi^2} \left(\frac{1}{r_{21}^2} - 2\frac{\boldsymbol{r}_{21} \cdot \boldsymbol{r}_{20}}{r_{21}^2 r_{20}^2} + \frac{1}{r_{20}^2} \right)$$

$$\times\, \Phi^{(0)}(\boldsymbol{r}_{10}, z_1) \qquad (3.9)$$

Note that the integral over $\boldsymbol{r}_{20}$ in (3.9) is ultra-violet divergent. This divergence will be treated more carefully in section 3.3. The origin of the three terms in the integrand of (3.9) is illustrated in fig. 3.3 . At this stage, it may be necessary to point out the advantage of using the impact parameter space representation. The time scale over which the soft gluon is emitted is much smaller than the time scales governing harder particles participating in the process and the soft gluon is therefore emitted independently of the quark and antiquark. One can think of the transverse coordinates of the quark and antiquark as being frozen during the emission of the soft gluon. The expression for $\Psi(\boldsymbol{k}_1, \boldsymbol{k}_2, z_1, z_2)$ in (3.5) depends on two initial wavefunctions $\Psi^{(0)}(\boldsymbol{k}_1, z_1)$ and $\Psi^{(0)}(\boldsymbol{k}_1 + \boldsymbol{k}_2, z_1)$ whereas the wavefunction $\Psi^{(1)}(\boldsymbol{r}_{10}, z_1)$ depends only on one initial onium configuration. Treatment of subsequent gluon emissions will therefore be simpler because of this reduction in the number of different states which must be considered.

The analysis is continued to the emission of a second soft gluon with longitudinal momentum fraction $z_3 \ll z_2$. Although it is possible to treat these higher order corrections to the onium wavefunction exactly, the process is simplified by invoking the large N_C limit [35]. In this limit, the colour structure of a gluon can be represented by a quark-antiquark pair signifying colour-anticolour structure. This step is not an approximation but arises from the SU(N_C) group product

$$\boldsymbol{N_C} \otimes \boldsymbol{N_C} \rightarrow \boldsymbol{N_C^2} - \mathbf{1} \oplus \mathbf{1} \tag{3.10}$$

The dynamical contribution of gluon emission from a quark is approximately equivalent to gluon emission from another gluon in the limit where the emitted particle is much softer than its parent which is the regime under consideration here. Using these facts, one can conclude that it is possible to treat the emission of a further soft gluon from an existing gluon or the original quark-antiquark pair in a similar manner. Effectively, an onium state of transverse size r_{10} having emitted a soft gluon with transverse position $\boldsymbol{r}_2$ can be viewed as two colour dipoles, with transverse sizes r_{20} and r_{21} (that is the first dipole consists of the original quark and the antiquark 'part' of the gluon at $\boldsymbol{r}_2$ and the second consists of the original antiquark and the quark 'part' of the gluon at r_2). The process of real soft gluon emission is a simple branching process where the parent dipole branches into two dipoles which have sizes determined by the position of the emitted soft gluon.

In constructing the expression for the squared wavefunction for two gluon emission $\Phi^{(2)}(\boldsymbol{r}_{10}, z_1)$, only terms which are leading in powers of N_C are retained. Leading order diagrams must not have any crossed internal lines and as such are termed *planar* diagrams. Examples of leading order diagrams in the case where the second soft gluon is emitted from the original quark or antiquark part of the first emitted gluon are illustrated in fig. 3.4(a) along with a non-leading diagram shown in fig. 3.4(b) which is neglected in the determination of $\Phi^{(2)}$. The double lines in the graphs represent the emitted gluons in the large N_C limit. All leading contributions to $\Phi^{(2)}$ consist of the second soft gluon being emitted by either

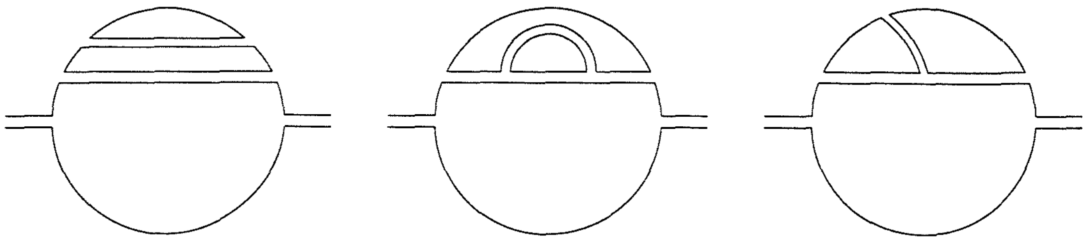

(a) Contributions to $\Phi^{(2)}$ where the second gluon is emitted from the original quark or anti-quark part of gluon 1 and is reabsorbed by this same dipole

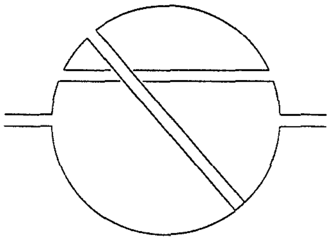

(b) A non-planar second order graph where the second gluon is emitted by one dipole and is reabsorbed by the other dipole

Figure 3.4: Examples of leading and non-leading N_C diagrams at 2nd order

of the colour dipoles and then being reabsorbed by that same dipole again. At leading order, there is no interference between different dipoles. This structure can be observed if the expression for $\Phi^{(2)}$ is examined

$$\Phi^{(2)}(\boldsymbol{r}_{10}, z_1) = \Phi^{(0)}(\boldsymbol{r}_{10}, z_1)\frac{\alpha_s N_c}{2\pi^2}\int_{z_0}^{z_1}\frac{\mathrm{d}z_2}{z_2}\int \mathrm{d}^2\boldsymbol{r}_{20}\frac{r_{10}^2}{r_{20}^2 r_{21}^2}$$
$$\left\{\frac{\alpha_s N_c}{2\pi^2}\int_{z_0}^{z_2}\frac{\mathrm{d}z_3}{z_3}\left(\int \mathrm{d}^2\boldsymbol{r}_{30}\frac{r_{20}^2}{r_{30}^2 r_{20}^2} + \int \mathrm{d}^2\boldsymbol{r}_{31}\frac{r_{21}^2}{r_{31}^2 r_{32}^2}\right)\right\} \qquad (3.11)$$

A lower limit z_0 has been introduced into the longitudinal momentum integrations in (3.11) and this lower cutoff is implicit in other such integrations in this chapter. This cutoff which has been inserted to avoid logarithmic divergences in z appearing will not be present in scattering cross sections or other physical quantities calculated using the dipole approach. The integrands in (3.11) have been simplified using the identity

$$\frac{r_{jk}^2}{r_{ik}^2 r_{ij}^2} = \left(\frac{1}{r_{ij}^2} - 2\frac{\boldsymbol{r}_{ij} \cdot \boldsymbol{r}_{ik}}{r_{ij}^2 r_{ik}^2} + \frac{1}{r_{ik}^2} \right) \tag{3.12}$$

In (3.11). the factor in curly brackets comes from the emission of the second soft gluon. Observe that there are two independent contributions from the second gluon emission which are identical in structure to the branching observed at the one gluon level (3.9). The first term in the round brackets describes the branching of the colour dipole of transverse size r_{20} and the second describes the branching of the dipole of size r_{21}. Note that in (3.11) the colour factor C_F has been replaced by $N_C/2$ which is consistent with the leading N_C approximation.

In order to perform calculations in both the fixed and running coupling regimes the change of integration variables

$$\mathrm{d}^2\boldsymbol{r}_{20} = \mathcal{J}(r_{10}, r_{20}, r_{21}) \mathrm{d}r_{20} \mathrm{d}r_{21} \tag{3.13}$$

is made where the Jacobian of the transformation can be written

$$\mathcal{J}(r_{10}, r_{20}, r_{21}) = 2\pi r_{20} r_{21} \int_0^\infty \mathrm{d}\kappa \kappa \mathrm{J}_0(\kappa r_{10}) \mathrm{J}_0(\kappa r_{20}) \mathrm{J}_0(\kappa r_{21}) \tag{3.14}$$

The generalisation to further gluon emission is now straightforward. Mueller [4, 33] uses a generating functional approach to encode the 1 → 2 dipole branching kernel which has been observed at each stage in the calculation so far, *ie.*

$$\frac{\alpha_s N_C}{2\pi^2} \frac{r_{10}^2}{r_{20}^2 r_{21}^2} \tag{3.15}$$

into an integral equation which demonstrates how the probability of dipole branching evolves with changes in longitudinal momentum fraction. The dipole branching process can also be described in terms of the density of dipoles with a given transverse size which is the approach employed in this study. The dipole density is introduced in section 3.3 after discussing how the virtual gluon corrections to the onium state are determined.

3.2 Virtual Corrections to the Onium Wavefunction

The analysis so far has concentrated on real gluon emission (or dipole branching when viewed in the leading N_C limit). Virtual corrections are calculated using unitarity arguments. Let $\Phi(\boldsymbol{r}_{10}, z_1)$ represent the inclusive probability of finding an onium state, that is the probability of finding an onium which includes the sum over all soft gluon contributions,

$$\begin{aligned}\Phi(\boldsymbol{r}_{10}, z_1) =& \Phi^{(0)}(\boldsymbol{r}_{10}, z_1) \\ & \times \left[1 + \int \mathrm{d}^2\boldsymbol{r}_{20} \int^{z_1} \frac{\mathrm{d}z_2}{z_2} \frac{\alpha_s C_F}{\pi^2} \left(\frac{1}{r_{21}^2} - 2\frac{\boldsymbol{r}_{21}\cdot\boldsymbol{r}_{20}}{r_{21}^2 r_{20}^2} + \frac{1}{r_{20}^2}\right)\right. \\ & \left. + V^{(1)}(\boldsymbol{r}_{10}, z_1) + \cdots\right] \end{aligned} \tag{3.16}$$

where the $\mathcal{O}(\alpha_s)$ contribution from real emission has been reproduced from (3.9) and where $V^{(1)}(\boldsymbol{r}_{10}, z_1)$ represents the virtual one gluon exchange term. Due to conservation of probability,

$$\int \mathrm{d}^2\boldsymbol{r}_{10} \int_0^1 dz_1 \Phi(\boldsymbol{r}_{10}, z_1) = 1 \tag{3.17}$$

If one recalls the normalisation of the lowest order onium state $\Phi^{(0)}(\boldsymbol{r}_{10}, z_1)$ defined by (3.3), then it can be seen that in order to satisfy (3.17) at the one gluon level, the virtual contribution $V^{(1)}(\boldsymbol{r}_{10}, z_1)$ must be given by

$$\begin{aligned} V^{(1)}(\boldsymbol{r}_{10}, z_1) &= -\int_{\Lambda} \mathrm{d}^2\boldsymbol{r}_{20} \int^{z_1} \frac{\mathrm{d}z_2}{z_2} \frac{\alpha_s C_F}{\pi^2} \left(\frac{1}{r_{21}^2} - 2\frac{\boldsymbol{r}_{21} \cdot \boldsymbol{r}_{20}}{r_{21}^2 r_{20}^2} + \frac{1}{r_{20}^2} \right) \\ &= -\frac{2\alpha_s N_C}{\pi} \ln\left(\frac{r_{10}}{\Lambda}\right) \ln z_1 \end{aligned} \tag{3.18}$$

The ultra-violet divergence in the integration over transverse coordinates has been performed using an ultra-violet cut-off Λ as the lower limit of the integration range. It shall be found that when real and virtual terms are combined, the overall result is finite.

The virtual corrections reflect the fact that after a dipole branches, the parent dipole is annihilated. Higher order virtual corrections are determined using the same unitarity argument order by order in perturbation theory.

3.3 The Dipole Evolution Equation

Later in this study, the dipole approach will be used to model scattering cross sections in the high energy limit. With this in mind, the rapidity variable Y is introduced into the dipole formalism. In the context of the variables introduced so far, Y has the structure $Y = \ln(1/z)$ which corresponds to the definition in chapter 2. The exact definition of the rapidity will be refined when the dipole cascade is implemented into a specific scattering process. The evolution of dipole number with Y in the fixed coupling limit was developed by Mueller [3, 33] .

To reflect the fact that the results quoted in this section are quite general and also to simplify the notation in future chapters, the transverse coordinate variables have been renamed as follows

$$\begin{aligned} \boldsymbol{r}_{10} &\rightarrow \boldsymbol{r} \\ \boldsymbol{r}_{20} &\rightarrow \hat{\boldsymbol{r}}' \\ \boldsymbol{r}_{21} &\rightarrow \boldsymbol{r}' \end{aligned} \tag{3.19}$$

with the relation

$$\boldsymbol{r}' = \hat{\boldsymbol{r}}' - \boldsymbol{r} \tag{3.20}$$

holding as before.

Consider an initial onium state of size r where the antiquark has longitudinal momentum fraction z_1. Assume that a dipole of size ρ is emitted from this initial state and that the smallest longitudinal momentum fraction in this dipole is greater than e^{-Y}. The dipole density $n(Y, r, \rho)$ is defined such that

$$N(Y, \rho) = \int_0^1 \mathrm{d}z_1 \int \mathrm{d}^2\boldsymbol{r}\Phi^{(0)}(\boldsymbol{r}, z_1) n(Y, r, \rho) \tag{3.21}$$

where $N(Y, \rho)$ is the number density of dipoles of transverse size ρ with smallest longitudinal momentum fraction greater than e^{-Y}. It is found [33] that the dipole density $n(Y, r, \rho)$ evolves with rapidity according to

$$\begin{aligned} n(Y, r, \rho) = {} & \exp\left(-\frac{2\alpha_s N_C}{\pi} \ln\left(\frac{r}{\Lambda}\right) Y\right) \rho\delta(\rho - r) + \\ & \frac{\alpha_s N_C}{\pi^2} \int_0^Y \mathrm{d}Y' \int_\Lambda \mathrm{d}^2\boldsymbol{r}' \exp\left(-\frac{2\alpha_s N_C}{\pi} \ln\left(\frac{r}{\Lambda}\right)(Y - Y')\right) \frac{r^2}{r'^2 \hat{r}'^2} n(Y', r', \rho) \end{aligned} \tag{3.22}$$

Note that the ultra-violet divergence present in the integral over impact parameter space is regularised by inserting an ultra-violet cutoff Λ. A diagrammatical

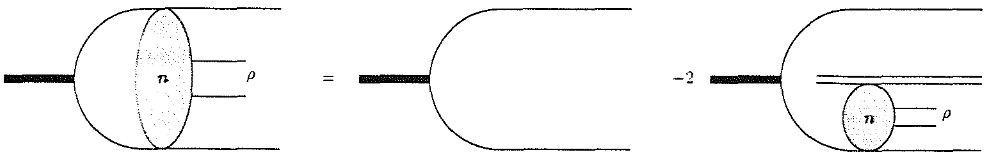

Figure 3.5: Schematic representation of the dipole evolution equation (3.22). The original dipole has transverse size r and the emitted dipole has transverse size ρ

representation of (3.22) is shown in fig. 3.5. The first term represents the possibility of the dipole being formed from the quark-antiquark pair whilst the second represents the branching of a dipole. Note that the second term contains the dipole branching factor (3.15) and is responsible for the creation of new dipoles. It should also be noted that a factor of 2 $n(Y', r', \rho)$ in the second term of (3.22) could be replaced by $n(Y', r', \rho) + n(Y', \hat{r}', \rho)$ to demonstrate explicitly that after a dipole has split into two, each new dipole can act as the parent for subsequent emissions. By symmetry, both representations produce identical results in the analysis which follows. The virtual corrections are accounted for by the factor

$$\exp\left(-\frac{2\alpha_s N_C}{\pi}\ln\frac{r}{\Lambda}Y\right) \equiv \exp(V^{(1)}(\boldsymbol{r}, z_1)) \tag{3.23}$$

which appears in both terms of (3.22). The form of virtual corrections can be deduced by using the method outlined in section 3.2 or by using the generating functional approach employed by Mueller [4]. Such exponentiation of soft gluon radiation can also be observed in jet physics where the jet evolution follows a sequential branching process [36].

In order to investigate the properties of the dipole density n, a Laplace transform is performed

$$n_\omega(r, \rho) = \int_0^\infty \mathrm{d}Y e^{-\omega Y} n(Y, r, \rho) \tag{3.24}$$

so that (3.22) can be written

$$
\begin{aligned}
n_\omega(r,\rho) = {} & \frac{1}{\omega}\rho\delta(\rho - r) + \\
& \frac{1}{\omega}\frac{2\alpha_s N_C}{\pi}\int_\Lambda \mathrm{d}r' \left(\int_\Lambda \mathrm{d}\hat{r}' \frac{1}{2\pi}\mathcal{J}(r,\hat{r}',r')\frac{r^2}{\hat{r}'^2 r'^2}\right. \\
& \left. -\delta(r'-r)\ln\frac{r}{\Lambda}\right) n_\omega(r',\rho) \qquad (3.25)
\end{aligned}
$$

where the integration over the transverse position of the soft gluon is performed according to the transformation (3.13). A kernel for the dipole evolution $\mathcal{K}_{DIP}$ can be deduced from (3.25) such that

$$
n_\omega(r,\rho) = \frac{1}{\omega}\rho\delta(\rho - r) + \frac{1}{\omega}\int_\Lambda \mathrm{d}r' \mathcal{K}_{DIP}(r,r') n_\omega(r',\rho) \qquad (3.26)
$$

where

$$
\begin{aligned}
\mathcal{K}_{DIP}(r,r') = {} & \frac{\alpha_s N_C}{\pi^2}\int_\Lambda \mathrm{d}\hat{r}' \mathcal{J}(r,\hat{r}',r')\frac{r^2}{\hat{r}'^2 r'^2} \\
& - \frac{2\alpha_s N_C}{\pi}\delta(r'-r)\ln\frac{r}{\Lambda} \qquad (3.27)
\end{aligned}
$$

The first term in (3.27) describes real gluon emission and the second corresponds virtual emission. An inverse Laplace transform can be easily performed to write (3.26) in terms of $n(Y,r,\rho)$ again if desired. Now consider the action of the kernel on the function $(r'^2)^\nu$. The result is

$$
\int \mathrm{d}r' \mathcal{K}_{DIP}(r,r')(r'^2)^\nu = \frac{\alpha_s N_C}{\pi}\chi^{(0)}(\nu)(r^2)^\nu \qquad (3.28)
$$

where $\chi^{(0)}(\nu)$ is given by (2.27). As the eigenvalue spectrum of the dipole and BFKL kernels is the same, these kernels are equivalent despite the differences between (2.24) and (3.27). By introducing a regularisation scheme, it is possible to show that $\mathcal{K}_{DIP}$ is ultra-violet finite. The ultra-violet singularities which are present in the virtual and the real terms cancel exactly leaving an ultra-violet regular kernel. The explicit cancellation of ultra-violet singularities will be demonstrated in a different manner in chapter 6 where the Borel plane variable b is used to regulate the divergences. Note that unlike the BFKL kernel (2.24), both real and virtual contributions to the dipole kernel are individually infra-red finite. The equivalence between the dipole and the BFKL approaches has been demonstrated in detail by Chen and Mueller [34].

Having determined the eigenvalue spectrum of the dipole kernel, the solution for the dipole density n in the leading logarithmic limit is found to be

$$n(Y, r, \rho) = \frac{r}{\rho} \frac{\exp(-\omega_L Y)}{\sqrt{C\pi Y}} \exp\left(-\frac{\ln^2(r/\rho)}{CY}\right) \tag{3.29}$$

where C and ω_L are the same factors that appear in the solution to the BFKL equation (2.29). The infra-red diffusion property which the BFKL amplitude F possesses is also present in (3.29). This can be seen in the $\ln^2(r/\rho)$ term indicating that the dipole density n can probe dipole sizes of large ρ.

3.4 Deep Inelastic Scattering in the Dipole Approach

The analysis of this chapter now moves away from the approach taken by Mueller and others and instead the equivalent terminology of Nikolaev and Zakharov is used. Both approaches model cross sections via onium-onium scattering. In the formulation introduced in this study, the entire dipole cascade is evolved from one of the onia and the dipole cascade then couples to the other onium by means of a convolution over transverse position and longitudinal momentum fraction. The approach taken by Mueller [3, 37] in order to investigate the unitarity problem in the semihard regime by onium-onium interactions employs a different partitioning of the scattering amplitude. In these studies, dipole cascades from both of the onia are evolved to an intermediate rapidity which interact via the exchange of two hard gluons, corresponding to the exchange of one hard pomeron. At the one pomeron exchange level (that is where there is only a single onium-onium interaction) these different partitionings of the scattering amplitude can be related by noting that as for the BFKL amplitude (2.21), there is no unique prescription for defining the amplitude because of the convolution property which the dipole density function n obeys, that is

$$n(Y, r, \rho) = \int_0^Y \mathrm{d}Y' n(Y - Y', r, \rho) n(Y', r, \rho) \tag{3.30}$$

Consider deep inelastic lepton-nucleon scattering in the rest frame of the nucleon which has mass m_N. As in chapter 2, the virtual photon (γ^*) proton cross section is studied. The squared wavefunction for the transition $\gamma^* \to q\bar{q}$ where the quark and antiquark have transverse separation r and the antiquark carries a longitudinal momentum fraction z is denoted by $\Phi^{(0)}(r, z)$. The virtual photon-proton cross section, $\sigma(x, Q^2)$ is defined by [38, 5, 39]

$$\sigma_L(x, Q^2) = \int_0^1 \mathrm{d}z \int \mathrm{d}^2\boldsymbol{r} \Phi_L^{(0)}(\boldsymbol{r}, z) \sigma_{dN}(Y, \boldsymbol{r}) \tag{3.31}$$

where σ_{dN} is the total dipole nucleon cross section and Y is defined by $\ln(z/x)$. The subscript L denotes a longitudinally polarised photon and an identical expression could be written down for a transversely polarised photon, however the exact functional forms for $\Phi_L^{(0)}$ and $\Phi_T^{(0)}$ would of course differ. The forms for $\Phi_L^{(0)}$ and $\Phi_T^{(0)}$ will be quoted in chapter 7 but at this stage, their definition is not important and the indices T and L are suppressed until chapter 7. Physically, one can interpret (3.31) by noting that the fluctuation $\gamma^* \to q\bar{q}$ occurs much earlier than interactions with the nucleon.

It is found that the lowest order dipole nucleon cross section $\sigma^{(0)}_{dN}$ takes the form

$$\sigma^{(0)}_{dN} = \frac{1}{N_C}\int \frac{\mathrm{d}^2 l}{(\boldsymbol{l}^2)^2}\alpha_s^2 V(\boldsymbol{l})\mathfrak{Re}(1-e^{-ilr}) \tag{3.32}$$

where $V(\boldsymbol{l})$ is proportional to the gluon-gluon-nucleon-nucleon vertex function. This chapter has discussed how the radiative corrections to this function can be developed using the dipole density $n(Y, r, \rho)$ which encodes the soft gluon radiation as a dipole cascade emanating from the initial $q\bar{q}$ pair with square wavefunction $\Phi(\boldsymbol{r}, z)$. The dipole density couples to the nucleon end by means of a convolution in transverse coordinate space and this permits the dipole-nucleon cross section to be written in the form

$$\sigma_{dN}(Y, r) = \int \frac{\mathrm{d}^2\rho}{2\pi\rho^2} n(Y, r, \rho)\sigma^{(0)}_{dN}(\rho) \tag{3.33}$$

so that the equation for the virtual photon-proton cross section (3.31) can be rewritten in the form

$$\sigma(x, Q^2) = \int_0^1 \mathrm{d}z \int \mathrm{d}^2\boldsymbol{r} \int \frac{dm^2\rho}{2\pi\rho^2}\Phi^{(0)}(\boldsymbol{r}, z) n(Y, r, \rho)\sigma^{(0)}_{dn}(\rho) \tag{3.34}$$

This representation of the virtual photon proton cross section is the analogue of (2.21) in the BFKL case where the universal part of the cross section is the dipole density n which is independent of the projectile or the target just like the universal BFKL amplitude F in (2.21). All dependence on hadronic momentum scales enters through $\sigma^{(0)}_{dN}$. Note that there is a difference in these equations. In the BFKL formulation, all dependence on longitudinal momentum fraction is concentrated in the BFKL amplitude F. In the dipole approach described by (3.34), the projectile and target functions contain depend on z and x respectively. This explains the presence of the convolution over the longitudinal momentum fraction z in (3.34).

In chapter 7 the properties of the dipole cascade incorporating a running coupling will be used to predict the form of the power corrections in inverse powers of Q^2 that are associated with $\sigma_L(x, Q^2)$ and hence with the structure function $F_L(x, Q^2)$ which is defined by (2.39). Before this however, it is necessary to introduce renormalons in QCD which is done in the next chapter. Renormalons will be used to identify the infra-red behaviour of the dipole density with a running coupling and in the next chapter, it shall be demonstrated that renormalon singularities are linked to power correction terms.

Chapter 4

The Borel Transform and Renormalons in QCD

In this chapter, the Borel transform and some of its properties will be introduced. Singularities in Borel transformed functions are discussed and the reason why these singularities lead one to deduce that non-perturbative power corrections to the perturbative result exist is also discussed. The application of the Borel transform to QCD was originally reported by 't Hooft [40] and the reader is referred to this reference for a more detailed treatment along with the papers of Mueller [41, 42] and Zakharov [43]. The use of of the Borel transform to probe perturbative QCD amplitudes has become a popular method in recent years and many applications of the basic procedure reviewed below can now be found in the literature. It should also be noted that there are other methods currently employed to probe the QCD perturbation series which include different definitions of the Borel transform and dispersive techniques [44]. These approaches will not be discussed any further here. It will become apparent that due to the nature of the QCD perturbation series, the results which are obtained from the Borel transformed amplitude cannot be uniquely translated into the usual perturbative framework however the functional dependence of the deduced power corrections is fixed by the results from the Borel transform.

4.1 The Borel Transform

Consider the perturbative expansion for an observable $O(\alpha_s(Q^2))$ where α_s is the running QCD coupling defined by (2.7) and Q^2 is some large external momentum scale in the process (*eg.* the photon virtuality in deep inelastic scattering). The perturbation expansion for O is

$$O(\alpha_s(Q^2)) = o + \sum_{n=0} o_n \alpha^{n+1}(Q^2) \tag{4.1}$$

It is known [40, 42] that the perturbative expansion of O is at best asymptotic however in many cases, it may be divergent or non-unique. An attempt to classify the causes of the problems in perturbation theory which cause this is the goal of renormalon analysis.

Consider the transformed function $\tilde{O}(b)$

$$\tilde{O}(b) = o\delta(b) + \sum o_n \frac{b^n}{n!} \tag{4.2}$$

It can be shown that the convergence properties of this series are much better than the series in (4.1). To illustrate this point, consider the following two simple examples. Firstly, assume that the perturbative coefficients o_n are of the form $o_n = (-1)^n n!$. The series in α_s space, (4.1) has zero radius of convergence whereas the transformed series given by (4.2) is analytic over the whole complex b plane and can easily be summed to give

$$\tilde{O}(b) = \frac{1}{1+b} \tag{4.3}$$

In this case, as there are no singularities on the positive real b axis, the function $O(\alpha_s)$ can be reconstructed using the Borel transform equation

$$O(\alpha_s(Q^2)) = \int_0^\infty \mathrm{d}b \tilde{O}(b) e^{-b/\alpha_s(Q^2)} \tag{4.4}$$

The reason for the requirement that the Borel transformed function $\tilde{O}(b)$ has no singularities on the positive b axis can be understood from the form of the transform (4.4) where the integration range is the semi-infinite interval $b \in [0, \infty)$. The series in this example is said to be Borel summable as it allows an expansion in α_s to be constructed without ambiguity using the transformation (4.4). An example of a non-Borel summable series is where the perturbative coefficients of (4.1) have the form $o_n = n!$. In this case, the Borel transformed function $\tilde{O}(b)$ can also be summed to all orders, the result being

$$\tilde{O}(b) = \frac{1}{1-b} \tag{4.5}$$

In this example however, the Borel transform has a singularity on the real axis at $b = 1$ and this prevents the transform integral (4.4) from being unambiguously performed in the complex b plane. Although it is possible to define a prescription which allows the transformation integral to be performed, this depends on the way in which the pole at $b = 1$ is circumnavigated in the complex plane and therefore is not unique.

The previous example showed how ambiguities can arise in the reconstruction of observables from their Borel transforms if the Borel transformed function contains poles on the positive real b axis. It would be convenient if the QCD perturbation series was Borel summable but of course this is not the case ! Unfortunately, it is found that there exists a series of pole in Borel space on the positive real axis at integer multiples of $1/\beta_0$, where β_0 is the first order expansion of the β function defined by (2.4). These Borel plane singularities prevent the Borel transformed expression for an observable $\tilde{O}(b)$ from being unambiguously transformed to give an expression in terms of the running coupling α_s and these poles are called infra-red renormalons. The existence of terms in QCD perturbation series which gives rise to these infra-red renormalons is discussed in the next section. A series of poles are also observed at negative integer multiples of $1/\beta_0$ and because these poles arise from diagrams which involve integrations over large internal loop momenta they are given the title ultra-violet renormalons. As the location of the ultra-violet renormalons is on the negative real b axis and therefore not on the integration path of (4.4) their presence is not such a serious problem. In this study, where the diffusion into low momentum regions in the Regge limit of QCD is being investigated, ultra-violet renormalons will not be considered in any detail and a recent review can be found in [45].

4.2 The Origin of Infra-Red Renormalons in the QCD Perturbation Series

For the case of QED, Lautrup [46] demonstrated that a class of Feynman diagrams at n^{th} order in perturbation theory can give rise to amplitudes which contribute factors of $n!$ and an example of such a diagram is illustrated in fig. 4.1. In the case of QCD, it is necessary to extend the analysis such that the non-Abelian nature of the theory is exposed. In this study, the common assumption that the analysis for QED can be simply 'non-Abelianised' will be adopted. By making this assumption, it is presumed that infra-red renormalons arise only from the

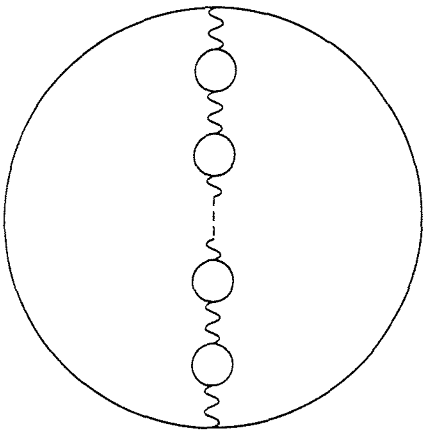

Figure 4.1: An example of an n loop diagram which grows as $n!$.

running of the coupling at not from other sources.

Contributions from diagrams such as fig. 4.1 lead to a singularity in the Borel plane located on the positive real axis. The reason that this singularity exists arises from the fact that the virtual loop momenta are much smaller than the momentum which is used to define the running coupling. Another way of relating the problematic fixed sign $n!$ growth of the perturbative series with infra-red effects is to rewrite the expression for the running coupling $\alpha_s(k^2)$ in terms of the scale μ^2 (2.5) as a series

$$\alpha_s(k^2) = \sum_0^\infty \left(-\beta_0 \ln \frac{k^2}{\mu^2}\right)^n \alpha(\mu^2)^{n+1} \tag{4.6}$$

Reparameterising the integral over k^2 which must be performed, the coefficient of $\alpha(\mu^2)^{n+1}$ then takes the form,

$$\int_0^1 \mathrm{d}u \left(ln\frac{1}{u}\right)^n = n! \tag{4.7}$$

and the origin of the $n!$ growth of the coefficient can be observed explicitly.

4.3 Power Corrections to QCD Amplitudes

Although it is not possible to uniquely invert the Borel transform of $\tilde{O}(b)$ when infra-red renormalon singularities are present, an estimation of the ambiguity present in $O(\alpha_s(Q^2))$ can be made if a prescription is chosen for the contour taken to avoid the Borel plane pole. Although this means that the residue of the pole and hence the magnitude of the infra-red renormalon singularity in α_s space is not known, it does allow the Q^2 dependence to be accurately determined. Consider a Borel transformed function $\tilde{O}$

$$\tilde{O}(b) = \frac{\mathcal{C}}{b_1 - b} + \tilde{O}_R(b) \tag{4.8}$$

where $\tilde{O}_R(b)$ contains no poles in b. The Borel transform exhibits an infra-red renormalon pole at $b = b_1$, which means that the integration path in (4.4) must be distorted around the point $b = b_1$ to avoid encountering the singularity. Define the expression for $O(\alpha_s(Q^2))$ in the following way

$$O(\alpha_s(Q^2)) = O_A(\alpha_s(Q^2)) + O_R(\alpha_s(Q^2)) \tag{4.9}$$

The transform of $\tilde{O}_R(b)$ to give $O_R(\alpha_s(Q^2))$ is well defined as there no non-integrable singularities in $\tilde{O}_R(b)$. The function $O_A(\alpha_s(Q^2))$ however cannot be determined without introducing an ambiguity. Making the assumption that the magnitude of the Cauchy integral is used to determine the contribution from the pole, this determines the coefficient of the pole at $b = b_1$ to be $2\pi\mathcal{C}$, the result for $O_A(\alpha_s(Q^2))$ which arises from using this prescription to transform the pole term in (4.8) is given by

$$O_A(\alpha_s(Q^2)) = 2\pi\mathcal{C}e^{-b_1/\alpha_s(Q^2)} \tag{4.10}$$

Using the expression (2.7) to write the running coupling $\alpha_s(Q^2)$ in terms of Λ_{QCD} allows (4.10) to be rewritten in the form

$$O_A(Q^2) = 2\pi C \left(\frac{\Lambda^2_{QCD}}{Q^2} \right)^{b_1 \beta_0} \tag{4.11}$$

and hence it can be observed that the infra-red renormalon singularity at $b = b_1$ leads to an power dependent term in the perturbation series. Note that the position of the pole in the Borel plane determines the order of the power dependence and this is not ambiguous. The coefficient of the power dependent term is not uniquely determined however as it relies on the method which is used to distort the contour of intergation in the complex plane in order to estimate the contribution of the pole term to the integral.

The ambiguous power dependent term is commonly interpreted to signal the presence of correction terms which are of the same order in (Λ^2_{QCD}/Q^2) and which are non-perturbative in origin. The reason behind this interpretation is quite simple: experimental determinations of $O(Q^2)$ are insensitive to the fact that the perturbative expression contains a power like ambiguity and so compensating non-perturbative power corrections are required to yield a unique result.

4.4 Convolution of Borel Transforms

The rest of this study will deal with Borel transformed quantities and it is necessary to understand how to multiply two Borel transformed functions. The Borel convolution of two functions is defined analogously to a Laplace convolution. The Borel transform of the product of two functions f and g whose Borel transforms are $\tilde{f}$ and $\tilde{g}$ respectively is given by

$$\tilde{f}(b) \otimes \tilde{g}(b) = \int_0^b \mathrm{d}b' \tilde{f}(b') \tilde{g}(b - b') \tag{4.12}$$

In the next chapter, the Borel transform techniques discussed here will be used to incorporate a running coupling into the dipole approach in order that the infrared singularity structure of the dipole evolution kernel with running coupling can be studied in chapter 6.

Chapter 5

Dipole Evolution Incorporating a Running Coupling

In this chapter, the colour dipole formalism of chapter 3 will be extended to include the effects of a running coupling in order that the asymptotic behaviour of the perturbation series in the small-x limit may be studied. It has already been established that due to the diffusive property of small-x dynamics, the coupling is driven towards the Landau pole so it is essential to formulate a systematic method of running the coupling in the small-x limit. In order to achieve this, the Borel transform defined in chapter 4 is employed. The Borel space formulation will allow the existence of power corrections to the perturbatively calculated result to be established. The type of power corrections present are reflected in the infra-red singularity structure of the perturbative dipole cascade in the Borel plane. In order to study the Borel singularities of the dipole cascade, the dipole evolution kernel incorporating a running coupling must be determined in Borel space.

Sections 5.1-5.3 concentrate wholly on incorporating a running coupling into the probability for one soft gluon emission from a quark-antiquark pair. For reasons of clarity and so that comparisons can be made with the discussion in chapter 3, the transverse coordinates of the quark, antiquark and emitted soft gluon will be represented by $\boldsymbol{r}_0$,$\boldsymbol{r}_1$ and $\boldsymbol{r}_2$ respectively. In section 5.4, where the discussion is generalised to multi-gluon emission by deriving an integral equation for the dipole density in Borel space and for the remainder of this thesis where the singularities of this kernel are studied, the relabelling introduced in (3.19) will be used.

5.1 Argument of the Running Coupling

The technique of renormalon analysis discussed in chapter 4 was constructed entirely in momentum space. The dipole branching evolution kernel developed in chapter 3 for fixed coupling uses an impact parameter space representation. It has been shown that the branching property of the dipole picture is only present when the evolution is viewed in terms of transverse coordinates because during the emission of a soft gluon, the impact parameters of all harder particles are frozen. It is therefore necessary to determine a prescription for the running coupling in terms of impact parameter space variables which is consistent order by order in dipole emission with the Borel singularity structure found in momentum space.

Recall that when viewed in momentum space, the dipole branching process occurs through the emission of a soft gluon with transverse momentum $\boldsymbol{k}_2$ and transverse coordinate $\boldsymbol{r}_2$ from a dipole of momentum p where the quark and antiquark have transverse separation $\boldsymbol{r}_{10}$ (see fig.3.2). The argument of the coupling in this process is taken to be $\boldsymbol{k}_2^2$ which is in accordance with the treatment of soft gluon radiation in the case of timelike cascades [36]. The radiative nature of the dipole branching process allows the analogy to be made with jet decay. Note that the virtuality of the soft gluon is determined by its transverse momentum, $k_2^2 \simeq \boldsymbol{k}_2^2$. The transverse momentum of the emitted gluon is the only information which is used to determine the running coupling. In order to incorporate this information into the dipole formalism, the one gluon emission process has to be viewed in transverse coordinate space, that is a dipole of transverse separation $\boldsymbol{r}_{10}$ emits a soft gluon with transverse coordinate $\boldsymbol{r}_2$. This may lead one to conclude that the correct argument with which to run the coupling is actually the transverse coordinate of the soft gluon $\boldsymbol{r}_2$. Although this assumption is correct for sufficiently small $\boldsymbol{r}_2$, it does not permit diffusion in $\boldsymbol{r}_2$ to large values where one approaches the Landau pole. In order to deduce the argument of the running coupling in impact parameter variables, the Borel transform is employed. Before developing an expression for the probability of one gluon emission in the Borel plane, it is necessary to define the Borel transform of $g_s(\boldsymbol{k}^2)$ and $\alpha_s(\boldsymbol{k}^2)$.

5.2 Borel transform of g_s

It can easily be verified from the definition of the Borel transform (4.4) that the Borel transform of the running coupling $\alpha_s(\boldsymbol{k}^2)$ in (2.5) is

$$\tilde{\alpha}_s(\boldsymbol{k}^2, b) = \left(\frac{\boldsymbol{k}^2}{Q^2}\right)^{-b\beta_0} \tag{5.1}$$

where Q^2 is an overall external momentum scale dependent on the physical process being considered. In the case of deep inelastic scattering which will be studied later, Q^2 is the virtuality of the photon which fluctuates into the dipole cascade before interacting with the nucleon target. Note that (5.1) encodes the naïve non-Abelianisation discussed in section 4.2 as it includes the leading behaviour in $\ln(\boldsymbol{k}^2/Q^2)$ of the probability for the emission of the soft gluon.

The Borel transform of $g_s(\boldsymbol{k}^2)$ related to $\alpha_s(\boldsymbol{k}^2)$ by (2.6) is determined by the requirement that the Borel convolution of $\tilde{g}_s(\boldsymbol{k}^2, b)$ with itself results in the Borel transformed quantity $4\pi\tilde{\alpha}_s(\boldsymbol{k}^2, b)$, that is

$$4\pi\left(\frac{\boldsymbol{k}^2}{Q^2}\right)^{-b\beta_0} = \int_0^b \mathrm{d}b'\tilde{g}_s(\boldsymbol{k}^2, b)\tilde{g}_s(\boldsymbol{k}^2, b-b') \tag{5.2}$$

From (5.2), it can be deduced that

$$\tilde{g}(\mathrm{k}^2, b) = \frac{2}{\sqrt{b}}\left(\frac{k^2}{Q^2}\right)^{-b\beta_0} \tag{5.3}$$

5.3 The Running Coupling in Impact Parameter Space

In order to determine the argument of the running coupling in impact parameter space, the Borel transformed probability for the emission of one soft gluon from a quark-antiquark pair is calculated, that is the configuration depicted in fig.3.2 is studied having implemented the running of the coupling in momentum space in accordance with section 5.1. After inserting the running coupling, the wavefunction for the quark-antiquark state with one real soft gluon emission becomes *cf.* (3.5)

$$\Psi^{(1)\,a}(\boldsymbol{k}_1, \boldsymbol{k}_2, z_1, z_2) = 2g_s(\boldsymbol{k}_2^2)t^a\left[\Psi^{(0)}(\boldsymbol{k}_1 + \boldsymbol{k}_2, z_1) - \Psi^{(0)}(\boldsymbol{k}_1, z_1)\right]\frac{\boldsymbol{k}_2 \cdot \boldsymbol{\epsilon}}{\boldsymbol{k}_2^2} \tag{5.4}$$

Using the expression (5.3) for $\tilde{g}_s(\boldsymbol{k}^2, b)$, the Borel transform of the wavefunction $\tilde{\Psi}^{(1)}$ is

$$\begin{aligned}\tilde{\Psi}^{(1)\,a}(\boldsymbol{k}_1, \boldsymbol{k}_2, z_1, z_2, b) =& \frac{4}{\sqrt{b}}\left(\frac{\boldsymbol{k}_2^2}{Q^2}\right)^{-b\beta_0} t^a \\ &\times \left[\Psi^{(0)}(\boldsymbol{k}_1 + \boldsymbol{k}_2, z_1) - \Psi^{(0)}(\boldsymbol{k}_1, z_1)\right]\frac{\boldsymbol{k}_2 \cdot \boldsymbol{\epsilon}}{\boldsymbol{k}_2^2}\end{aligned} \tag{5.5}$$

The Borel transformed wavefunction is obtained as a function of the impact parameters $\boldsymbol{r}_{10}$ and $\boldsymbol{r}_{20}$ by Fourier transforming over the transverse momenta $\boldsymbol{k}_1$ and $\boldsymbol{k}_2$ which yields

$$\tilde{\Psi}^{(1)\,a}(\boldsymbol{r}_{10}, \boldsymbol{r}_{20}, z_1, z_2, b) = -\frac{1}{\sqrt{b}}\frac{2i}{\pi} t^a \Psi^{(0)}(\boldsymbol{r}_{10}, z_1)$$
$$\int_0^\infty \mathrm{d}\tau \mathrm{J}_1(\tau) \left[\left(\frac{Q^2 r_{20}^2}{\tau^2} \right)^{b\beta_0} \frac{\boldsymbol{\epsilon} \cdot \boldsymbol{r}_{20}}{r_{20}^2} - \left(\frac{Q^2 r_{21}^2}{\tau^2} \right)^{b\beta_0} \frac{\boldsymbol{\epsilon} \cdot \boldsymbol{r}_{21}}{r_{21}^2} \right] \tag{5.6}$$

where J_1 is the first order Bessel function. In arriving at (5.6), the two dimensional integral over transverse coordinate space has been transformed into polar coordinates and the angular integration has been performed. The parameter τ has been introduced to simplify integrals of the form

$$\begin{aligned} \frac{1}{2\pi^2} \int \mathrm{d}^2\boldsymbol{k} e^{i\boldsymbol{k}\cdot\boldsymbol{r}} \frac{\boldsymbol{k}}{\boldsymbol{k}^{2\gamma}} &= \frac{i}{2\pi} \int_0^\infty \frac{\mathrm{d}k}{(k^2)^{\gamma-1}} \mathrm{J}_1(kr) \frac{\boldsymbol{r}}{r} \\ &= \frac{i}{2\pi} \int_0^\infty \mathrm{d}\tau \mathrm{J}_1(\tau) \left(\frac{r^2}{\tau^2} \right)^{\gamma-1} \frac{\boldsymbol{r}}{r^2} \end{aligned} \tag{5.7}$$

The Borel transformed probability for one gluon emission $\tilde{\Phi}^{(1)}(\boldsymbol{r}_{10}, z_1, b)$ is obtained from $\tilde{\Psi}^{(1)}$ in (5.6) in the same manner as the fixed coupling case, however when the amplitude is 'squared' this should be understood to mean that a Borel convolution of $\tilde{\Psi}^{(1)}$ with its hermitian conjugate is performed, that is

$$\tilde{\Phi}^{(1)}(\boldsymbol{r}_{10}, z_1, b) = \int \frac{\mathrm{d}^2\boldsymbol{r}_{20}}{2\pi} \int^{z_1} \frac{\mathrm{d}z_2}{2z_2} \int_0^b \mathrm{d}b'$$
$$\sum_a \tilde{\Psi}^{(1)\,a}(\boldsymbol{r}_{10}, \boldsymbol{r}_{20}, z_1, z_2, b') \tilde{\Psi}^{\dagger\,(1)\,a}(\boldsymbol{r}_{10}, \boldsymbol{r}_{20}, z_1, z_2, b - b') \tag{5.8}$$

The complete expression for $\tilde{\Phi}^{(1)}(\boldsymbol{r}_{10}, z_1, b)$ was found to be

$$\tilde{\Phi}^{(1)}(\boldsymbol{r}_{10}, z_1, b) = \frac{N_C}{2\pi^3} \int^{z_1} \frac{\mathrm{d}z_2}{z_2} \int \mathrm{d}^2\boldsymbol{r}_{20} \int_0^\infty \mathrm{d}\tau \mathrm{d}\tau' \mathrm{J}_1(\tau)\mathrm{J}_1(\tau') \int_0^1 \frac{\mathrm{d}\omega}{\omega^{\frac{1}{2}}(1-\omega)^{\frac{1}{2}}}$$
$$\times \left(\frac{1}{\tau^2}\right)^{\omega b\beta_0} \left(\frac{1}{\tau'^2}\right)^{(1-\omega)b\beta_0} \frac{(Q^2)^{b\beta_0}}{\boldsymbol{r}_{20}^2 \boldsymbol{r}_{21}^2}$$
$$\times \left[(\boldsymbol{r}_{20}^2)^{b\beta_0}\boldsymbol{r}_{21}^2 + (\boldsymbol{r}_{21}^2)^{b\beta_0}\boldsymbol{r}_{20}^2 - 2\boldsymbol{r}_{20}\cdot\boldsymbol{r}_{21}(\boldsymbol{r}_{20}^2)^{\omega b\beta_0}(\boldsymbol{r}_{21}^2)^{(1-\omega)b\beta_0}\right]$$
$$\times \Phi^{(0)}(\boldsymbol{r}_{10}, z_1) \tag{5.9}$$

A change of variables has been made by defining $\omega = b'/b$ to simplify (5.9). It is possible to perform the integrals over $\boldsymbol{r}_{20}$,τ,τ' and ω analytically making use of the standard integral [47]

$$\int_0^\infty \mathrm{d}x x^\mu \mathrm{J}_\nu(ax) = 2^\mu a^{-\mu-1} \frac{\Gamma(\frac{1}{2}+\frac{1}{2}\nu+\frac{1}{2}\mu)}{\Gamma(\frac{1}{2}+\frac{1}{2}\nu-\frac{1}{2}\mu)} \tag{5.10}$$

and this yields

$$\tilde{\Phi}^{(1)}(\boldsymbol{r}_{10}, z_1, b) = -\frac{N_C}{\pi} \int^{z_1} \frac{\mathrm{d}z_2}{z_2} \frac{\Gamma(-b\beta_0)}{\Gamma(1+b\beta_0)} \left(\frac{Q^2\boldsymbol{r}_{10}^2}{4}\right)^{b\beta_0} \Phi^{(0)}(\boldsymbol{r}_{10}, z_1) \tag{5.11}$$

The gamma function in the numerator of (5.11) exhibits poles at positive integer values of $b\beta_0$ corresponding to infra-red renormalon singularities. The singularity at $b = 0$ is of ultra-violet origin and is also present in the fixed coupling case. As before, it can be regularised by the introduction of a short distance cut-off Λ in the integration over $\boldsymbol{r}_{20}$. It shall be demonstrated explicitly in chapter 6 that the singularity at $b = 0$ cancels between the real and virtual terms.

As a check on these calculations, $\tilde{\Phi}^{(1)}(\boldsymbol{r}_{10}, z_1, b)$ was also determined by squaring the amplitude for single gluon emission calculated in momentum space (5.4), taking the Borel transform of the running coupling using (5.1) and then Fourier transforming in the transverse momentum $\boldsymbol{k}_1$ of the antiquark only. The result of these calculations gives

$$\tilde{\Phi}^{(1)}(\boldsymbol{r}_{10}, z_1, b) = \frac{N_C}{2\pi^2} \int^{z_1} \frac{\mathrm{d}z_2}{z_2} \int \frac{\mathrm{d}^2\boldsymbol{k}_2}{\boldsymbol{k}_2^2} \left(\frac{Q^2}{\boldsymbol{k}_2^2}\right)^{b\beta_0} \times \left[2 - e^{i\boldsymbol{k}_2\cdot\boldsymbol{r}_{10}} - e^{-i\boldsymbol{k}_2\cdot\boldsymbol{r}_{10}}\right] \Phi^{(0)}(\boldsymbol{r}_{10}, z) \tag{5.12}$$

Integrating (5.12) over $\boldsymbol{k}_2$ yields (5.11). This is not surprising and confirms that one is at liberty to commute Fourier and Borel transforms.

Having calculated the Borel transformed probability for the emission of one gluon in impact parameter space it is now possible to identify the argument of the running coupling in terms of impact parameter variables. In order to do this, the unintegrated form of $\tilde{\Phi}^{(1)}(\boldsymbol{r}_{10}, z_1, b)$, (5.9) is used. Firstly note that the scalar product in (5.9) can be written as

$$\boldsymbol{r}_{20} \cdot \boldsymbol{r}_{21} = \frac{1}{2}(\boldsymbol{r}_{20}^2 + \boldsymbol{r}_{21}^2 - \boldsymbol{r}_{10}^2) \tag{5.13}$$

Defining functions λ and $\boldsymbol{R}$ by

$$\lambda^2(\tau, \tau', \omega) = \tau^{2\omega}\tau'^{2(1-\omega)} \tag{5.14}$$

$$\boldsymbol{R}^2(\omega) = (\boldsymbol{r}_{20}^2)^{\omega}(\boldsymbol{r}_{21}^2)^{(1-\omega)} \tag{5.15}$$

then $\tilde{\Phi}^{(1)}(\boldsymbol{r}_{10}, z_1, b)$ can be written as

$$\tilde{\Phi}^{(1)}(\boldsymbol{r}_{10}, z_1, b) = \frac{N_C}{2\pi^3}\Phi^{(0)}(\boldsymbol{r}_{10}, z_1)\int^{z_1}\frac{\mathrm{d}z_2}{z_2}\int \mathrm{d}^2\boldsymbol{r}_{20}\int \mathrm{d}\tau \mathrm{d}\tau' \mathrm{J}_1(\tau)\mathrm{J}_1(\tau')$$

$$\times \int_0^1 \frac{\mathrm{d}\omega}{\omega^{\frac{1}{2}}(1-\omega)^{\frac{1}{2}}}\frac{(Q^2)^{b\beta_0}}{\boldsymbol{r}_{20}^2\boldsymbol{r}_{21}^2}$$

$$\times \left[\boldsymbol{r}_{10}^2\frac{(\boldsymbol{R}^2)^{b\beta_0}}{\lambda^{2b\beta_0}} + \boldsymbol{r}_{21}^2\frac{(\boldsymbol{r}_{20}^2)^{b\beta_0} - (\boldsymbol{R}^2)^{b\beta_0}}{\lambda^{2b\beta_0}} + \boldsymbol{r}_{20}^2\frac{(\boldsymbol{r}_{21}^2)^{b\beta_0} - (\boldsymbol{R}^2)^{b\beta_0}}{\lambda^{2b\beta_0}}\right] \tag{5.16}$$

The inverse Borel transform of (5.16) can now be taken which exposes the argument of the running coupling for gluon emission in impact parameter space

$$\Phi^{(1)}(\boldsymbol{r}_{10}, z_1) = \frac{N_C}{2\pi^3}\Phi^{(0)}(\boldsymbol{r}_{10}, z_1)\int^{z_1}\frac{\mathrm{d}z_2}{z_2}\int \mathrm{d}^2\boldsymbol{r}_{20}\int_0^\infty \mathrm{d}\tau \mathrm{d}\tau' \mathrm{J}_1(\tau)\mathrm{J}_1(\tau')$$

$$\times \int_0^1 \frac{\mathrm{d}\omega}{\omega^{\frac{1}{2}}(1-\omega)^{\frac{1}{2}}}\frac{1}{\boldsymbol{r}_{20}^2\boldsymbol{r}_{21}^2}$$

$$\times \left[\alpha_s(\lambda^2/\boldsymbol{R}^2)\boldsymbol{r}_{10}^2 + \left(\alpha_s(\lambda^2/\boldsymbol{r}_{20}^2) - \alpha_s(\lambda^2/\boldsymbol{R}^2)\right)\boldsymbol{r}_{21}^2\right.$$

$$\left. + \left(\alpha_s(\lambda^2/\boldsymbol{r}_{21}^2) - \alpha_s(\lambda^2/\boldsymbol{R}^2)\right)\boldsymbol{r}_{20}^2\right] \tag{5.17}$$

In the limit where the coupling is fixed the integrations over τ, τ' and ω give a factor of π and the first term on the in the square brackets of (5.17) coincides with the expression (3.9) which was obtained by using a fixed coupling in the derivation. In the limit of fixed coupling, the second two terms in the square brackets of (5.17) vanish.

In the case of dipole evolution with a running coupling, the prescription which must be used is that which is defined in (3.9), namely that the kernel has three terms each of which has a different running coupling and for each of these terms the argument of the running coupling is not expressed simply in terms of the impact parameters $\boldsymbol{r}_{10}$ and $\boldsymbol{r}_{20}$ as one might have expected initially, but also in terms of three further parameters, τ, τ', ω, the emission probability being a weighted integral over these parameters. It should be noted that the weight function peaks when $\lambda(\tau, \tau', \omega)$ is equal to unity, so that although one has to integrate over all possible arguments for the running coupling, the integral is highly peaked in the region where the running depends only on $\boldsymbol{r}_{20}^2$ or $\boldsymbol{r}_{21}^2$ or some mean of the two.

If the Fourier transform of the wavefunction $\Psi^{(1)\,a}$ in eq.(5.4) had been taken and then squared to construct $\Phi^{(1)}(\boldsymbol{r}_{10}, z_1)$ as in eq.(5.17), there would have been a product of the form $(g_s(\tau/\boldsymbol{r}_{20}^2)\ g_s(\tau'/\boldsymbol{r}_{21}^2))$ in the result. It is the use of the Borel representation that enables this product to be expressed in terms of running α_s of a single argument. This then is a consistent and systematic way to introduce the running of the coupling, valid to all orders in perturbation theory.

The virtual contribution to the one gluon exchange probability is $-\tilde{\Phi}^{(1)}(\boldsymbol{r}_{10}, z_1, b)$ in order to unitarise the inclusive probability for the existence of an onium *cf.* section 3.2.

5.4 The Dipole Evolution Kernel with a Running Coupling

Having determined the Borel transformed probability for one gluon emission in impact parameter space, the analysis can be simply extended to encompass subsequent emission of more gluons.

In exact analogy with the treatment in section 3.3, the dipole branching process can be iterated to account for the emission of any number of soft gluons (or colour dipoles when viewed in the leading N_C limit). The Borel transformed dipole density for emission of dipoles of size ρ from an initial onium state with transverse size r, $\tilde{n}(Y, r, \rho, b)$ is defined analogously to $n(Y, r, \rho)$ discussed in section 3.3.

Correspondingly, an equation describing the dipole evolution with Y, incorporating the running coupling by means of the Borel transform was determined. Due to the lengthy functional form of this equation, due in part to the multiple convolutions which must be performed, it is not instructive to reproduce the analogue of (3.22) here. However, using the standard Laplace transform techniques which were also employed in section 3.3 it is possible to transform the dipole evolution equation into a more manageable format and the dipole density $\tilde{n}(Y, r, \rho, b)$ can be represented in terms of a compact integral equation

$$\begin{aligned}\tilde{n}(Y, r, \rho, b) =& \rho\delta(r-\rho)\delta(b) \\ &+ \int_0^b \mathrm{d}b' \int_0^Y \mathrm{d}Y' \int_0^\infty \mathrm{d}r' \tilde{\mathcal{K}}(r, r', b')\tilde{n}(Y', r', \rho, b-b')\end{aligned} \tag{5.18}$$

with kernel

$$\begin{aligned}\tilde{\mathcal{K}}(r, r', b) &= \frac{N_C}{\pi}\left(\frac{Q^2r^2}{4}\right)^{b\beta_0} \frac{\Gamma(-b\beta_0)}{\Gamma(1+b\beta_0)}\delta(r'-r) \\ &+ \frac{N_C}{\pi^3}\left(\frac{Q^2}{4}\right)^{b\beta_0} \int_0^1 \frac{\mathrm{d}\omega}{\omega^{\frac{1}{2}}(1-\omega)^{\frac{1}{2}}} \frac{\Gamma(1-\omega b\beta_0)\Gamma(1-(1-\omega)b\beta_0)}{\Gamma(1+\omega b\beta_0)\Gamma(1+(1-\omega)b\beta_0)} \\ &\int \mathrm{d}\hat{r}' \mathcal{J}(r, \hat{r}', r') \left[(r^2)(\hat{r}'^2)^{\omega b\beta_0 - 1}(r'^2)^{(1-\omega)b\beta_0-1} + (\hat{r}'^2)^{b\beta_0-1}\right. \\ &\left. -(\hat{r}'^2)^{\omega b\beta_0-1}(r'^2)^{(1-\omega)b\beta_0} + (r'^2)^{b\beta_0-1} - (\hat{r}'^2)^{\omega b\beta_0}(r'^2)^{(1-\omega)b\beta_0-1}\right]\end{aligned} \tag{5.19}$$

The first term in (5.19) is the contribution from virtual gluon emission and the second term corresponds to real gluon emission. The form of the second term can be traced from the expression for the emission of one real gluon (5.9). Note that the ω dependent Γ functions in the second term arise from performing the integrals over τ and τ' using the standard integral (5.10). The two dimensional integration over transverse coordinates of the emitted real gluon has been transformed according to (3.13) and this explains the presence of the Jacobian $\mathcal{J}$ in the term corresponding to real emission. The properties of this kernel will be investigated in more depth in chapter 6.

It is possible to use the kernel in the form of (5.19) to integrate simple functions analytically and an important application of this will be studied in chapter 6 where deviations from the fixed coupling limit will be examined.

In the realistic case of deep inelastic scattering considered in chapter 7, it is not possible to use analytic methods and computational methods will be employed. In order to write the kernel in a form which is amenable to numerical analysis, the integral over $\hat{r}'$ and the integral over κ, implicit in the definition of the Jacobian $\mathcal{J}$ (3.14) were performed to yield

$$\begin{aligned}
\tilde{\mathcal{K}}(r,r';b) &= \frac{N_c}{\pi}\left(\frac{Q^2r^2}{4}\right)^{b\beta_0}\frac{\Gamma(-b\beta_0)}{\Gamma(1+b\beta_0)}\delta(r-r') \\
&+ 2\frac{N_c}{\pi^2}\frac{1}{r'}\left(\frac{Q^2r'^2}{4}\right)^{b\beta_0} \\
&\times\int_0^1\frac{d\omega}{\omega^{1/2}(1-\omega)^{1/2}}\frac{\Gamma(1-\omega b\beta_0)\,\Gamma(1-(1-\omega)b\beta_0)}{\Gamma(1+\omega b\beta_0)\,\Gamma(1+(1-\omega)b\beta_0)} \\
&\times\left\{\left(\frac{r_>^2}{r'^2}\right)^{b\beta_0-1}{}_2\mathrm{F}_1\left(1-b\beta_0,1-b\beta_0;1;\frac{r_<^2}{r_>^2}\right)\right. \\
&\quad+\left(\frac{r^2-r'^2}{r_>^2}\right)\left(\frac{r_>^2}{r'^2}\right)^{\omega b\beta_0}{}_2\mathrm{F}_1\left(1-\omega b\beta_0,1-\omega b\beta_0;1;\frac{r_<^2}{r_>^2}\right) \\
&\quad\left.-\left(\frac{r_>^2}{r'^2}\right)^{\omega b\beta_0}{}_2\mathrm{F}_1\left(-\omega b\beta_0,-\omega b\beta_0;1;\frac{r_<^2}{r_>^2}\right)\right\} \qquad (5.20)
\end{aligned}$$

where $r_< = \min(r,r')$, $r_> = \max(r,r')$ and ${}_2\mathrm{F}_1$ is the Gauss hypergeometric function. The reader who wishes to perform this transformation explicitly may wish to note that the standard integral involving Bessel functions (5.10) and the integral [47]

$$\int_0^\infty \mathrm{d}x \mathrm{J}_\nu(\alpha x)\mathrm{J}_\mu(\beta x)x^{-\lambda} = \frac{\alpha^\nu}{2^\lambda \beta^{\nu-\lambda+1}} \frac{\Gamma\left(\frac{\nu+\mu-\lambda+1}{2}\right)}{\Gamma\left(\frac{-\nu+\mu+\lambda+1}{2}\right)\Gamma(\nu+1)}$$

$$ {}_2\mathrm{F}_1\left(\frac{\nu+\mu-\lambda+1}{2}, \frac{\nu+\mu-\lambda+1}{2}; \nu+1; \frac{\alpha^2}{\beta^2}\right) \tag{5.21}$$

with $0 < \alpha < \beta$ were required to derive (5.20).

In the next chapter, it shall be shown that an analytic form exists for the result of the action of (5.19) on the function $(r'^2)^\gamma$. This analytic expression will allow the singularity structure of the kernel to be established. The integrated expression for the kernel given by (5.20) will be used in a numerical procedure to confirm these analytical findings.

Chapter 6

Deviations from the Fixed Coupling Limit

In this chapter, the properties of the dipole evolution kernels (5.19) and (5.20) which incorporate a running coupling in Borel space will be studied in depth. A procedure for analysing iterations of the kernel numerically is also introduced and a check that this numerical method produces consistent results is described.

6.1 The Borel Plane Singularity at $b = 0$

At first sight it may appear worrying that the virtual term of the dipole evolution kernel in the Borel plane possesses a pole at $b = 0$ in (5.19) and (5.20) , where $b = 0$ is exactly the point which corresponds to the fixed coupling limit. It was pointed out in chapter 5 that this Borel singularity was ultra-violet in origin and was the Borel space analogue of the logarithmic divergence as $r \to 0$ in the fixed coupling limit. Following Mueller [4], the divergence was regulated by using an ultraviolet cutoff Λ. Alternatively, when considering the kernel with running coupling in Borel space, the Borel space variable b can be used as a dimensional regulator. The $b = 0$ pole in the virtual contribution to $\tilde{\mathcal{K}}$ cancels exactly with an identical singularity which arises from the real contribution. In order to appreciate this, it is necessary to recall some of the properties of the hypergeometric function ${}_2\mathrm{F}_1\left(\alpha, \alpha; 1; x\right)$. The hypergeometric function ${}_2\mathrm{F}_1\left(\alpha, \alpha; 1; x\right)$ is convergent at $x = 1$ only if $2\alpha < 1$ [47]. Define $\zeta_{<>}$ by

$$\zeta_{<>} = \frac{r_<}{r_>} \tag{6.1}$$

Examining the hypergeometric functions of (5.20) in the limit $b \to 0$, it is observed that the only divergent contribution in this limit comes from the hypergeometric function ${}_2\mathrm{F}_1\left(1 - b\beta_0, 1 - b\beta_0; 1; \zeta_{<>}^2\right)$ with $\zeta_{<>} = 1$. When $\zeta_{<>} = 1$, this is the region where a gluon is emitted at an impact parameter almost equal to that of the parent dipole. It is possible to specify the divergence of ${}_2\mathrm{F}_1\left(1 - b\beta_0, 1 - b\beta_0; 1; \zeta_{<>}^2\right)$ more exactly by using the linear transformation property of the ${}_2\mathrm{F}_1$ function. For a hypergeometric function ${}_2\mathrm{F}_1\left(1 - \alpha, 1 - \alpha; 1; x\right)$ the transformation [47]

$${}_2\mathrm{F}_1\left(1 - \alpha, 1 - \alpha; 1; x\right) = (1 - x)^{-1+2\alpha}{}_2\mathrm{F}_1\left(\alpha, \alpha; 1; x\right) \tag{6.2}$$

parameterises the divergent term. Using this transformation, the kernel takes the form

$$\begin{aligned} \tilde{\mathcal{K}}(r, r', b) = \frac{N_C}{\pi}\left(\frac{Q^2 r^2}{4}\right)^{b\beta_0} \Bigg\{ & -\frac{1}{b\beta_0} \\ & + \frac{2}{r'}(1 - \zeta_{<>}^2)^{-1+2b\beta_0}{}_2\mathrm{F}_1\left(b\beta_0, b\beta_0; 1; \zeta_{<>}^2\right) + (\text{Finite Terms}) \Bigg\} \end{aligned} \tag{6.3}$$

in the limit $b \to 0$. Note that ${}_2\mathrm{F}_1\left(0,0;1;x\right) = 1$ for all x. The singular factor $(1-\zeta_{<>}^2)^{-1+2b\beta_0}$ can be expressed in terms of distributions as

$$(1-\zeta_{<>}^2)^{-1+2b\beta_0} = 2\left(\frac{1}{4b\beta_0}\delta(1-\zeta_{<>}) + \frac{1}{2}\left(\frac{1}{1-\zeta_{<>}}\right)_+ + \cdots\right) \tag{6.4}$$

where the overall factor of two reflects the fact that the $\zeta_{<>} \to 1$ limit can be approached from above or below. By substituting this expansion into (6.3) and simplifying the δ functions it can be seen that the singular parts of the real and virtual terms cancel in the limit as $b \to 0$ leaving a finite result. From this analysis, it can be concluded that the Borel transformed kernel is finite in the fixed coupling limit and in the next section, it will be demonstrated that the action of the kernel on a function of the form $(r'^2)^\gamma$ yields the same results in the fixed coupling regime as the BFKL kernel. The cancellation between real and virtual terms will be considered in a related fashion in section 6.3 where the algorithm for implementing the kernel into a numerical framework is discussed.

6.2 The Borel Singularity of the Dipole Cascade

In order to study the Borel singularity generated by the dipole kernel $\tilde{\mathcal{K}}$, consider its action on a test function of the form $(r'^2)^\gamma$. Although the form of this test function is not physically realistic, the integrals can be performed analytically and the analysis will reveal results which are independent of the nature of the test function. Using the representation of the kernel defined by (5.19) the integral

$$\int_0^\infty \mathrm{d}r' \tilde{\mathcal{K}}(r, r', b)(r'^2)^\gamma =$$

$$\frac{N_C}{\pi} \int_0^\infty \mathrm{d}r' \left(\frac{Q^2 r'^2}{4}\right)^{b\beta_0} \frac{\Gamma(-b\beta_0)}{\Gamma(1+b\beta_0)} (r'^2)^\gamma \delta(r - r')$$

$$+ \int_0^\infty \mathrm{d}r' \int_0^\infty \mathrm{d}\hat{r}' \mathcal{J}(r, \hat{r}', r') \int_0^1 \frac{\mathrm{d}\omega}{\omega^{\frac{1}{2}}(1-\omega)^{\frac{1}{2}}}$$

$$\frac{\Gamma(1-\omega b\beta_0)}{\Gamma(1+\omega b\beta_0)} \frac{\Gamma(1-(1-\omega)b\beta_0)}{\Gamma(1+(1-\omega)b\beta_0)}$$

$$\Big[(r^2)(\hat{r}'^2)^{\omega b\beta_0 - 1}(r'^2)^{2(1-\omega)b\beta_0+\gamma-1} - (\hat{r}'^2)^{2\omega b\beta_0-1}(r'^2)^{2(1-\omega)b\beta_0+\gamma}$$

$$+(\hat{r}'^2)^{b\beta_0-1}(r'^2)^\gamma + (r'^2)^{b\beta_0+\gamma-1} - (\hat{r}'^2)^{2\omega b\beta_0}(r'^2)^{(1-\omega)b\beta_0-1+\gamma}\Big] \tag{6.5}$$

must be performed. Standard Feynman parameterisation methods allow one to develop the integral

$$\int \frac{\mathrm{d}^2\hat{\boldsymbol{r}}'}{(\hat{\boldsymbol{r}}'^2)^\alpha(\boldsymbol{r}'^2)^\beta} = \pi \frac{\Gamma(\alpha+\beta-1)\Gamma(1-\alpha)\Gamma(1-\beta)}{\Gamma(\alpha)\Gamma(\beta)\Gamma(2-\alpha-\beta)}(\boldsymbol{r}^2)^{1-\alpha-\beta} \tag{6.6}$$

Recall that $\boldsymbol{r}^2 \equiv r^2$ and that $\boldsymbol{r}' = \hat{\boldsymbol{r}}' - \boldsymbol{r}$. By using (3.13) to rewrite the integrals over transverse sizes as an integral over the two dimensional coordinate $\hat{\boldsymbol{r}}'$ again, relation (6.6) can be used to perform the transverse coordinate integration analytically. Defining the function $\chi(\gamma, b)$ through the equation

$$\int_0^\infty \mathrm{d}r' \, \tilde{\mathcal{K}}(r, r', b)(r'^2)^\gamma = \frac{N_c}{\pi}\chi(\gamma, b)\left(\frac{Q^2 r^2}{4}\right)^{b\beta_0}(r^2)^\gamma, \tag{6.7}$$

it is found after some manipulation of Γ functions that $\chi(\gamma, b)$ takes the form

$$\begin{aligned}\chi(\gamma,b) &= \frac{\Gamma(-b\beta_0)}{\Gamma(1+b\beta_0)} \\ &+ \frac{\Gamma(-\gamma-b\beta_0)}{\Gamma(1+\gamma+b\beta_0)}\frac{1}{\pi}\int_0^1 \frac{d\omega}{\omega^{1/2}(1-\omega)^{1/2}}\frac{\Gamma(1-\omega b\beta_0)}{\Gamma(1+\omega b\beta_0)}\frac{\Gamma(1-(1-\omega)b\beta_0)}{\Gamma(1+(1-\omega)b\beta_0)} \\ &\times\left[\frac{\Gamma(1+\gamma)}{\Gamma(-\gamma)}\frac{\Gamma(b\beta_0)}{\Gamma(1-b\beta_0)} - 2\frac{\Gamma(1+\gamma+(1-\omega)b\beta_0)}{\Gamma(1-\gamma-(1-\omega)b\beta_0)}\frac{\Gamma(1+\omega b\beta_0)}{\Gamma(1-\omega b\beta_0)}\right] \qquad (6.8)\end{aligned}$$

where the first term is due to virtual correction and the second from real emission. The virtual contribution to $\chi(\gamma, b)$ contains a series of poles at $b\beta_0 = 1, 2, 3...$ which are identified with infra-red renormalons and correspond to power corrections of $\mathcal{O}((\Lambda^2_{QCD}/Q^2)^n)$, $n = 1, 2, ...$ Note that these poles are independent of the specific form of the test function. This set of poles, resulting from the exponentiation of soft radiation, has also been derived in the context of the Drell-Yan process [48]. In addition, the presence of a series of poles at $b\beta_0 = n - \gamma$, $n = 0, 1, 2...$ is also observed and these poles are generated by the $\Gamma(-\gamma - b\beta_0)$ dependence of the real contribution to $\chi(\gamma, b)$. For $Re(\gamma) \geq m$ these poles correspond to infra-red renormalons for $n > m$. Their infra-red origin is established by observing that these singularities arise from the $r' > r$ integration region of eq. (6.7), where the offspring dipole is emitted with size larger than the parent dipole. At first inspection, the γ-dependent poles indicate the presence of $\mathcal{O}((\Lambda^2_{QCD}/Q^2)^{n-\gamma})$ power corrections. At this stage, it suffices to note that in this section the properties of the dipole cascade are being studied independently of its embedding in a particular physical process. The interpretation of the γ-dependent power corrections in terms of OPE matrix elements is not an issue here. In the case of deep inelastic scattering no such singularities will be present and this shall be explained in chapter 7.

As the kernel is regular around $b = 0$ the power series expansion in b of $\chi(\gamma, b)$

was computed. From the analytic form (6.8) the expansion

$$\chi(\gamma,b)=\chi^{(0)}(\gamma)+b\beta_0\chi^{(1)}(\gamma)+\mathcal{O}(b^2\beta_0^2)\,. \tag{6.9}$$

was obtained, where

$$\chi^{(1)}(\gamma)=-\frac{1}{\gamma}\chi^{(0)}(\gamma)-2\Psi(1)\chi^{(0)}(\gamma)+\frac{1}{2}\chi^{(0)}(\gamma)^2+\frac{1}{2}\chi^{(0)\prime}(\gamma) \tag{6.10}$$

The $\mathcal{O}(1/b)$ singular terms have cancelled as anticipated and the $\mathcal{O}(b^0)$ term is the BFKL spectral function $\chi^{(0)}(\gamma)$, (2.27). The intercept of the trajectory of the perturbative pomeron is determined by $\chi(1/2)$. The term linear in b in (6.9) determines the correction to this intercept from the running coupling to the first non-trivial order in perturbation theory. Thus to order α_s^2, the intercept becomes

$$\alpha_P(0)=1+\frac{4\ln 2\,\alpha_s N_c}{\pi}\left(1-2\alpha_s\beta_0(1-\ln 2+\Psi(1))\right)\,. \tag{6.11}$$

In order to study the Borel singularities of the dipole cascade after multiple iterations of the kernel, it is convenient to view the dipole density $n(Y,r,\rho)$ in terms of its Laplace and Mellin transforms. Returning to the dipole evolution equation (5.18) the Laplace is taken with respect to the rapidity Y

$$\tilde{n}_\omega(r,\rho,b)=\int_0^\infty \mathrm{d}Y e^{-\omega Y}\tilde{n}(Y,r,\rho.b)\,, \tag{6.12}$$

and the anomalous dimension γ is introduced via the Mellin transform

$$\tilde{n}_{\omega,\gamma}(b)=\int_0^\infty \frac{\mathrm{d}r^2}{r^2}\left(\frac{r^2}{\rho^2}\right)^{-\gamma}\tilde{n}_\omega(r,\rho,b)\,. \tag{6.13}$$

Implementing these transforms and using the defining equation for $\chi(\gamma,b)$, (6.7), converts (5.18) into an equation for the spectral amplitudes $\tilde{n}_{\omega,\gamma}(b)$,

$$\begin{aligned}\omega\,\tilde{n}_{\omega,\gamma}(b) =&2\delta(b)\\ &+\frac{N_c}{\pi}\int_0^b \mathrm{d}b'\,\chi(\gamma-b'\beta_0,b')\left(\frac{Q^2\rho^2}{4}\right)^{b'\beta_0}\tilde{n}_{\omega,\gamma-b'\beta_0}(b-b')\,. \qquad (6.14)\end{aligned}$$

This equation is universal for all semihard processes. The dipole density is reconstructed from the spectral amplitudes as

$$\tilde{n}(Y,r,\rho,b)=\int\frac{\mathrm{d}\omega}{2\pi i}e^{\omega Y}\int\frac{\mathrm{d}\gamma}{2\pi i}\left(\frac{r^2}{\rho^2}\right)^{\gamma}\tilde{n}_{\omega,\gamma}(b)\,. \qquad (6.15)$$

The equation governing the spectral amplitudes (6.14) is an integral equation of the Volterra type. Such equations are known not to have eigenfunctions for bounded kernels. One way of constructing solutions is by iteration. In this case, the iterative solution is given by the formal expression

$$\tilde{n}_{\omega,\gamma}(b)=\sum_{k=0}^{\infty}\tilde{n}^{(k)}_{\omega,\gamma}(b)\,, \qquad (6.16)$$

with

$$\begin{aligned}\tilde{n}^{(0)}_{\omega,\gamma}(b)&=\frac{2}{\omega}\delta(b)\\ \tilde{n}^{(1)}_{\omega,\gamma}(b)&=\frac{2}{\omega}\left(\frac{N_c}{\pi\omega}\right)\left(\frac{Q^2\rho^2}{4}\right)^{b\beta_0}\chi(\gamma-b\beta_0,b) \qquad (6.17)\\ & \qquad (6.18)\end{aligned}$$

and

$$\tilde{n}^{(k)}_{\omega,\gamma}(b) = \frac{2}{\omega}\left(\frac{N_c}{\pi\omega}\right)^k \left(\frac{Q^2\rho^2}{4}\right)^{b\beta_0} \int_0^b db_{k-1}\,\chi(\gamma - (b-b_{k-1})\beta_0, b - b_{k-1})$$
$$\times \int_0^{b_{k-1}} db_{k-2}\,\chi(\gamma - (b-b_{k-2})\beta_0, b_{k-1} - b_{k-2}) \ldots$$
$$\times \int_0^{b_3} db_2\,\chi(\gamma - (b-b_2)\beta_0, b_3 - b_2)$$
$$\times \int_0^{b_2} db_1\,\chi(\gamma - (b-b_1)\beta_0, b_2 - b_1)\,\chi(\gamma - b\beta_0, b_1)\,, \tag{6.19}$$

for $k \geq 2$. The index k counts the number of iterations of the kernel in eq. (6.14).

Having identified the infra-red renormalon poles of $\chi(\gamma, b)$, through (6.8), the Borel singularities of the spectral amplitude $\tilde{n}_{\omega,\gamma}(b)$ can be studied using (6.19). The contribution to $\tilde{n}^{(k)}_{\omega,\gamma}(b)$ from the virtual (γ-independent) terms only is

$$\frac{2}{\omega}\left(\frac{N_c}{\omega\pi}\right)^k \left(\frac{Q^2\rho^2}{4}\right)^{b\beta_0} \times \int_0^b db_{k-1}\,\frac{\Gamma(-(b-b_{k-1})\beta_0)}{\Gamma(1+(b-b_{k-1})\beta_0)}$$
$$\times \int_0^{b_{k-1}} db_{k-2}\,\frac{\Gamma(-(b_{k-1}-b_{k-2})\beta_0)}{\Gamma(1+(b_{k-1}+b_{k-2})\beta_0)}\cdots$$
$$\times \int_0^{b_2} db_1\,\frac{\Gamma(-(b_2-b_1)\beta_0)}{\Gamma(1+(b_2+b_1)\beta_0)}\,\frac{\Gamma(-b_1\beta_0)}{\Gamma(1+b_1\beta_0)}\,. \tag{6.20}$$

As the b-integrals are nested, for $b < 1/\beta_0$ no new singularity is introduced in the solution from these virtual corrections. For $b > 1/\beta_0$ some of the Γ-function poles will be encountered on the b-integration paths turning the leading $b = 1/\beta_0$ pole into a branch cut. Real contributions introduce singularities on the positive b-semiaxis for real γ, and for $0 < \gamma < 1$, the leading singularity is found from (6.18, 6.19) to be located at $b = \gamma/\beta_0$. Note that for $b\beta_0 < \gamma$ the real contributions to $\tilde{n}^{(k)}_{\omega,\gamma}(b)$ will not generate singularities because none of the poles of the χ-functions in (6.19) are encountered along the nested b-integration paths. For $b\beta_0 > \gamma$, as in the case of virtual contributions, poles are found along some of the b-paths turning the leading $b = \gamma/\beta_0$ pole into a branch cut. From (6.8, 6.19) it follows that there are also singularities for negative values of b. This means that $b = \gamma/\beta_0$ is the position of the leading singularity for positive b *only* when γ is in the range $0 < \gamma < 1$. If we were to take γ in the range $n < \gamma < n+1$, $n \in Z$, then the leading infra-red singularity would be at $\gamma - n$, and the singularities for negative b would be displaced further to the left on the negative b-semiaxis. Although these singularities do not affect the estimate of the power corrections from the non-perturbative effects, they reflect the fact that as γ increases the dipole densities generated from these test functions become increasingly infra-red divergent.

The above argument can be repeated for the contributions to the solution from cross products of virtual terms for some of the χ-functions and real terms for the rest. The net result of this analysis is that the region of analyticity in Borel space of $\tilde{n}_{\omega,\gamma}(b)$ with $0 < \gamma < 1$ contains the interval $0 < b < \gamma/\beta_0$ and the leading singularity is a branch cut at $b = \gamma/\beta_0$. In the asymptotic limit $Y \to \infty$ the anomalous dimension is $\gamma = 1/2 + i\nu$ with ν the spectral parameter to be integrated over in eq. (6.15). Such a $Re(\gamma)$ implies the presence of power corrections of $\mathcal{O}(\Lambda_{QCD}/Q)$ for the dipole density $n(Y, r, \rho)$. These $1/Q$ power corrections have also been reported in the context of conventional BFKL approach [30]. These renormalon singularities herald an ambiguity in the $1/Q$ corrections to the effective pomeron trajectory. Therefore, it is not possible to calculate the effect of such singularities on the pomeron intercept. One can, however, easily imagine that these non-perturbative power corrections could be important in resolving the conflict between the intercepts of the perturbative pomeron and the soft pomeron discussed in chapter 2.

The evolution equation (5.18) is not conformally invariant because the action of the dipole kernel results in a shift of γ by $b'\beta_0$ in eq. (6.14). However, having established a region of analyticity in Borel space that contains $b = 0$, the b-expansion can be employed as a measure of deviation from the conformal limit. From (6.9, 6.19) the b-expansion of the spectral amplitude generated after k iterations of the kernel is

$$\begin{aligned}\tilde{n}^{(k)}_{\omega,\gamma}(b)\frac{2}{\omega}\left(\frac{N_c}{\pi\omega}\right)^k \Bigg\{ & \frac{b^{k-1}}{(k-1)}\chi(\gamma)^k \\ & + \frac{b^k}{(k-1)!}\left[\beta_0 \ln\left(\frac{Q^2\rho^2}{4}\right)\chi(\gamma)^k + \beta_0\chi^{(1)}(\gamma)\chi(\gamma)^{k-1}\right] \\ & -\frac{b^k}{2}\frac{(k+1)}{(k-1)!}\beta_0\chi(\gamma)^{k-1}\frac{\mathrm{d}\chi(\gamma)}{\mathrm{d}\gamma} + \mathcal{O}(b^{k+1})\Bigg\}\end{aligned} \tag{6.21}$$

The full spectral amplitude $n_{\omega,\gamma}(b)$, defined in eq. (6.16), can be constructed in the small-b region from summing the powers of b. Summation of the leading powers of b, *ie.* retaining only the $\mathcal{O}(b^{k-1})$ terms in eq. (6.21) is required in the region

$$b \ll 1, \qquad \frac{N_c\chi(\gamma)}{\pi\omega}b \sim 1\,. \tag{6.22}$$

This 'resummation' of the $\mathcal{O}(N_c\chi(\gamma)b/(\omega\pi))$ terms is well defined if the $\mathcal{O}(b^k)$ terms are small relative to the $\mathcal{O}(b^{k-1})$ terms in eq. (6.21). For the $\mathcal{O}(b^k\ln(Q^2\rho^2/4))$ term this translates to the requirement

$$b\beta_0 \ln\frac{Q^2\rho^2}{4} \ll 1 \Leftrightarrow b\left(\frac{1}{\alpha_s(Q^2)} - \frac{1}{\alpha_s(1/\rho^2)}\right) \ll 1\,. \tag{6.23}$$

Hence, leading b-power resummation is valid in the conformal limit of fixed coupling. In this case the Borel transform can be readily inverted in terms of a fixed

α_s to yield the well known answer for the BFKL spectral amplitude

$$\begin{aligned} n_{\omega,\gamma} &= \sum_{k=0}^{\infty} \frac{2}{\omega}\left[1+\frac{N_c\alpha_s\chi(\gamma)}{\pi\omega}+\left(\frac{N_c\alpha_s\chi(\gamma)}{\pi\omega}\right)^2+\ldots\right] \\ &= \frac{2}{\omega-N_c\alpha_s\chi(\gamma)/\pi} \end{aligned} \tag{6.24}$$

and via eq. (6.15) the asymptotic solution for the dipole density is obtained (3.29). The dipole density in Borel space can therefore be identified with the usual asymptotic solution for n in the fixed coupling limit.

6.3 A Numerical Procedure to Integrate $\tilde{\mathcal{K}}$

The test function $(r'^2)^\gamma$ allowed a closed form for the action of the kernel on $(r'^2)^\gamma$ to be determined, that is $\chi(\gamma, b)$ in (6.8). In the case of deep inelastic scattering which is considered in chapter 7, the integrals which have to be performed do not lend themselves to such an analysis and instead, computational methods will be employed. In order to test the numerical implementation of the kernel (5.20), the integral which defines the analytic χ function was performed numerically. The translation of (5.20) into a framework which permits an efficient and accurate numerical analysis of the dipole kernel is described below. In this section it shall be assumed that the function upon which the kernel acts is $f(r')\delta(b)$. In general, the b dependence of the function upon which the kernel acts will be more complex than this and an explicit convolution over the Borel variable will be required but the transformations to the kernel discussed in this section do not involve the Borel variable explicitly so the freedom exists to make this simplifying assumption.

Firstly, note that the ω dependence in the part of the kernel corresponding to real emission (the second term of (5.20)) can be written in the form

$$\tilde{\mathcal{K}}_R = \int_0^1 \frac{d\omega}{\omega^{\frac{1}{2}}(1-\omega)^{\frac{1}{2}}} R(r, r', \omega) \tag{6.25}$$

where the subscript R has been used to signify that the real part of the kernel only is being considered. From inspection of (5.20) it can be observed that the function $R(r, r', \omega)$ contains no singularities in ω. The end point singularities which occur in (6.25) are integrable but it was found that the numerical quadrature routines used in this study introduced inaccuracies when the ω integration was performed according to (6.25). Instead, the change of variables

$$\omega = \sin^2\left(\frac{\omega'}{2}\right) \tag{6.26}$$

was made which converts (6.25) into the more manageable form

$$\tilde{\mathcal{K}}_R = \int_0^{\pi} d\omega' R(r, r', \omega') \tag{6.27}$$

Recall that the variables $r_< \equiv \min(r, r')$ and $r_> \equiv \max(r, r')$ were used in the expression of $\tilde{\mathcal{K}}_R$, (5.20). The introduction of these variables was necessary because of the structure of the standard integral (5.21). In order to integrate the kernel numerically, it is more convenient to split the r' integration region into two parts where the sectioning embodies the requirements demanded by (5.21), that is two integrations over r' with ranges $0 \leq r' \leq r$ and $r \leq r' < \infty$ are considered.

$$\int_0^{\infty} dr' \tilde{\mathcal{K}}(r, r', b) f(r') = \int_0^{r} dr' \tilde{\mathcal{K}}(r, r', b) f(r') + \int_r^{\infty} dr' \tilde{\mathcal{K}}(r, r', b) f(r') \tag{6.28}$$

A change of variables from r' to ζ is then performed on each of these integrals where

$$\zeta = \frac{r'}{r} \quad \text{in the range} \quad 0 \leq r' \leq r \tag{6.29}$$

$$\zeta = \frac{r}{r'} \quad \text{in the range} \quad r \leq r' < \infty \tag{6.30}$$

which converts the integrations on the right hand side of (6.28) as follows

$$\int_0^\infty \mathrm{d}r' \tilde{\mathcal{K}}(r, r'. b) f(r') = \int_0^1 \mathrm{d}\zeta \tilde{\mathcal{K}}_{1R}(r, \zeta, b) f(r\zeta) + \int_0^1 \mathrm{d}\zeta \tilde{\mathcal{K}}_{2R}(r, \zeta, b) f(r/\zeta) \tag{6.31}$$

and where $\tilde{\mathcal{K}}_{1R}$ and $\tilde{\mathcal{K}}_{2R}$ have the form

$$\begin{aligned} \tilde{\mathcal{K}}_{1R} = {} & \frac{2N_C}{\pi^2} \left(\frac{Q^2 r^2}{4} \right)^{b\beta_0} \int_0^\pi \mathrm{d}\omega' \frac{\Gamma(1-(1-s(\omega'))b\beta_0)}{\Gamma(1+(1-s(\omega'))b\beta_0)} \frac{\Gamma(1-s(\omega')b\beta_0)}{\Gamma(1+s(\omega')b\beta_0)} \\ & \times \left[\zeta (1-\zeta^2)^{-1+2b\beta_0} {}_2\mathrm{F}_1 \left(b\beta_0, b\beta_0; 1; \zeta^2 \right) \right. \\ & \quad + \zeta^{2b\beta_0(1-s(\omega'))-1} (1-\zeta^2)^{2s(\omega')b\beta_0} {}_2\mathrm{F}_1 \left(s(\omega')b\beta_0, s(\omega')b\beta_0; 1; \zeta^2 \right) \\ & \quad \left. - \zeta^{2b\beta_0(1-s(\omega'))-1} {}_2\mathrm{F}_1 \left(-s(\omega')b\beta_0, -s(\omega')b\beta_0; 1; \zeta^2 \right) \right] \end{aligned} \tag{6.32}$$

$$\begin{aligned} \tilde{\mathcal{K}}_{2R} = {} & \frac{2N_C}{\pi^2} \left(\frac{Q^2 r^2}{4} \right)^{b\beta_0} \int_0^\pi \mathrm{d}\omega' \frac{\Gamma(1-(1-s(\omega'))b\beta_0)}{\Gamma(1+(1-s(\omega'))b\beta_0)} \frac{\Gamma(1-s(\omega')b\beta_0)}{\Gamma(1+s(\omega')b\beta_0)} \\ & \times \left[\zeta^{-2b\beta_0-1} (1-\zeta^2)^{-1+2b\beta_0} {}_2\mathrm{F}_1 \left(b\beta_0, b\beta_0; 1; \zeta^2 \right) \right. \\ & \quad - \zeta^{-2b\beta_0-1} (1-\zeta^2)^{2s(\omega')b\beta_0} {}_2\mathrm{F}_1 \left(s(\omega')b\beta_0, s(\omega')b\beta_0; 1; \zeta^2 \right) \\ & \quad \left. - \zeta^{-2b\beta_0-1} {}_2\mathrm{F}_1 \left(-s(\omega')b\beta_0, -s(\omega')b\beta_0; 1; \zeta^2 \right) \right] \end{aligned} \tag{6.33}$$

and $s(\omega')$ has been defined as

$$s(\omega') \equiv \sin^2(\omega'/2) \tag{6.34}$$

in an effort to simplify the expressions for $\tilde{\mathcal{K}}_{1R}$ and $\tilde{\mathcal{K}}_{2R}$. Note that the hypergeometric functions have been written in terms of their transformed representation according to (6.2). When the kernel is supplied with a Borel argument b greater than $0.5/\beta_0$, the untransformed hypergeometric functions are convergent at $\zeta = 1$ and these convergent functions are used in the numerical analysis, *eg.* ${}_2\mathrm{F}_1\left(1 - b\beta_0, 1 - b\beta_0; 1; \zeta^2\right)$ is used instead of $(1-\zeta^2)^{-1+2b\beta_0}{}_2\mathrm{F}_1\left(b\beta_0, b\beta_0; 1; \zeta^2\right)$ for $b\beta_0 > 0.5$ and so on.

It was demonstrated in section 6.1 that the ultra-violet singularities at $b = 0$ present in both the real and virtual contributions to the kernel cancelled against each other. Despite this, the numerical treatment of the $b = 0$ region requires careful attention to ensure that this cancellation between the real and virtual parts actually occurs. Recall that only the first terms in (6.32) and (6.33) are responsible for the singularity as $\zeta \to 1$. Consider the integral over ζ of the first term in (6.32) as an example. It can be written in the form

$$\int_0^1 \mathrm{d}\zeta \frac{\mathcal{P}_1(\zeta, b)}{(1-\zeta)^{1-2b\beta_0}} = \frac{\mathcal{P}_1(\zeta = 1, b)}{2b\beta_0} + \int_0^1 \frac{\mathcal{P}_1(\zeta, b) - \mathcal{P}_1(\zeta = 1, b)}{(1-\zeta)^{1-2b\beta_0}} \tag{6.35}$$

where the function $\mathcal{P}_1(b, \zeta)$ is constructed from the first term of $\tilde{\mathcal{K}}_{1R}$ and takes the form

$$\mathcal{P}_1(\zeta, b) = \frac{2N_C}{\pi^2}\left(\frac{Q^2r^2}{4}\right)^{b\beta_0} \int_0^\pi \mathrm{d}\omega' \frac{\Gamma(1-(1-s(\omega'))b\beta_0)\,\Gamma(1-s(\omega')b\beta_0)}{\Gamma(1+(1-s(\omega'))b\beta_0)\,\Gamma(1+s(\omega')b\beta_0)}$$
$$\times\, \zeta(1+\zeta)^{-1+2b\beta_0}{}_2\mathrm{F}_1\left(b\beta_0, b\beta_0; 1; \zeta^2\right) f(r\zeta) \tag{6.36}$$

The same procedure is applied to the first term of $\tilde{\mathcal{K}}_{2R}$ and a function $\mathcal{P}_2(\zeta, b)$ can be constructed in the same way. Note that this rearrangement of the ζ integral is analogous to the parameterisation of the singular part of the kernel in terms of distributions (6.4) with the overall factor of 2 in (6.4) being accounted for by the fact that two integrals, one with kernel $\tilde{\mathcal{K}}_{1R}$ and the other with kernel $\tilde{\mathcal{K}}_{2R}$ are being performed. It should be noted that both $\mathcal{P}_1(\zeta, b)$ and $\mathcal{P}_2(\zeta, b)$, reproduced in (6.37), coincide at $\zeta = 1$ by definition.

$$\mathcal{P}_2(\zeta, b) = \frac{2N_C}{\pi^2}\left(\frac{Q^2r^2}{4}\right)^{b\beta_0} \int_0^{\pi} d\omega' \frac{\Gamma(1-(1-s(\omega'))b\beta_0)}{\Gamma(1+(1-s(\omega'))b\beta_0)} \frac{\Gamma(1-s(\omega')b\beta_0)}{\Gamma(1+s(\omega')b\beta_0)}$$

$$\times\, \zeta^{-2b\beta_0-1}(1+\zeta)^{-1+2b\beta_0}\,{}_2\mathrm{F}_1\left(b\beta_0, b\beta_0; 1; \zeta^2\right) f(r/\zeta) \qquad (6.37)$$

Also, $\mathcal{P}_1(\zeta, b)$ and $\mathcal{P}_2(\zeta, b)$ approach $\mathcal{P}_1(\zeta = 1, b)$ faster than $(1-\zeta)$ so that the integrations over ζ give finite results. Examining the structure of (6.36) and (6.37) at $\zeta = 1$ demonstrates that the coefficients of the $b = 0$ pole terms in $\tilde{\mathcal{K}}_{1R}$,$\tilde{\mathcal{K}}_{2R}$ and the virtual part of the kernel sum to zero so that the overall kernel is finite. Numerical tests showed that this method of rewriting the real part of the kernel was sufficient to guarantee finite results as $b \to 0$. The procedures which have been described were found to provide the most efficient way of incorporating the Borel transformed dipole evolution kernel (5.20) into a numerical quadrature routine. In the next section, results are presented to show that the transformations on (5.20) in this section are entirely consistent and that the function $\chi(\gamma, b)$ is returned when the kernel acts on the test function $(r'^2)^\gamma$.

6.4 Numerical Evaluation of $\chi(\gamma, b)$

In this section, results are presented which demonstrate that performing the numerical integration of the kernel (6.7) using the algorithm discussed in section 6.3 returns the χ function defined by (6.8). The results are presented here for

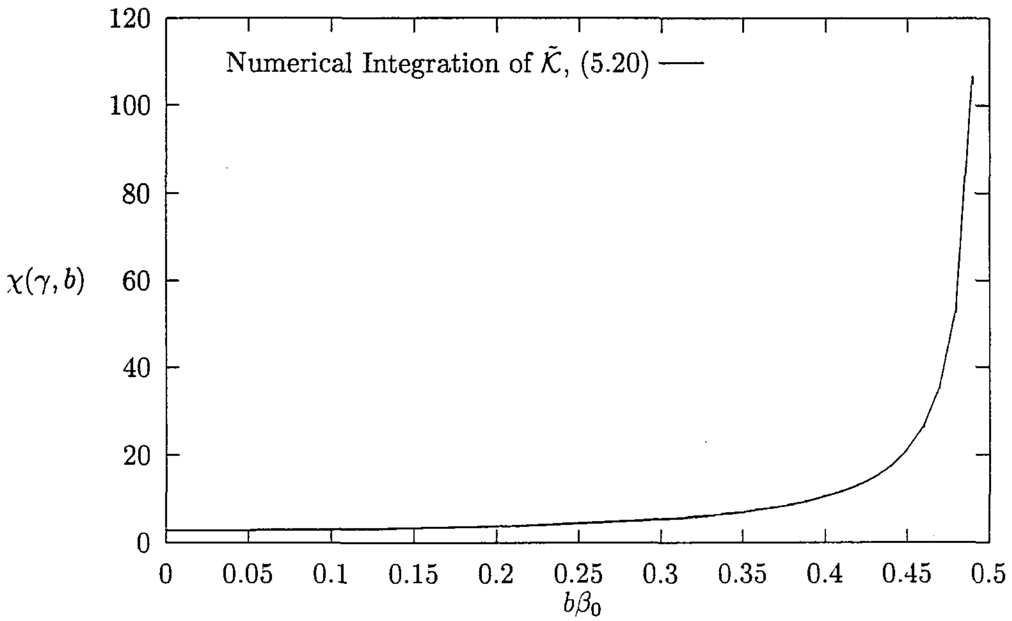

Figure 6.1: Numerically evaluated $\chi(\gamma, b)$ plotted against $b\beta_0$ demonstrating the singularity as $b\beta_0 \to 0.5$

the case $\gamma = 0.5$.

From the analytical expression for $\chi(\gamma, b)$ and the discussion which follows equation (6.8), it is expected that the χ function will be finite at $b = 0$ with a value of $\chi^{(0)}(0.5)$. A pole term is also expected to be present at $b\beta_0 = \gamma = 0.5$. The graph illustrated in fig. 6.1 shows $\chi(\gamma, b)$ determined by numerical integration of $\tilde{\mathcal{K}}$ acting on $(r'^2)^\gamma$ plotted against $b\beta_0$ over the range $0 \leq b\beta_0 < 0.5$. The singular behaviour of $\chi(\gamma, b)$ is clearly present as $b\beta_0 \to 0.5$. The data near $b\beta_0 = 0.5$ was fitted to the form

$$\frac{1.05}{0.5 - b\beta_0} \tag{6.38}$$

confirming the presence of a simple pole at $b\beta_0 = 0.5$. To check the consistency of the numerical integration over $\tilde{\mathcal{K}}$, (5.20) over the full range of b, the ω integration in the analytic expression for $\chi(\gamma, b)$, (6.8) was evaluated numerically using

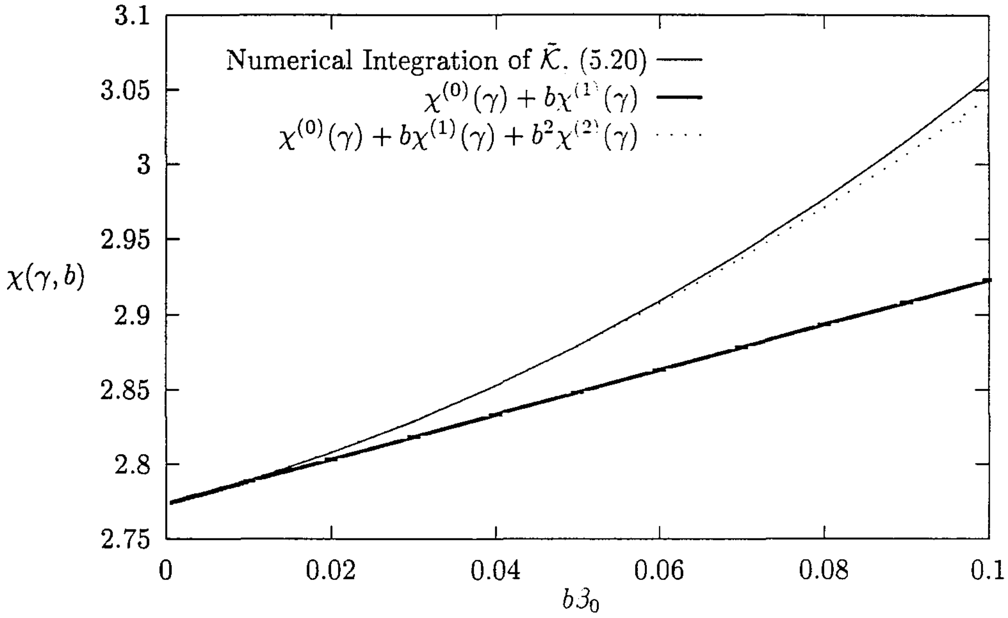

Figure 6.2: Numerically evaluated $\chi(\gamma, b)$ plotted against $b\beta_0$ in the region of $b = 0$. Linear and quadratic approximations in b derived from the analytic expression for $\chi(\gamma, b)$ near $b = 0$ are also plotted.

the transformation described in (6.26). As one might expect, the same results were obtained by using this method to determine $\chi(\gamma, b)$ as were obtained by integrating the kernel numerically. It was observed however that the results obtained in the region of the singularity at $b\beta_0 = 0.5$ were slightly more unstable in the case where $\tilde{\mathcal{K}}$ was integrated numerically. These instabilities were not serious however and it was concluded that the algorithm used to integrate $\tilde{\mathcal{K}}$ numerically was satisfactory.

The region of Borel space near $b = 0$ in fig. 6.1 is magnified in fig. 6.2. Numerical evaluation of $\chi(\gamma, b)$ was performed for b values as low as $b \simeq 1.0 \times 10^{-3}$ and finite results were obtained, confirming that the procedure introduced in section 6.3 to ensure the cancellation between real and virtual singularities at $b = 0$ is effective. The other plots in fig. 6.2 show the linear and quadratic power series approximations in b to $\chi(\gamma, b)$ near $b = 0$. When $\gamma = 0.5$, the coefficient functions

$\chi^{(0)}(\gamma), \chi^{(1)}(\gamma)$ and $\chi^{(2)}(\gamma)$ used to construct the power series expansion in b take the numerical values

$$\begin{aligned} \chi^{(0)}(0.5) &= 2.773 \\ \chi^{(1)}(0.5) &= 1.500 \\ \chi^{(2)}(0.5) &= 12.19 \end{aligned} \tag{6.39}$$

The $b = 0$ intercept of χ evaluated numerically was found to be $\chi^{(0)}(0.5) = 4 \ln 2$ which is the numerical factor found in the BFKL case.

In chapter 7, no analytic expressions for the integral of the kernel are available and numerical methods will provide the only results. The success of the numerical method to determine χ accurately is therefore encouraging.

Chapter 7

The Borel Singularity Structure of Small-x DIS

The analysis of chapter 6 examined the singularity structure of the Borel transformed evolution kernel and the dipole density n in some detail. The objective of this chapter is to apply the dipole formalism to describe deep inelastic scattering at small-x. The analysis will be carried out in the Borel plane and the Borel singularity structure of the small-x structure functions will be determined numerically.

Although the operator product expansion can be used to determine higher twist power contributions to deep inelastic scattering functions this approach is only valid outside the high energy limit because of the two large ordered scales which characterise the small-x limit of QCD. It is found that order of the power corrections that the approach used in this study predicts are consistent with those obtained by the conventional operator product expansion.

7.1 The Borel Transform of the DIS Structure Functions

The form of the structure function $F_L(x, Q^2)$ where L denotes the longitudinal structure function can be constructed in the dipole approach from the defining equation (2.39) and the expression derived for the cross section for the interaction between a longitudinally polarised virtual photon and a proton (3.34). Accordingly, in the Borel plane, the Borel transformed expression for the structure function $\tilde{F}_L(x, Q^2, b)$ is given by

$$\begin{aligned}\tilde{F}_L(x, Q^2, b) &= \frac{Q^2}{4\pi\alpha_{em}} \int_0^1 \mathrm{d}z \mathrm{d}^2\boldsymbol{r} \Phi_L^{(0)}(\boldsymbol{r}, z) \tilde{\sigma}_{dN}(Y = \ln(z/x), r, b) \\ &= \frac{Q^2}{4\pi\alpha_{em}} \int_0^1 \mathrm{d}z \mathrm{d}^2\boldsymbol{r} \Phi_L^{(0)}(\boldsymbol{r}, z) \int \frac{\mathrm{d}^2\boldsymbol{\rho}}{2\pi\rho^2} \tilde{n}(Y, r, \rho, b) \sigma_0(\rho) \qquad (7.1)\end{aligned}$$

where $Y = \ln(z/x)$ is the large rapidity. Recall that $\Phi^{(0)}(\boldsymbol{r}, z)$ represents the contribution from the $\gamma^* \to q\bar{q}$ fluctuation which is the initial perturbative onium state from which the dipole cascade evolves. The exact functional forms for $\Phi_L^{(0)}(\boldsymbol{r}, z)$ and $\Phi_T^{(0)}(\boldsymbol{r}, z)$ (for the transversely polarised photon) can be calculated in perturbation theory [38, 49] and when expressed in terms of transverse coordinates, they take the form

$$\Phi_L^{(0)}(\boldsymbol{r}, z) = \frac{8N_C e^2 Z_q^2}{(2\pi)^2} z^2 (1-z)^2 Q^2 \mathrm{K}_0(\mu r)^2 \qquad (7.2)$$

$$\Phi_T^{(0)}(\boldsymbol{r}, z) = \frac{2N_C e^2 Z_q^2}{(2\pi)^2} \left[(z^2 + (1-z)^2)\mu^2 \mathrm{K}_1(\mu r)^2 + m_q^2 \mathrm{K}_0(\mu)^2\right] \qquad (7.3)$$

where μ is defined by

$$\mu^2 = z(1-z)Q^2 + m_q^2 \qquad (7.4)$$

and where K_ν is the modified Bessel function of order ν, Z_q is the quark charge and m_q is the quark mass. The virtuality of the photon is Q^2. In the numerical analysis performed, the limit of zero mass quarks is taken and the electronic charge e is scaled to 1. Also, in the initial quark-antiquark pair formed from the γ^*, the quark and antiquark are assumed to have equal longitudinal momentum fractions which maximises the z dependence of $\Phi_T^{(0)}$ and $\Phi_L^{(0)}$ in (7.2) and (7.3). The initial $\gamma^* \to q\bar{q}$ fluctuation can be thought of as having transverse size of order $1/Q$ using this assumption.

In (7.1), the Borel transformed dipole-nucleon cross section $\tilde{\sigma}_{dN}$ is a solution to the Borel plane evolution equation

$$\frac{\partial}{\partial Y}\tilde{\sigma}_{dN}(Y,r,b) = \int_0^\infty \mathrm{d}r' \int_0^b \mathrm{d}b'\, \tilde{\mathcal{K}}(r,r',b')\, \tilde{\sigma}_{dN}(Y,r',b-b')\,, \tag{7.5}$$

where $\tilde{\mathcal{K}}$ is given by (5.20) and this integro-differential equation has boundary condition

$$\tilde{\sigma}_{dN}(Y=0,r) = \delta(b)\,\sigma_0(r)\,. \tag{7.6}$$

This has the same form as the evolution equation for fixed coupling discussed in section 3.4. The structure functions always contain a non-perturbative part labelled by σ_0, the cross section for the absorption of a dipole by the nucleon at impact parameter r. The mass scale which governs σ_0 is m_N, where m_N represents a typical nucleon mass. The dipole cascade $\tilde{n}$ is generated from the initial $q\bar{q}$ wavefunction $\Phi^{(0)}$ and is governed by the perturbative scale Q^2. It is this perturbative scale which appears in the integration kernel $\tilde{\mathcal{K}}$. Borel singularities present in $\tilde{n}$ will therefore correspond to leading power correction terms to the perturbative result which are of order $(1/Q^2)^p$ where p represents the position of the leftmost pole on the positive real b axis. The b dependence in (7.1) is present only through the dipole density $\tilde{n}$.

Recall that the physical rôle which $\Phi^{(0)}$ fulfils is that it determines the distribution of the initial $q\overline{q}$ pair in transverse coordinate space. A more precise understanding of this distribution comes from noting the asymptotic behaviour of a modified Bessel function $K_\nu(u)$ as $u \to \infty$

$$K_\nu(u) \to \sqrt{\frac{\pi}{2u}}\, e^{-u} \left(1 + \mathcal{O}\left(\frac{1}{u}\right)\right) . \tag{7.7}$$

Note that the leading term in this asymptotic expansion is independent of the order of the Bessel function and hence both γ^* polarisations scale in the same asymptotic manner. When the expressions $\Phi^{(0)}$ are viewed in this context, the scale Q^2 can be seen to act as an infra-red regulator where $q\overline{q}$ dipole configurations with large Qr will be suppressed by virtue of (7.7).

At the end of the dipole cascade, where the convolution with the dipole-nucleon cross section $\sigma_0(\rho)$ occurs, $\sigma_0(\rho)$ is the quantity which regulates the emission of dipoles of large sizes. Dipoles of size $\rho \gg (1/m_N)$, where $(1/m_N)$ represents the nucleon size, will not couple to the target.

7.2 The Borel Singularity Structure of the Small-x Structure Functions

Before presenting numerical results illustrating the Borel dependence of $\tilde{\sigma}_{dN}$, the differences between the analysis in this section and that carried out in chapter 6 is discussed. In chapter 6, the action of the kernel on the test function $(r'^2)^\gamma$ was studied and an analytic expression for the Borel singularity structure was determined (6.8). The test functions were then used as a basis for decomposing the dipole density in terms of the spectral amplitudes (6.13) and it was observed that this led to infra-red renormalons whose position were dependent on the value of γ. If this procedure were applicable for constructing the structure functions in this section, it would yield a leading infra-red renormalon at $b\beta_0 = \gamma$ which would be to the left of $b\beta_0 = 1$ if $0 < \gamma < 1$ and would correspond to a power correction of order $(1/Q^2)^\gamma$. This would be in contradiction with the usual Wilson operator product expansion developed for deep inelastic scattering structure functions away from small-x which predicts leading power corrections of order $(1/Q^2)$. This apparent contradiction between the operator product expansion and the approach followed here does not arise however.

In section 6.2 it was noted that the infra-red renormalon singularities arise from the $r' \gg r$ region in the integral over r' in (6.7), that is where dipoles are emitted with large impact parameters. In terms of the dipole nucleon density evolution, (7.5) the infra-red renormalon singularities arise from the large r' region. Although the dipole-nucleon absorption cross section $\sigma_0(r')$ is not calculable within perturbative QCD some of its properties can be deduced. The cross section $\sigma_0(r')$ is controlled by a nucleon wave function which is suppressed at large r' (where the scale 'large' is relative to the nucleon radius). This leads one to the conclusion that the probability of finding a sufficiently large primary dipole inside a nucleon is negligible. The cross section σ_0 can be modelled to incorporate this large impact parameter and this is the procedure which is employed in the numerical analysis which follows.

It has been argued that the nucleon wave function is rapidly suppressed at large impact parameter. In this study, it is assumed that this suppression is exponential for asymptotically large impact parameter. The model chosen is to adopt the impact parameter dependence calculated for the virtual photon (7.2). Note that for the realistic case of DIS this is a model whereas if the scattering of two virtual photons were being considered (onium-onium scattering) then this model would be exact as both ends of the dipole cascade would link to objects which were calculable in perturbation theory. It is required that the model of the nucleon wavefunction is normalisable and for this reason the functional dependence of the nucleon wavefunction part of σ_0 is taken to be $\mathrm{K}_0(m_N\rho)^2$. Choosing the impact parameter space dependence of the transversely polarised photon would not give rise to a normalisable wavefunction as it would exhibit an ultra-violet divergence which can be observed by noting that $\mathrm{K}_1(\rho)$ behaves like $1/\rho$ as $\rho \to 0$. In the case of the transverse photon, this divergence is associated with the wavefunction renormalisation of the photon. Note that from the property of the modified Bessel functions (7.7), it can be seen that the asymptotic dependence is independent of the order ν of K_ν. The choice of K_0 is normalisable and reproduces the assumed large impact parameter behaviour. The function used to model the cross section $\sigma_{dN}^{(0)}$ is

$$\sigma_{dN}^{(0)}(\rho) = \rho^2 \mathrm{K}_0(m_N\rho)^2 \tag{7.8}$$

with Borel transform

$$\tilde{\sigma}_{dN}^{(0)} = \rho^2 \mathrm{K}_0(m_N\rho)\delta(b) \tag{7.9}$$

One should not think that this model for σ_0 determines the non-perturbative quantity σ_0 exactly and it should be emphasised that the structure functions will *always* contain a non-perturbative component which cannot be calculated.

Returning to the discussion regarding the leading infra-red renormalon, note that the modified Bessel function cannot be decomposed into a set of basis functions of the form $(r^2)^\gamma$. It is for this reason that γ dependent renormalon singularities will not appear to the left of $b\beta_0 = 1$ in the Borel plane expression for $\tilde{\sigma}_{dN}$ determined by (7.5). Note that this does not mean that one should conclude that infra-red renormalons do not arise from real emission, however it does mean that the leading infra-red renormalon in the Borel transformed dipole density function in deep inelastic scattering is predicted to appear at $b\beta_0 = 1$ which indicates that leading power corrections of order $1/Q^2$ are present. This result is then consistent with the usual operator product expansion result. These predictions were tested numerically and the results are discussed in section 7.3.

It is pertinent to note the interplay of the two momentum scales present in the scattering process at this point, namely the soft, hadronic scale denoted by m_N and the hard scale Q. The small scale m_N acts as an infrared regulator and normalises the measured structure functions. In the numerical analysis presented in section 7.3, this scale is set to $m_N = 1GeV$. However, in the short distance part of the process the scale is determined by Q, the inverse size of the γ^* probe, and this approach aims at determining the power corrections with respect to this hard scale. It is the suppression of the wavefunction for the dipole produced by this probe for sizes $r > 1/Q$ that leads to the appearance of the first renormalon singularity at $b\beta_0 = 1$, giving rise to the first Q^2 dependent power correction. The structure of the power corrections is a property of the short distance part and does not depend on the specific model that is chosen for σ_0. It is due to this property that renormalon analysis can be used to determine the structure of the power corrections as signalled by perturbation theory itself, using a method similar to that discussed in chapter 4. Note that the coefficient of the power correction involves a factor which is dependent on the modelling of σ_0. This same undetermined factor also multiplies the contributions to the structure functions which come from inverting the terms which are non-singular in Borel space. This common undetermined factor will not affect estimates of the relative importance of power corrections with regard to the perturbative result and is a signal that in order to calculate the structure functions absolutely, some experimental input from outside perturbation theory is required. In this study, the structure functions are not determined absolutely but the estimated size of the power corrections relative to the perturbative contribution is discussed. In chapter 8 a prescription will be introduced to invert the Borel transform numerically and estimate the importance of the power correction term.

Before discussing the numerical results obtained, it is appropriate to introduce one further piece of notation which will be used in the next section and also in chapter 8. The quantity $\tilde{f}_L(Y, Q^2, b)$ is defined by

$$\tilde{f}(Y, Q^2, b) = \int \mathrm{d}^2\boldsymbol{r}\Phi_L^{(0)}(r, z)\tilde{\sigma}_{dN}(Y, r, b) \tag{7.10}$$

To arrive at the expression for $\tilde{f}_L$, all integrations over impact parameter variables have been performed. The dependence on Q^2 which arises from the hard scale present in $\Phi_L^{(0)}$ and $\tilde{n}$ has been shown explicitly as this is the scale with which the Borel transform of the running coupling was defined in (5.1). A similar quantity $\tilde{f}_T$ could be defined in the case where a transversely polarised virtual photon probe is present. In this study, only $\tilde{f}_L$ will be considered. Both transverse and longitudinal polarisations possess the same large r asymptotic bahaviour by virtue of the Bessel function expansion (7.7) which leads to the same type of power corrections in both cases. However it has already been remarked that the expression for the transversely polarised photon (7.3) is ultra-violet divergent because of the small r form of the first order modified Bessel function. A numerical subtraction procedure could be implemented to regulate this divergence, however in this study, the case of longitudinal polarisation only is considered.

7.3 Numerical Analysis of the Borel Singularity Structure in DIS

In this section, the numerical algorithm used to construct the dipole density $\tilde{\sigma}_{dN}$ is discussed and results which demonstrate that that this function is regular in the region $0 \leq b\beta_0 < 1$ are presented along with evidence that the first Borel singularity is encountered at $b\beta_0 = 1$.

The functional form of σ_0 (7.9) prevents an analytic solution to (7.5) from being found. Numerical methods must be used to perform the integrals over r' and b' in (7.5) and the integral over ω present in the integration kernel (5.20). Specifically, the Borel transformed dipole density $\tilde{\sigma}_{dN}$ is approximated by a power series expansion in rapidity Y

$$\tilde{\sigma}_{dN}(Y, r, b) = \sum \frac{Y^n}{n!} \tilde{\sigma}_{dN}^{(n)}(r, b) \,, \tag{7.11}$$

so as to bring the evolution equation into the form

$$\tilde{\sigma}_{dN}^{(n)}(r, b) = \int \mathrm{d}r' \int_0^b \mathrm{d}b' \tilde{\mathcal{K}}(r, r', b - b') \tilde{\sigma}_{dN}^{(n-1)}(r', b') \,. \tag{7.12}$$

Functions $\tilde{f}^{(n)}(Q^2, b)$ are defined from the coefficient functions $\tilde{\sigma}_{dN}^{(n)}(r, b)$ of the power series expansion (7.11) in an analogous way to (7.10). In this chapter, the results are discussed primarily in terms of the functions $\tilde{\sigma}_{dN}^{(n)}$ (and $\tilde{f}^{(n)}(Q^2, b)$ is employed in chapter 8). This is because the integration over r performed in the construction of $\tilde{f}$ takes place after the procedure (7.12) is carried out. Discussing the behaviour of $\tilde{\sigma}_{dN}^{(n)}(r, b)$ allows the method of generating the power series coefficients $\tilde{\sigma}^{(n)}$ to be examined in more detail.

The first convolution of the kernel with $\tilde{\sigma}(\rho, b)$, denoted by $\tilde{\sigma}^{(1)}$ is slightly simpler

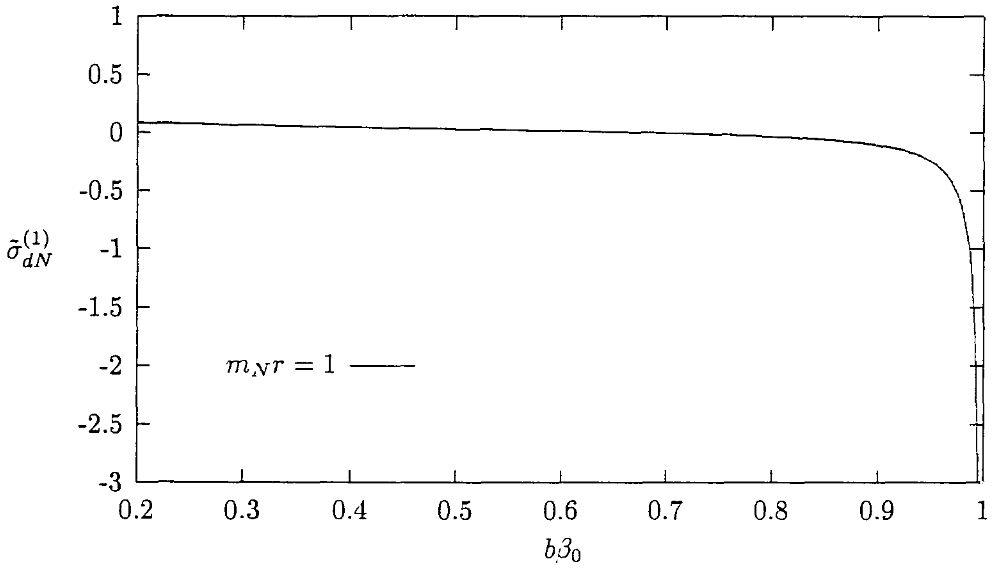

Figure 7.1: The behaviour of $\tilde{\sigma}^{(1)}_{dN}(r, b)$ plotted against $b\beta_0$ for $m_N r = 1$

to perform numerically than subsequent iterations because the b dependence of $\tilde{\sigma}^{(0)}_{dN}$ is a simple Dirac-delta function in b and hence no numerical convolution integral in b has to be performed. The integration over the transverse size r' in (7.12) is performed using the transformations discussed in section 6.3, that is the r' integration is converted into two integrations over ζ , where $0 \leq \zeta \leq 1$ and the algorithm described for parameterising the $\zeta \to 1$ behaviour is implemented.

It is found that $\tilde{\sigma}^{(1)}$ exhibits the singularity structure anticipated from the discussion in section 7.2. This is illustrated in fig. 7.1 where $\tilde{\sigma}^{(1)}$ is plotted against $b\beta_0$ for $m_N r = 1$. Recall that the integration over r is not performed in the determination of $\tilde{\sigma}^{(1)}$ and so $\tilde{\sigma}^{(1)}$ has been plotted in terms of the dimensionless quantity $m_N r$. Observe that the leftmost singularity in the Borel plane appears at $b\beta_0 = 1$ and this is identified as the leading infra-red renormalon. The most singular behaviour of $\tilde{\sigma}^{(1)}$ as $b\beta_0 \to 1$ was found to be a simple pole in Borel space. For the first iteration, the pole term arises entirely from the virtual correction contribution to $\tilde{\sigma}^{(1)}$.

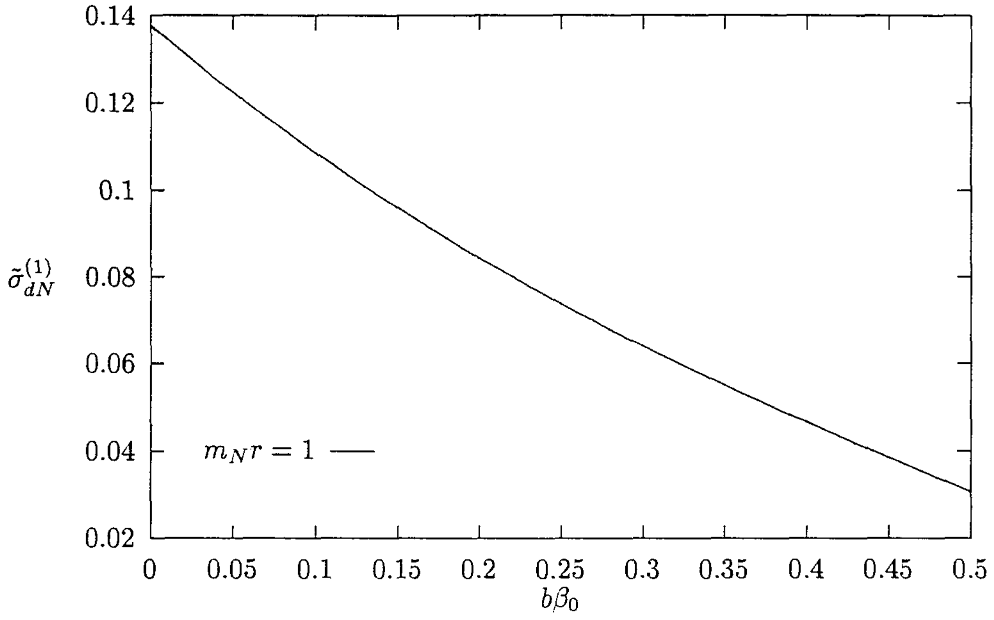

Figure 7.2: The behaviour of $\tilde{\sigma}^{(1)}_{dN}(r, b)$ plotted against $b\beta_0$ near $b = 0$ for $m_N r = 1$

There is no evidence of any singular behaviour in the region $0 \leq b\beta_0 < 1$ and this is illustrated in fig. 7.2 where $\tilde{\sigma}^{(1)}$ is plotted over an intermediate range of $b\beta_0$. No singularities can be detected near $b = 0$ and it was concluded that the algorithm used to encode the $b = 0$ region has again been effective in handling the cancellation between the real and virtual terms. In order to generate subsequent iterations, it is necessary to know the large r behaviour of $\tilde{\sigma}^{(1)}$. It is found that there is a distinct difference between the asymptotic behaviour of $\tilde{\sigma}^{(0)}_{dN}(r, b)$ and $\tilde{\sigma}^{(1)}_{dN}(r, b)$ as $m_N r \to \infty$. The large r behaviour of $\tilde{\sigma}^{(1)}$ is illustrated in fig. (7.3) for an intermediate value of $b\beta_0 = 0.25$. Whereas $\tilde{\sigma}^{(0)}_{dN}(r, b)$ decays exponentially at large $m_N r$, (7.7), the asymptotic behaviour of $\tilde{\sigma}^{(1)}_{dN}(r, b)$ can be parameterised by

$$\tilde{\sigma}^{(1)}_{dN}(r, b) \to (m_N r)^{2(b\beta_0 - 1)} . \tag{7.13}$$

Examination of the kernel (5.20) reveals that $\tilde{\mathcal{K}}$ scales as $(m_N r')^{2b\beta_0 - 1}$ at large

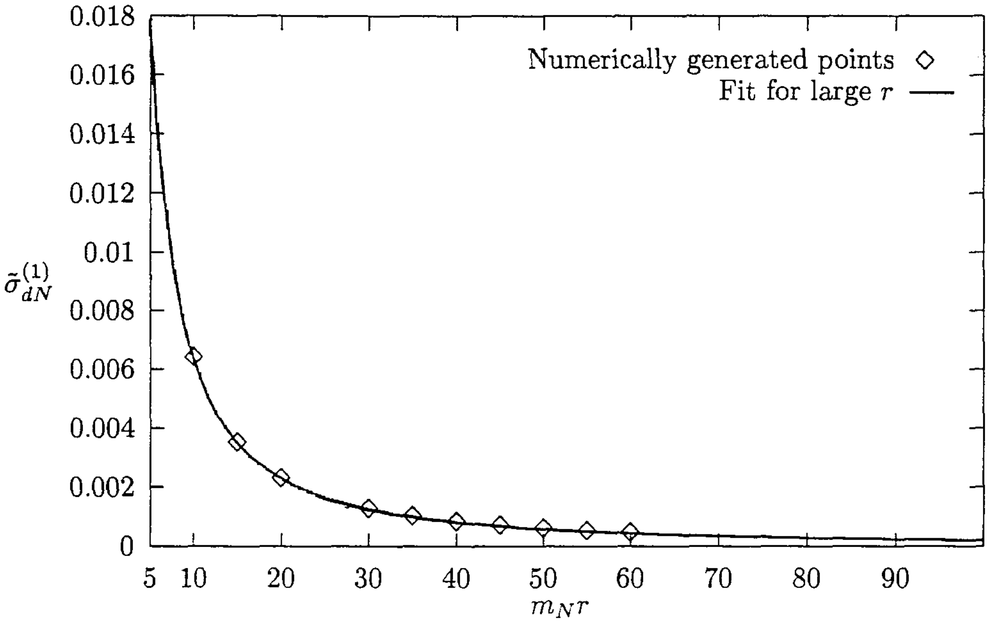

Figure 7.3: The behaviour of $\tilde{\sigma}^{(1)}_{dN}(r, b)$ plotted against $m_N r$ at $b\beta_0 = 0.25$

$m_N r'$ and this is the scaling behaviour which dominates in the convolution to determine the behaviour of $\tilde{\sigma}^{(1)}_{dN}$. For intermediate values of $m_N r$, the result obtained can be fitted accurately if the parameterisation is extended to include logarithmic correction terms and it is found that the large r behaviour can be fitted by

$$\tilde{\sigma}^{(1)}_{dN}(r, b) \simeq (m_N r)^{2(b\beta_0 - 1)}(a_1 + a_2 \ln(m_N r) + a_3 \ln(m_N r)^2)\,, \tag{7.14}$$

where a_1, a_2 and a_3 are fit parameters. This fit is exhibited in fig. (7.3) where the points represent actual data points generated and the fit is plotted as a solid line. In section 7.2, it was argued that the exponential nature of $\tilde{\sigma}^{(0)}$ at large $m_N r$ was responsible for the Borel singularity structure observed in the result of the first iteration. The power like behaviour of $\tilde{\sigma}^{(1)}_{dN}(r, b)$ at large $m_N r$ does not imply that new singularities will appear in the Borel plane to the left of $b\beta_0 = 1$ in subsequent iterations. The action of the convolution in b' in each subsequent iteration guarantees this. For large r', the convolution integrand has a factor $r'^{(2b'\beta_0-1)}$ arising from the kernel and a factor $r'^{2((b-b')\beta_0-1)}$ from the behaviour of $\tilde{\sigma}^{(1)}_{dN}(r',b)$ and the integration introduces a factor of r; the result of this being that the second convolution also exhibits a power dependence of the form parameterised in eq. (7.13) for large r. This large r behaviour is sufficient to predict the position of the leading Borel plane singularity for subsequent iterations. Since the infrared singularities are determined by the infrared (large r) behaviour of the function on which the kernel acts, consider

$$\int_0^b \mathrm{d}b' \int \mathrm{d}r' \tilde{\mathcal{K}}(r,r',b-b')(r'^2)^{b'\beta_0-1} =$$

$$\frac{N_c}{\pi}\int_0^b \mathrm{d}b' \chi(b'\beta_0-1,b-b')\left(\frac{Q^2r^2}{\pi}\right)^{b\beta_0}(r^2)^{b'\beta_0-1}. \qquad (7.15)$$

Then, from (6.8) and the discussion that follows, it can be observed that (by replacing γ by $b\beta_0-1$ and b by $b-b'$ in (6.8)) $\chi(b'\beta_0-1,b-b')$ has a leading singularity at $b\beta_0=1$, which is where the leading singularity will be found for *all* subsequent iterations.

This is confirmed by carrying out a subsequent iteration numerically to generate $\tilde{\sigma}^{(2)}(r,b)$. The numerical procedure now becomes more complex. The two dimensional grid (in (r,b) space) of values taken by $\tilde{\sigma}^{(1)}(r,b)$ which was generated in the first iteration is used as the basis for a surface interpolation algorithm [50, 51] to return values of $\tilde{\sigma}^{(1)}(r,b')$ to the convolution integral (7.12). In performing the convolution over b, care was also taken to ensure that the algorithm selected the appropriate form of the hypergeometric function (6.2) depending on whether $b\beta_0$ was greater or less than 0.5. Requests from the numerical integration routine for $\tilde{\sigma}^{(1)}(r',b-b')$ at large r' were handled by using the fit described in (7.14). The results for $m_N r = 1$ are illustrated in fig. 7.4 where the leftmost singularity is located at $b\beta_0 = 1$ supplying evidence for the argument involving Borel trans-

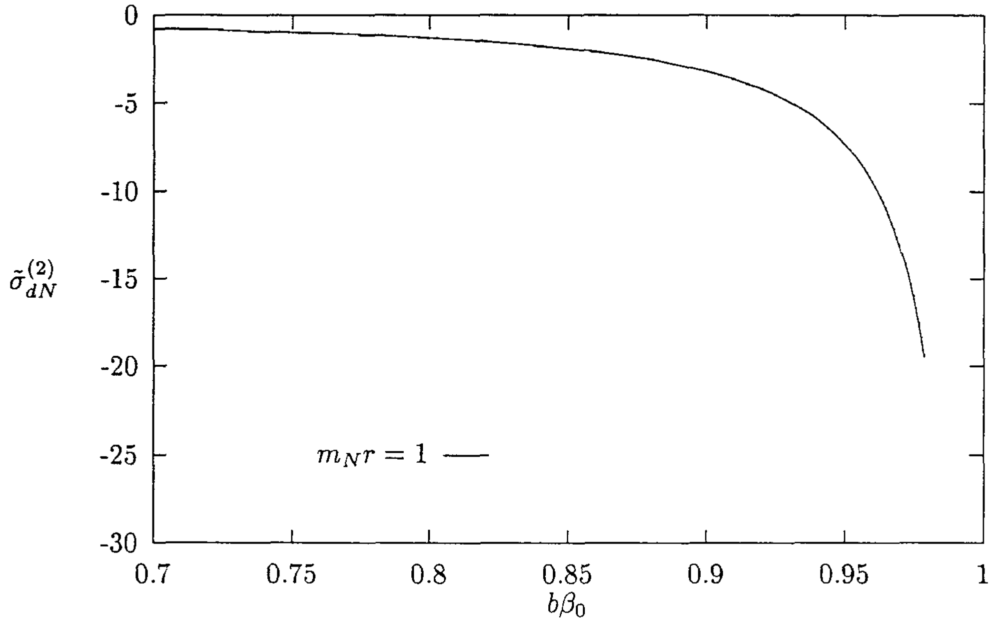

Figure 7.4: The behaviour of $\tilde{\sigma}^{(2)}_{dN}(r, b)$ plotted against $b\beta_0$ at $m_N r = 1$

forms given above. It was also observed that the functional form of $\tilde{\sigma}^{(2)}(r, b)$ near $b\beta_0 = 1$ was a simple pole. However, due to the complexity of the real part of the kernel and the added complexity which is added by the Borel convolution , sub leading terms in $(1 - b\beta_0)$ could not be conclusively determined. It was found however that the coefficient of the pole term could be determined with sufficient accuracy for it to be used in the analysis of chapter 8 despite the ambiguity in the functional form of the sub leading terms. Note that the shape of the distribution is broader near $b\beta_0 = 1$ than in the first iteration . For the second and subsequent iterations, the leading singularity at $b\beta_0$ is converted into a cut with a branch point at $b\beta_0 = 1$ which receives singular contributions from both the virtual correction and real emission part of the kernel.

Note that the convolution also leads to a linear fall off as $b\beta_0 \to 0$. In higher iterations of the kernel, it is the intermediate $b\beta_0$ range which will be of the most significance. The $b \to 0$ behaviour of $\tilde{\sigma}^{(2)}(r, b)$ can be seen more clearly in fig. 7.5

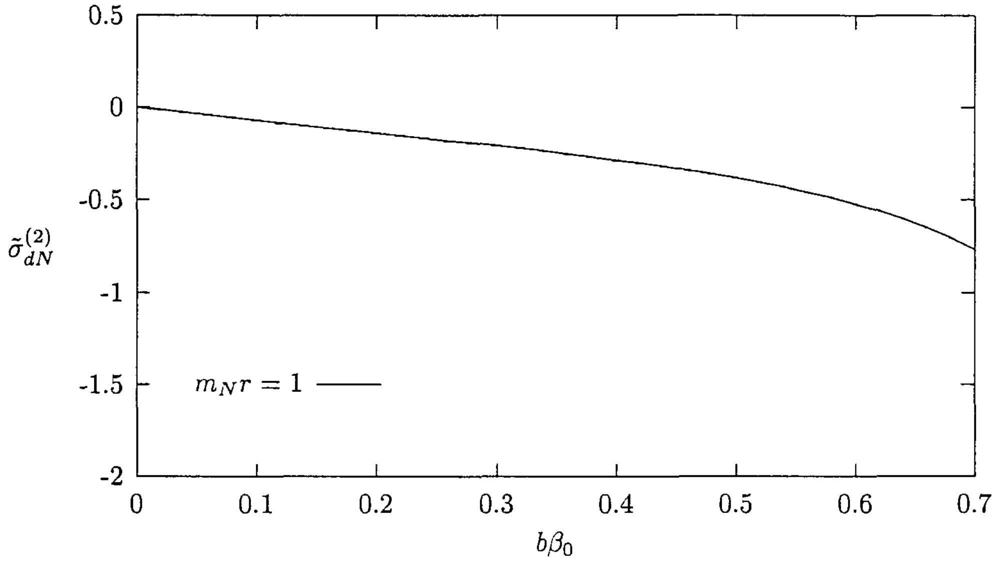

Figure 7.5: The behaviour of $\tilde{\sigma}^{(2)}_{dN}(r, b)$ near $b = 0$ plotted against $b\beta_0$ at $m_N r = 1$

where a more restricted range of $b\beta_0$ values is plotted compared to fig. 7.4 . The generation of these iterations proved to be a numerically intensive task. It became increasingly difficult to isolate the coefficient of the pole for higher iterations and because the coefficient of the pole is an important quantity in estimating the importance of the power correction terms to the perturbative result, in the next chapter only the first three iterations will be used to make estimations. In these iterations, fitting algorithms could determine the pole coefficient to a sufficiently reliable degree of accuracy for the analysis in chapter 8.

Although only the first three iterations will be used to estimate the size of the power correction terms, fourth and fifth iterations were performed and the dependence on b is demonstrated in fig. 7.6 and fig. 7.7 respectively. Although the results are slightly more unstable in the region of the pole, it is still clear that the first singularity in the Borel plane appears at $b\beta_0 = 1$.

Note that the fifth iteration exhibits a turning point near $b\beta_0 = 0.8$. The exact function which was responsible for this could not be determined but it was

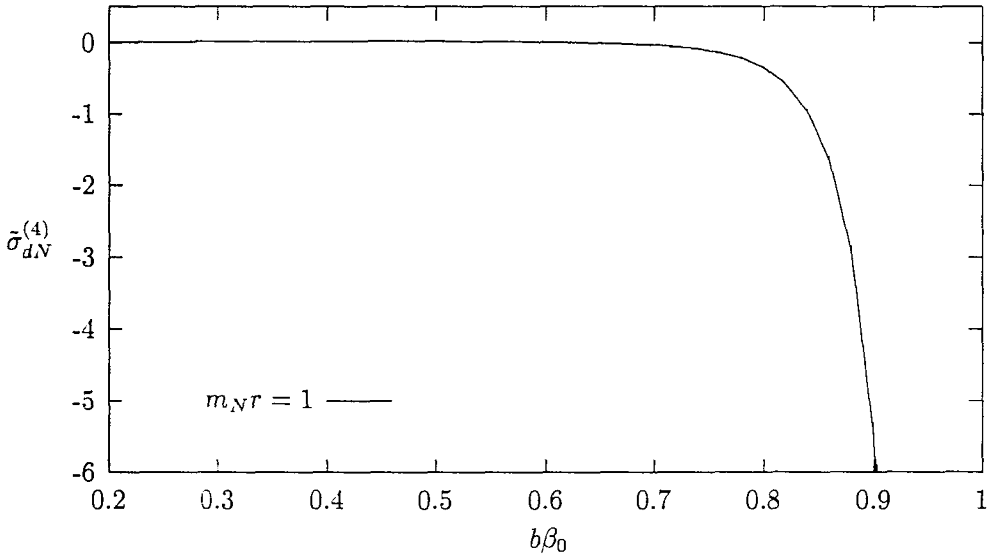

Figure 7.6: The behaviour of $\tilde{\sigma}^{(4)}_{dN}(r, b)$ near $b = 0$ plotted against $b\beta_0$ at $m_N r = 1$

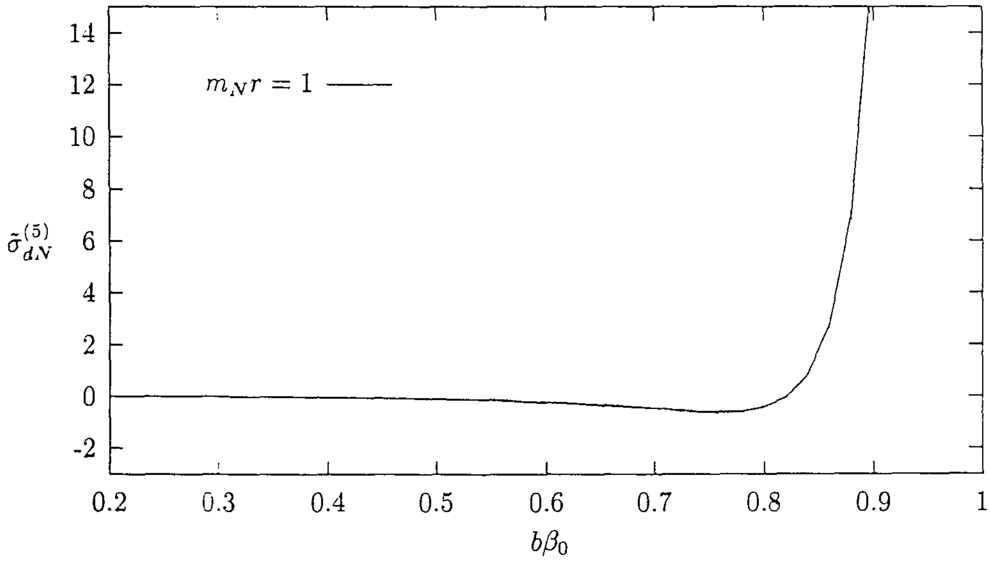

Figure 7.7: The behaviour of $\tilde{\sigma}^{(5)}_{dN}(r, b)$ near $b = 0$ plotted against $b\beta_0$ at $m_N r = 1$

found that above $b\beta_0 = 1$ the pole term became dominant and $\tilde{\sigma}^{(5)}_{dN}(r, b) \to +\infty$ monotonically.

In this chapter, it has been demonstrated that the leading Borel plane singularity for the deep inelastic structure functions is located at $b\beta_0 = 1$ and this was confirmed using a numerical procedure. In the next chapter, the size of the power correction terms due to this singularity in Borel space and the effects of running the coupling will be studied by implementing a prescription to invert the Borel transform.

Chapter 8

Physical Significance of the DIS Power Corrections

In chapter 7, the Borel singularity structure of the deep inelastic scattering structure functions was determined in the leading logarithmic $(1/x)$ limit by determining the Borel singularities of the function $\tilde{\sigma}_{dN}(Y, r, b)$. In this chapter, the functions $\tilde{f}^{(n)}(Q^2, b)$ defined by (7.10) are used to investigate the properties of the leading $(1/Q^2)$ power corrections which are predicted by these Borel plane singularities. It is emphasised again that an absolute prediction for the structure functions $F(x, Q^2)$ will not be made. Instead, the relative contributions of the fixed coupling, perturbative and power correction terms to the structure functions are estimated. This estimation is independent of the unknown but common non-perturbative factor which is present in the analysis of chapter 7.

8.1 Inverting the Borel Transform

The reader will recall from chapter 4 that an observable $O(Q^2)$ can be reconstructed from the Borel transformed $\tilde{O}(b)$ by using the Borel transformation (4.4). It was noted that the transformation was only unique if there were no singularities on the positive real axis. In the presence of infra-red renormalons a specific prescription has to be used to distort the path of the b integration in the complex b plane around the renormalon and it was noted that the prescription adopted introduces an ambiguity into the theory. In this chapter a specific prescription for the treatment of the Borel transform in the region of the pole is used. It is assumed that the contribution from integrating around a pole term at $b\beta_0 = 1$ is given by the magnitude of the Cauchy integral

$$-i \oint \mathrm{d}b \frac{C e^{-b/\alpha_s(Q^2)}}{1 - b\beta_0} = 2\pi C \left(\frac{\Lambda^2_{QCD}}{Q^2} \right) \tag{8.1}$$

where QCD scale parameter has been introduced using (2.7) and C is the residue of the pole term in Borel space. Recall that the order of the power correction is not ambiguous and that the presence of an infra-red renormalon at $b\beta_0 = 1$ leads to the existence of terms with power dependence $(1/Q^2)$ when viewed in terms of the running coupling. It is the non-unique nature of the method which is employed to estimate the contribution from the pole region which introduces an ambiguity. It is therefore recognised that the prescription set out by (8.1) may under or over estimate the importance of power corrections however it is expected that this only results in a ambiguity of order one. This estimate therefore provides an order of magnitude estimate of the non-perturbative higher twist effects.

In the specific case of $\tilde{f}_L^{(n)}(Q^2, b)$, the specific procedure used to invert this Borel transform can be traced from (4.2) and (4.4). Using the prescription defined above, $f_L^{(n)}(Q^2)$, the transform of $\tilde{f}_L^{(n)}(Q^2, b)$, can be written as the sum of three terms

$$f_L^{(n)}(Q^2) = f_{LF}^{(n)}(Q^2) + f_{LR}^{(n)}(Q^2) + f_{LP}^{(n)}(Q^2) \tag{8.2}$$

where the these terms are defined by

$$f_{LF}^{(n)}(Q^2) = \int \mathrm{d}b e^{-b/\alpha_s(Q^2)} \tilde{f}_L^{(n)}(Q^2, b)\delta(b) \tag{8.3}$$

$f_{LF}^{(n)}(Q^2)$ is the result which arises from the fixed coupling regime, that is the regime where the coupling is determined by the external momentum Q^2, so by 'fixed coupling' one should understand that the quantity $f_{LF}^{(n)}(Q^2)$ is governed by $\alpha_s(Q^2)$. The presence of the fixed coupling term, $f_{LF}^{(n)}(Q^2)$, in the Borel can be traced from (4.2). In terms of the scattering process under consideration, it is the term which arises from acting n times on $\sigma^{(0)}(r)$ with the kernel $\tilde{\mathcal{K}}$ at $b = 0$ or equivalently, with the fixed coupling kernel $\tilde{\mathcal{K}}_{DIP}$ (3.27) where α_s is evaluated at scale Q^2 and then multiplying by the perturbative $q\bar{q}$ onium and integrating over the remaining transverse size.

The term which is explicitly dependent on the prescription for treating the pole contribution is $f_{LP}^{(n)}(Q^2)$ where

$$\begin{aligned} f_{LP}^{(n)}(Q^2) &= -i \oint \mathrm{d}b \frac{\mathcal{C}}{1 - b\beta_0} e^{-b/\alpha_s(Q^2)} \\ &= 2\pi\mathcal{C}\left(\frac{\Lambda_{QCD}^2}{Q^2}\right) \end{aligned} \tag{8.4}$$

where (8.1) has been used to perform the integral.

The term $f_{LR}^{(n)}(Q^2)$ arises from the running of the coupling and is defined by

$$f_{LR}^{(n)}(Q^2) = \int_0^{1/\beta_0} \mathrm{d}b \left(\tilde{f}_L^{(n)}(Q^2, b) - \frac{\mathcal{C}}{1 - b\beta_0}\right) e^{-b/\alpha_s(Q^2)} \tag{8.5}$$

The integrand in (8.5) is integrable over b as $b\beta_0 \to 1$ as all pole terms have been subtracted. Up to systematic factors which are related to the determination of the pole coefficient, $f_{LR}^{(n)}(Q^2)$ is not an ambiguously defined quantity. The inverse transform integral in (8.5) should be performed over the range $0 \leq b < \infty$. In this case, values of the function $\tilde{f}_L^{(n)}(Q^2, b)$ were not available above $b\beta_0 = 1$ and an upper limit of $b\beta_0 = 1$ was imposed. This imposed cutoff introduces an artificial correction term of order $(\Lambda_{QCD}^2/Q^2)\frac{1}{\ln(Q^2/\Lambda_{QCD}^2)}$ which must be subtracted. This can be observed from the integral (8.5). Rescaling the integration variable in terms of $u = b\beta_0$ and inserting the explicit form for $\alpha_s(Q^2)$ from (2.7), (8.5) can be rewritten as

$$\int_0^1 du \left(\frac{\Lambda_{QCD}^2}{Q^2}\right)^u \left[\tilde{f}_L^{(n)}(Q^2, u) - \frac{C}{1-u}\right] \tag{8.6}$$

The term in the square brackets in (8.6) is defined so that it is integrable at $u = 1$. Assume that the term in square brackets is actually constant near $u = 1$ and equal to R, then the integral in (8.6) can be performed analytically and the result is

$$R\frac{1}{\ln(Q^2/\Lambda_{QCD}^2)}\left(1 - \frac{\Lambda_{QCD}^2}{Q^2}\right) \tag{8.7}$$

The term containing the factor (Λ_{QCD}^2/Q^2) is due to the artificial upper cut-off which has been imposed. In order to remove this explicit dependence on the value of the upper limit a term proportional $(\Lambda_{QCD}^2/Q^2)\frac{1}{\ln(Q^2/\Lambda_{QCD}^2)}$ was subtracted from the result of (8.5) and the exact coefficient was determined numerically. Another approximation which has been made in this treatment of inverting the Borel transform is that the contribution from the exponential integral function which would arise from a more analytical treatment of the integral in (8.1) has been neglected. The next section contains a brief description of how the terms $f_{LF}^{(n)}$ and $f_{LR}^{(n)}$ were determined numerically.

Iteration	Coefficient of pole at $b\beta_0 = 1$
1	-0.00034
2	-0.015
3	0.045

Table 8.1: Pole coefficients of $\tilde{f}^{(n)}(Q^2, b)$ for $n = 1, 2, 3$

8.2 Numerical Evaluation of $f_{LF}^{(n)}$ and $f_{LR}^{(n)}$

It has been demonstrated that the numerical algorithm used to code the kernel effectively handles the $b = 0$ region. The fixed coupling term $f_{LF}^{(n)}(Q^2)$ was arrived at numerically by iterating the b dependent kernel on $\sigma^{(0)}(\rho)$ at a very small value of b, where the singularities between real and virtual terms still cancelled numerically. It was found that a value of $b = 1.0 \times 10^{-3}$ could be used without difficulty.

The calculation of $f_{LF}^{(n)}(Q^2)$ required knowledge of the $b\beta_0 = 1$ pole coefficient in order that the term in parentheses in (8.5) could be calculated accurately. It was found that although the form of the subleading terms near $b\beta_0 = 1$ could not be determined, the difference that this made to the coefficient of the pole term in the first three iterations was not severe enough to invalidate the subtraction procedure used in (8.5) and consistent finite results were obtained by performing the b integration numerically. Lack of confidence in the coefficient of the pole at $b\beta_0 = 1$ for the fourth and subsequent iterations generated led to those iterations being discarded in this analysis. The coefficients obtained for the first three iterations are presented in table 8.2. The coefficient of the pole term at $b\beta_0 = 1$ after the first iteration is much smaller than subsequent iterations. This can be explained by noting that the pole dependence of $\tilde{f}_L(Q^2, b)$ arises entirely from the term corresponding to virtual emission in the first iteration. In second and subsequent iterations, the convolution over b is responsible for the larger pole

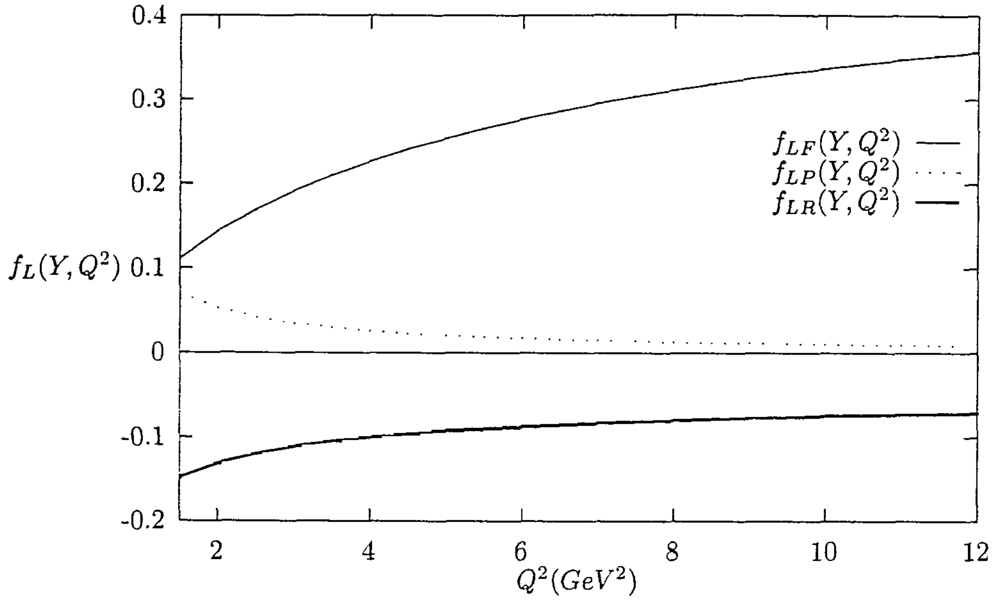

Figure 8.1: $f_{LF}(Y,Q^2)$,$f_{LR}(Y,Q^2)$,$f_{LP}(Y,Q^2)$ plotted against Q^2 at $Y=3$

coefficients. From iteration 2 onwards, the pole coefficients alternated in sign.

8.3 Numerical Results

The results obtained for each iteration are not presented independently but instead they are treated as the coefficients in the expansion of $f_L(Y,Q^2)$ where

$$f_L(Y,Q^2)=\sum_n \frac{Y^n}{n!} f_L^{(n)}(Q^2) \tag{8.8}$$

and $f_L^{(n)}(Q^2)$ is expanded in terms of (8.2). In fig. 8.1, the three terms which contribute to $f_L(Y,Q^2)$ are plotted for the case where $Y=3$. The dependence of $f_L(Y,Q^2)$ on Q^2 at $Y=4$ is illustrated in fig. 8.2. In both graphs, the fixed coupling term gives rise to the largest contribution to $f_L(Y,Q^2)$ at low Q^2. The contributions to $f_L(Y,Q^2)$ from the terms arising from considering a running

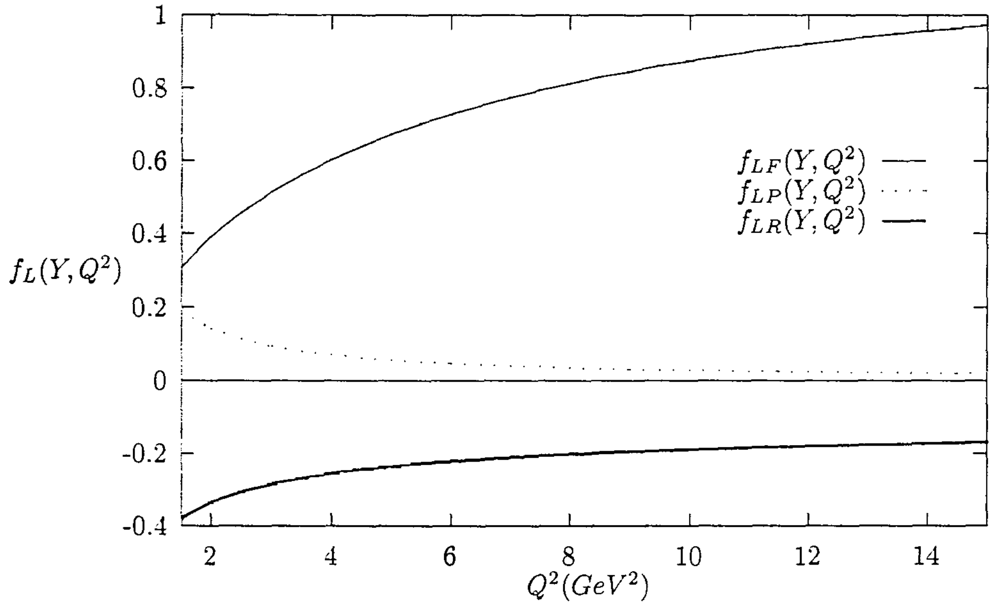

Figure 8.2: $f_{LF}(Y,Q^2)$,$f_{LR}(Y,Q^2)$,$f_{LP}(Y,Q^2)$ plotted against Q^2 at $Y = 4$

coupling at low Q^2 for $Y = 3$ and $Y = 4$ are smaller than the fixed coupling case but not insignificant, indicating that predictions for structure functions in the small-x limit at low values of Q^2 may require the terms arising from running the coupling to be included. At low Q^2, the power correction term f_{LP} has a $1/Q^2$ dependence and rises rapidly as Q^2 decreases. The Q^2 dependence of the term arising from the running coupling, f_{LR} is less severe and behaves like $(\ln(Q^2))^{-1}$. At high values of Q^2, the power correction terms fall off as $(1/Q^2)$ and the fixed coupling term $f_{LF}(Y,Q^2)$ term dominates. At high values of Q^2, it is expected that the usual BFKL result should provide a reasonable estimate of the structure functions calculated by resumming leading logarithms in longitudinal momentum. From the discussion in 2.4.2, the probability of diffusion into the region of transverse momenta where the coupling becomes large decreases with increasing Q^2 and the result for $f_L(Y,Q^2)$ should become less sensitive to non-perturbative effects.

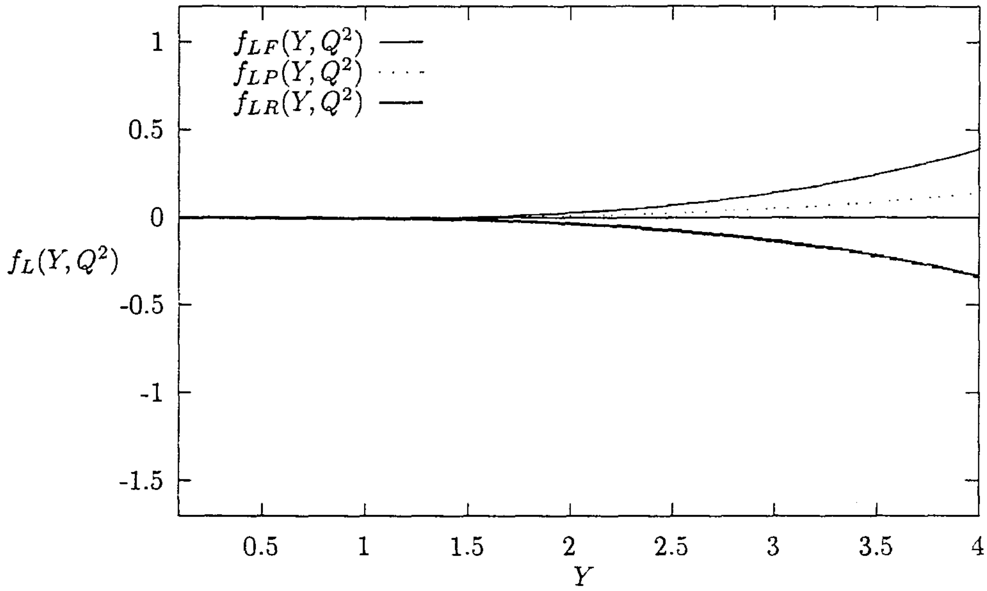

Figure 8.3: $f_L(Y, Q^2)$ plotted against Y for $Q^2 = 2GeV^2$

It is also interesting to consider how the individual components of $f_L(Q^2, Y)$ behave with rapidity. The graphs shown in figs. 8.3,8.4,8.5 show the evolution of $f_{LF}(Y, Q^2)$, $f_{LP}(Y, Q^2)$ and $f_{LR}(Y, Q^2)$ with Y as determined by the power series expansion (8.8). The evolution of each component of $f_L(Y, Q^2)$ is plotted for three different values of Q^2, $Q^2 = 2GeV^2$, $Q^2 = 5GeV^2$ and $Q^2 = 10GeV^2$ respectively.

The graph in fig. 8.3 indicate that as larger rapidities are considered, the contribtion to $f_L(Y, Q^2)$ still has a small but increasing component from $f_{LR}(Y, Q^2)$ and $f_{LP}(Y, Q^2)$ indicating that the fixed coupling term $f_{LF}(Y, Q^2)$ may not be sufficient to describe the structure functions completely at large rapidities and low Q^2. At $Q^2 = 10GeV^2$ however, the fixed coupling term $f_{LF}(Y, Q^2)$ dominates and appears to be increasing fastest with rapidity indicating that at this value of Q^2, the power correction terms and the effects from running the coupling are only of very slight importance.

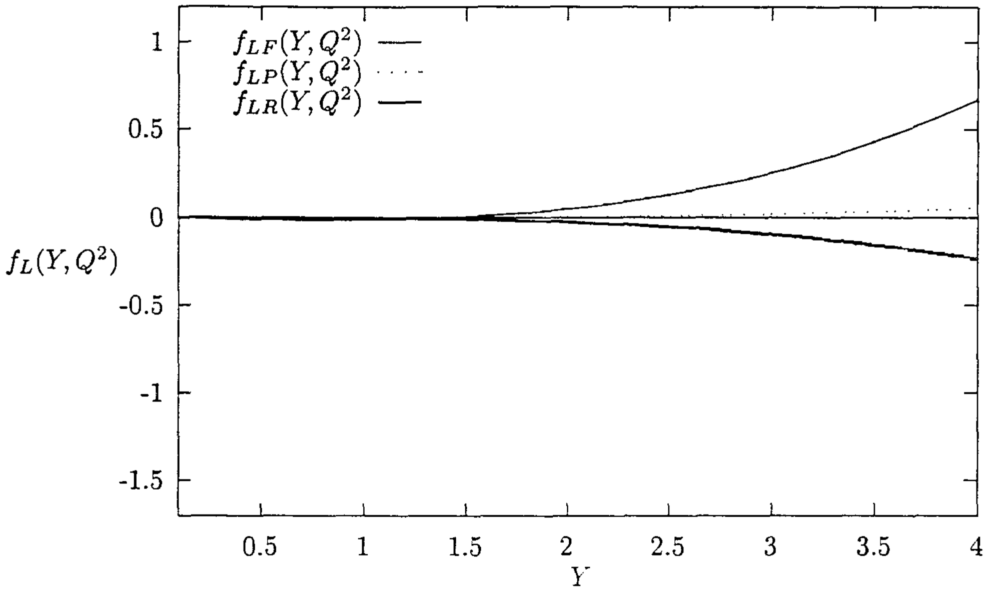

Figure 8.4: $f_L(Y, Q^2)$ plotted against Y for $Q^2 = 5GeV^2$

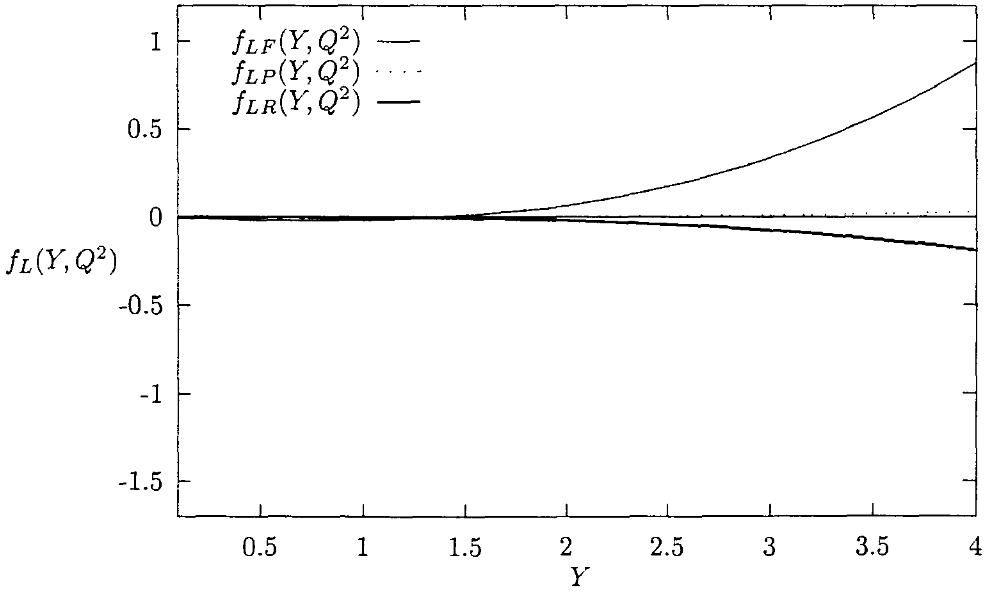

Figure 8.5: $f_L(Y, Q^2)$ plotted against Y for $Q^2 = 10GeV^2$

Chapter 9

Concluding Remarks

In this thesis, the high energy limit of QCD has been discussed. Using the BFKL approach in chapter 2, it was argued that a running coupling should be implemented into the leading logarithmic resummation. The complexities involved in the t-channel gluon ladder picture which results from the BFKL equation did not provide a framework into which the running QCD coupling could be inserted in a systematic way. Instead, the QCD dipole approach was introduced and it was demonstrated that the radiation of gluons (colour dipoles in the large N_C limit) was equivalent to the BFKL formalism. The analogues between the dipole evolution and jet cascades were observed and this provided a guide in the incorporation of a running coupling into the QCD dipole approach. In order to identify the infra-red singularity structure of the dipole evolution equation, the Borel transform was introduced.

After determining the Borel transformed probability for one gluon emission from a dipole, the explicit form for the probability for one gluon emission with a running coupling expressed in terms of impact parameters was deduced and it was found that the argument of the running coupling could not be simply expressed in terms of the transverse coordinates of the dipole and the emitted gluon alone.

An integral equation describing the evolution of the dipole density with rapidity was formulated in Borel space which allowed identification of an evolution kernel $\tilde{\mathcal{K}}$. It was demonstrated that $\tilde{\mathcal{K}}$ reduced to the dipole evolution kernel developed with a fixed coupling in the limit where the Borel plane variable $b \to 0$. The exact cancellation of a singularity at $b = 0$ between the terms responsible for real and virtual gluon exchange was also demonstrated proving that $\tilde{\mathcal{K}}$ was ultra-violet finite when both real and virtual contributions were considered.

By acting with the kernel $\tilde{\mathcal{K}}$ on a test function of the form $(r'^2)^\gamma$, an expression was developed for the function $\chi(\gamma, b)$ which revealed the Borel singularity structure of the kernel. It was found that in the $b \to 0$ limit, $\chi(\gamma, b)$ reduced to the well known BFKL spectral function. Poles on the positive real b-axis identified with infra-red renormalons were observed at values of n/β_0 and also at $b\beta_0 = n - \gamma$ where n is a positive integer. A numerical procedure was developed to integrate the kernel numerically and it was confirmed that numerical analysis reproduced the function $\chi(\gamma, b)$ when the kernel was allowed to act upon $(r'^2)^\gamma$.

The analysis was continued to model the Borel transformed deep inelastic scattering structure functions using the dipole approach. It was argued that due to the form of the impact factors in this case, the leading Borel plane singularity would appear at $b\beta_0 = 1$, a result which is consistent with the operator product expansion for deep inelastic scattering. Using a model for the impact parameter dependence of the dipole-nucleon cross section, the location of the Borel plane singularities were found numerically using an iterative scheme and it was found that the leading Borel plane singularity appeared at $b\beta_0 = 1$ for every iteration, corresponding to an infra-red renormalon giving rise to $(1/Q^2)$ power correction terms.

In order to estimate the importance of the power corrections arising from the renormalon singularity, a specific prescription was used to determine the residue of the pole in the Borel plane at $b\beta_0 = 1$ and it was found that at low values of Q^2, the fixed coupling prediction provided by the BFKL result is not sufficient to wholly describe the structure functions at large rapidities and that the terms which arise from running the coupling become increasingly relevant. In summary, the analysis performed on the DIS structure functions suggests that power corrections of order $(1/Q^2)$ are present when a running coupling is employed but the analysis presented here indicates that their magnitude relative to the fixed coupling contribution is not very important. It is unclear whether the effects discovered in this study would have any major impact in resolving the contradiction between the intercept of the soft pomeron described in chapter 2 and the result arrived at from the BFKL approach at fixed coupling. An investigation into how the intercept of the BFKL pomeron is modified, which may include generation of higher iterations with a modified treatment of the convolution in Borel space, may prove to be an exciting area for further study.

Bibliography

[1] E.A. Kuraev, L.N. Lipatov and V.S. Fadin, Sov. Phys. JETP 45 (1977) 199.

[2] Y.Y. Balitskii and L.N. Lipatov, Sov. J. Nucl. Phys. 28 (1978) 822.

[3] A.H. Mueller, Nucl. Phys. B437 (1995) 107, hep-ph/9408245.

[4] A.H. Mueller, Nucl. Phys. B415 (1994) 373.

[5] N.N. Nikolaev and B.G. Zakharov, Phys. Lett. B327 (1994) 149, hep-ph/9402209.

[6] R.K. Ellis, W.J. Stirling and B.R. Webber, QCD and Collider Physics (Cambridge University Press, 1996).

[7] G. Sterman, An Introduction to Quantum Field Theory (Cambridge University Press, 1993).

[8] D.J. Gross and F. Wilczek, Phys. Rev. Lett. 30 (1973) 1343.

[9] H.D. Politzer, Phys. Rev. Lett. 30 (1973) 1343.

[10] R. Eden et al., The Analytic S-matrix (Cambridge University Press, 1966).

[11] T. Regge, Nuov. Cim. 14 (1959) 951.

[12] P. Collins, An introduction to Regge theory and high energy physics (Cambridge University Press, 1977).

[13] A. Sommerfeld, Partial Differential Equations in Physics (Academic Press, 1949).

[14] G.N. Watson, Proc. Roy. Soc. 95 (1918) 83.

[15] G.F. Chew and S.C. Frautschi, Phys. Rev. Lett. 7 (1961) 394.

[16] G.F. Chew and S.C. Frautschi, Phys. Rev. Lett. 8 (1962) 41.

[17] I. Pomeranchuk, Sov. Phys 7 (1958) 499.

[18] A. Donnachie and P.V. Landshoff, Phys. Lett. B296 (1992) 227.

[19] P.V. Landshoff and O. Nachtmann, Z. Phys. C35 (1987) 405.

[20] D.S. Henty, C. Parrinello and D.G. Richards, Phys. Lett. B369 (1996) 130, hep-lat/9511031.

[21] Y.L. Dokshitser, Sov. Phys. JETP 46 (1977) 641.

[22] V.N. Gribov and L.N. Lipatov, Sov. J. Nucl. Phys. 15 (1972) 675.

[23] L.N. Lipatov, Sov. J. Nucl. Phys. 20 (1975) 94.

[24] G. Altarelli and G. Parisi, Nucl. Phys. B126 (1977) 298.

[25] E.A. Kuraev, L.N. Lipatov and V.S. Fadin, Sov. Phys. JETP 45 (1976) 443.

[26] J.R. Forshaw and D.A. Ross, Quantum Chromodynamics and the Pomeron (Cambridge University Press, 1997).

[27] L.V. Gribov, E.M. Levin and M.G. Ryskin, Phys. Rept. 100 (1983) 1.

[28] L.N. Lipatov, Sov. Phys. JETP 63 (1986) 904.

[29] J.C. Collins, D.E. Soper and G. Sterman, in Perturbative Quantum Chromodynamics ed. A. H. Mueller (World Scientific, 1989).

[30] E. Levin, Nucl. Phys. B453 (1995) 303.

[31] R.G. Roberts, The Structure of the Proton (Cambridge University Press, 1990).

[32] M. Derrick et al., Z. Phys. C72 (1996) 399, hep-ex/9607002.

[33] A.H. Mueller and B. Patel, Nucl. Phys. B425 (1994) 471, hep-ph/9403256.

[34] Z. Chen and A.H. Mueller, Nucl. Phys. B451 (1995) 579.

[35] G. 't Hooft, Nucl. Phys. B72 (1974) 461.

[36] Y.L. Dokshitser et al., Basics of perturbative QCD (Gif-sur-Yvette, France: Ed. Frontieres, 1991).

[37] A.H. Mueller and G.P. Salam, Nucl. Phys. B475 (1996) 293, hep-ph/9605302.

[38] N.N. Nikolaev and B.G. Zakharov, Z. Phys. C49 (1991) 607.

[39] N.N. Nikolaev, B.G. Zakharov and V.R. Zoller, Phys. Lett. B328 (1994) 486, hep-th/9401052.

[40] G. 't Hooft, Lectures given at Int. School of Subnuclear Physics, Erice, Sicily, Jul 23 - Aug 10, 1977 .

[41] A.H. Mueller, Nucl. Phys. B250 (1985) 327.

[42] A.H. Mueller, Phys. Lett. B308 (1993) 355.

[43] V.I. Zakharov, Nucl. Phys. B385 (1992) 452.

[44] Y.L. Dokshitser, G. Marchesini and B.R. Webber, Nucl. Phys. B469 (1996) 93, hep-ph/9512336.

[45] V.I. Zakharov, (1997), hep-ph/9802416.

[46] B. Lautrup, Phys. Lett. B76 (1977) 109.

[47] I. Gradshteyn and I.M. Ryzhik, Tables of Integrals, Series and Products (Academic Press, 1994).

[48] G.P. Korchemsky and G. Sterman, Nucl. Phys. B437 (1995) 415, hep-ph/9411211.

[49] J.D. Bjorken, J.B. Kogut and D.E. Soper, Phys. Rev. D3 (1971) 1382.

[50] R.L. Renka, ACM Trans. Math. Softw. 10 (1984) 440.

[51] A.K. Cline and R.L. Renka, Rocky Mountain J. Math. 14 (1984) 223.